Polypeptides synthesized by common bacteria in the human gut improve rodent metabolism

Fan, Yong; Lyu, Liwei; Vazquez-Uribe, Ruben; Zhang, Wanliang; Bongers, Mareike; Koulouktsis, Andreas; Yang, Mengliu; Sereika-Bejder, Vita; Arora, Tulika; Stankevic, Evelina; Armetta, Jeremy; Zosel, Franziska; de la Cour, Charlotta D.; Simonsen, Lotte; Kulakova, Alina; Wierer, Michael; Harris, Pernille; Gæde, Joachim; Rossing, Peter; Knop, Filip K.; Pers, Tune H.; Hansen, Tue Haldor; Nielsen, Trine; Li, Ling; Strømgaard, Kristian; Yang, Gangyi; Sommer, Morten Otto Alexander; Pedersen, Oluf

Published in:
Nature Microbiology

DOI:
10.1038/s41564-025-02064-x

Publication date:
2025

Document version
Publisher's PDF, also known as Version of record

nature microbiology

Article

https://doi.org/10.1038/s41564-025-02064-x

Polypeptides synthesized by common bacteria in the human gut improve rodent metabolism

Received: 6 February 2025

Accepted: 18 June 2025

Published online: 31 July 2025

Check for updates

Yong Fan[1,14], Liwei Lyu[1,2,14], Ruben Vazquez-Uribe[3], Wanliang Zhang[4], Mareike Bongers[3], Andreas Koulouktsis[3], Mengliu Yang[5], Vita Sereika-Bejder[6], Tulika Arora[1], Evelina Stankevic[1], Jeremy Armetta[3], Franziska Zosel[7], Charlotta D. de la Cour[7], Lotte Simonsen[7], Alina Kulakova[8], Michael Wierer[9], Pernille Harris[8], Joachim Gæde[2,10], Peter Rossing[11,12], Filip K. Knop[2,10,12], Tune H. Pers[1], Tue Haldor Hansen[1,12,13], Trine Nielsen[1,12,13], Ling Li[4], Kristian Strømgaard[6], Gangyi Yang[5], Morten Otto Alexander Sommer[3] & Oluf Pedersen[1,2,10,12] ✉

The human gut microbiota has the potential to synthesize proteins that may influence host metabolism. Here we report two polypeptides, RUMTOR-derived peptide (RORDEP) 1 and RORDEP2, circulating in human blood and synthesized by specific strains of gut commensal *Ruminococcus torques* that correlate inversely with adiposity in humans. Oral gavage with RORDEP-expressing strains improved glucose tolerance, increased bone density and reduced fat mass with an enhanced expression of genes and proteins involved in thermogenesis and lipolysis in lean mice on a high-fat diet and diet-induced obese mice. Recombinant RORDEP1 given to rats intraperitoneally decreased plasma gastric inhibitory polypeptide but increased glucagon-like peptide 1, peptide YY and insulin. Intestinal delivery of recombinant RORDEP1 to rats potentiated insulin-mediated inhibition of hepatic glucose production by downregulating genes and proteins controlling liver gluconeogenesis, glycogenolysis and lipogenesis but upregulating those involved in insulin signalling, glycogenesis and glycolysis. These preclinical findings warrant the exploration of RORDEPs for the prevention and treatment of human metabolic disorders.

Human biology is contextual on trillions of various microorganisms that interact with their host[1]. Central to this interaction is the collection of microbial genes, the microbiome, which in a human individual may represent a repertoire of protein-coding genes that is more than one order of magnitude larger than the number of genes in the human nuclear genome[2,3].

Despite the daunting task of annotating this multitude of microbial genes, large-scale computational mapping of thousands of human microbiome genes and their predicted proteins has been initiated[2,4–7]. Many of the annotated proteins have functions within their microbial communities including housekeeping, microorganism–microorganism communication, adaptation and defence against other microorganisms. In addition, other specific microbial compounds have been mapped including antimicrobial peptides, antibiotics, and proteins or lipids that in preclinical and for a few cases also in clinical settings modulate host biology[8–17].

A full list of affiliations appears at the end of the paper. ✉e-mail: oluf@sund.ku.dk

Among host functions that are influenced by gut microbiota, those involved in metabolism are of particular interest for developing novel approaches to prevent or treat widespread human metabolic disorders such as obesity, diabetes and osteoporosis[18]. *Ruminococcus torques* (RT) is a prevalent and abundant member of the commensal human gut microbiota[19], yet its functional role in host metabolic regulation remains largely unexplored.

Here we tested the hypothesis that gut bacteria coexisting with humans produce and release proteins that impact host metabolism[20,21]. We identified multiple strains of RT, which are predicted to harbour a known protein, RUMTOR_00181, the structure of which includes two fibronectin type III (FN3) protein domains. The two FN3 protein domains of RUMTOR_00181 share 73% amino acid residue identity, and they have 24% and 25% amino acid residue identity with irisin, a known human polypeptide hormone[22]. We have named the two bacterial FN3 protein domains RUMTOR-derived peptide (RORDEP) 1 and RORDEP2. In human epidemiological studies, we show that the abundance of RT strains expressing RUMTOR_00181 is inversely correlated with body mass index (BMI) and body adiposity. Following interventions in mice with an RT strain expressing both RORDEPs or an *Escherichia coli* strain engineered to express RORDEP1, we find an improvement of glucose tolerance, a higher bone density and a reduction of weight gain driven by a high-fat diet. Culture experiments suggest that the two RORDEPs are released from a RUMTOR_00181-expressing RT strain into culture supernatants and are present in human blood. Intraperitoneal delivery of recombinant RORDEP1 (r-RORDEP1) in rodents improves glucose tolerance and, in response to an oral glucose load, elicits an increase of plasma glucagon-like peptide 1 (GLP1), peptide YY (PYY) and insulin but a decline in gastric inhibitory polypeptide (GIP). Following intestinal delivery to rats, r-RORDEP1 lowers blood glucose by a potentiation of insulin-mediated inhibition of liver glucose production.

Results

Some RT strains are predicted to synthesize RORDEPs

We undertook a computational search by aligning RefSeq[23] prokaryote representative genomes containing 285,952 sequences (as of 17 October 2018) stored at the National Center for Biotechnology Information (NCBI) with amino acid sequences annotated to 118 human ligands and their precursor proteins (Fig. 1a and Supplementary Table 1). Alignment criteria are shown in the illustration of the bioinformatics pipeline in Fig. 1a.

We find a significant similarity between a sequence annotated as human irisin and its precursor protein FN3-containing protein 5 (FNDC5), and a coding sequence annotated as RUMTOR_00181 (UniProt: A5KIY5) in the genome of the RT Amercian Type Culture Collection (ATCC) 27756 strain isolated from human microbiota. The bacterial genome has been deposited at NCBI as the reference genome for the RT species.

The identified RUMTOR_00181 is predicted to have a signal peptide, two FN3 sandwich structure domains and one hydrophobic domain, the latter probably needed for membrane insertion, followed by a seven-amino acid C-terminus (Fig. 1b,c and Supplementary Fig. 1). Moreover, within the 244 available metagenomic or culturomic RT strain genomes, we find 161 strains isolated from *Homo sapiens* with a high homology (>99%) to RUMTOR_00181 from RT ATCC 27756 (Supplementary Table 2).

RORDEPs are released in cultures of RT expressing the precursor protein

RUMTOR_00181 is predicted to be proteolytically cleaved by trypsin-like endopeptidases present within the genome of the RT ATCC 27756 strain (Supplementary Table 3) as well as in the intestinal lumen into two polypeptides. These we named RORDEP1 and RORDEP2, consisting of 87 and 88 amino acid residues, respectively (Fig. 1c). Phylogenetic analysis comparing RORDEPs with 1,077 sequences of known FN3-containing human proteins shows that both RORDEP1 (Supplementary Fig. 2a) and RORDEP2 (Supplementary Fig. 2b) have homology to FNDC5, with identities of 13% (28 out of 214 amino acid residues for RORDEP1 and 27 out of 214 amino acid residues for RORDEP2; Supplementary Fig. 3). The alignment of RORDEP1 and RORDEP2 shows a 73% (65 out of 89 amino acid residues) identity (Supplementary Fig. 3).

To experimentally validate the computational predictions, we performed liquid chromatography coupled with tandem mass spectrometry (LC–MS/MS). The analysis focused on identifying RORDEPs in culture supernatants of RT ATCC 27756. As shown in Extended Data Fig. 1, for the mass spectrometric analysis of each RORDEP, two unique proteotypic peptides were chosen as markers to unambiguously identify RORDEP1 and RORDEP2. Given the molecular weights of RORDEPs (approximately 10 kDa), we selected the 3–30-kDa fractions from culture supernatants of RT ATCC 27756 synthesizing RUMTOR_00181 to develop the assays (Supplementary Fig. 4). The presence of RORDEPs in culture media was confirmed by the high mass accuracy of the b- and y-ion series in the MS^2 spectra, comparing the predicted and observed data for the unique proteotypic peptides (Extended Data Fig. 1 and Supplementary Table 4). The presence of RORDEP1 and RORDEP2 in the RT ATCC 27756 culture supernatants therefore aligns with the predicted proteolytical cleavage and release of the two polypeptides from the RT ATCC 27756 strain as fragments with a molecular size below 30 kDa.

RORDEP-synthesizing RT strains associate inversely with adiposity

It has been reported that the RT species has a relatively high prevalence and abundance in human gut microbiota[19]. In analyses of 1,493 intestinal metagenomes from three public datasets[24–26], we confirm the presence of the RT species in 93% of the metagenomes and with a mean relative abundance of 1% although the latter varies from 0 to 22% at the individual level (Supplementary Fig. 5 and Table 5).

We quantitated the absolute number of specific RT strains encoding RUMTOR_00181 and thereby releasing RORDEPs in human stools by integrating qPCR readouts of primers specifically targeting the RORDEP1 sequence of RT genomes followed by flow cytometric enumeration and staining of faecal bacterial cell counts. In an analysis of 59 healthy adults (Supplementary Table 6), we found RT strains encoding RUMTOR_00181 in all examined individuals with an absolute cell count that varied 10^5-fold (ranging from 5.6×10^6 to 4.3×10^{11} bacterial cells per gram of faeces) (Fig. 2a). In addition, in gut microbiota analyses of the absolute count of RT strains carrying the gene encoding RUMTOR_00181 from vegans and omnivores[27], we find no significant difference between the dietary groups, suggesting that choice of diet may not be a major factor driving the abundance of RUMTOR_00181-synthesizing RT strains (Fig. 2b and Supplementary Table 7).

In human epidemiological studies, the absolute counts of RUMTOR_00181-synthesizing RT strains correlate inversely with BMI and body fat percentage (Fig. 2c). To further validate our initial observations, we analysed the LifeLines DEEP 2016 cohort[28] (661 females and 471 males, aged 45 ± 14 years) in which information on BMI was publicly available. Among the 1,135 individuals, we confirmed an inverse association between BMI and the relative abundance of the RUMTOR_00181 gene in the 359 metagenomes where the gene was detectable ($\beta = -0.151$, $P = 0.002$; Fig. 2d).

RORDEPs are present in human plasma

We established and applied an absolute quantification (AQUA) peptide approach combined with SureQuant targeted proteomics (Methods, Extended Data Fig. 2a and Supplementary Table 8), using isotope-labelled unique proteotypic peptides derived from each of the two RORDEPs as internal standards, achieving the lowest limit of quantification at 2.5 pM. In healthy adults (Supplementary Table 6), the plasma concentrations of RORDEP1 and RORDEP2 after an overnight

https://doi.org/10.1038/s41564-025-02064-x

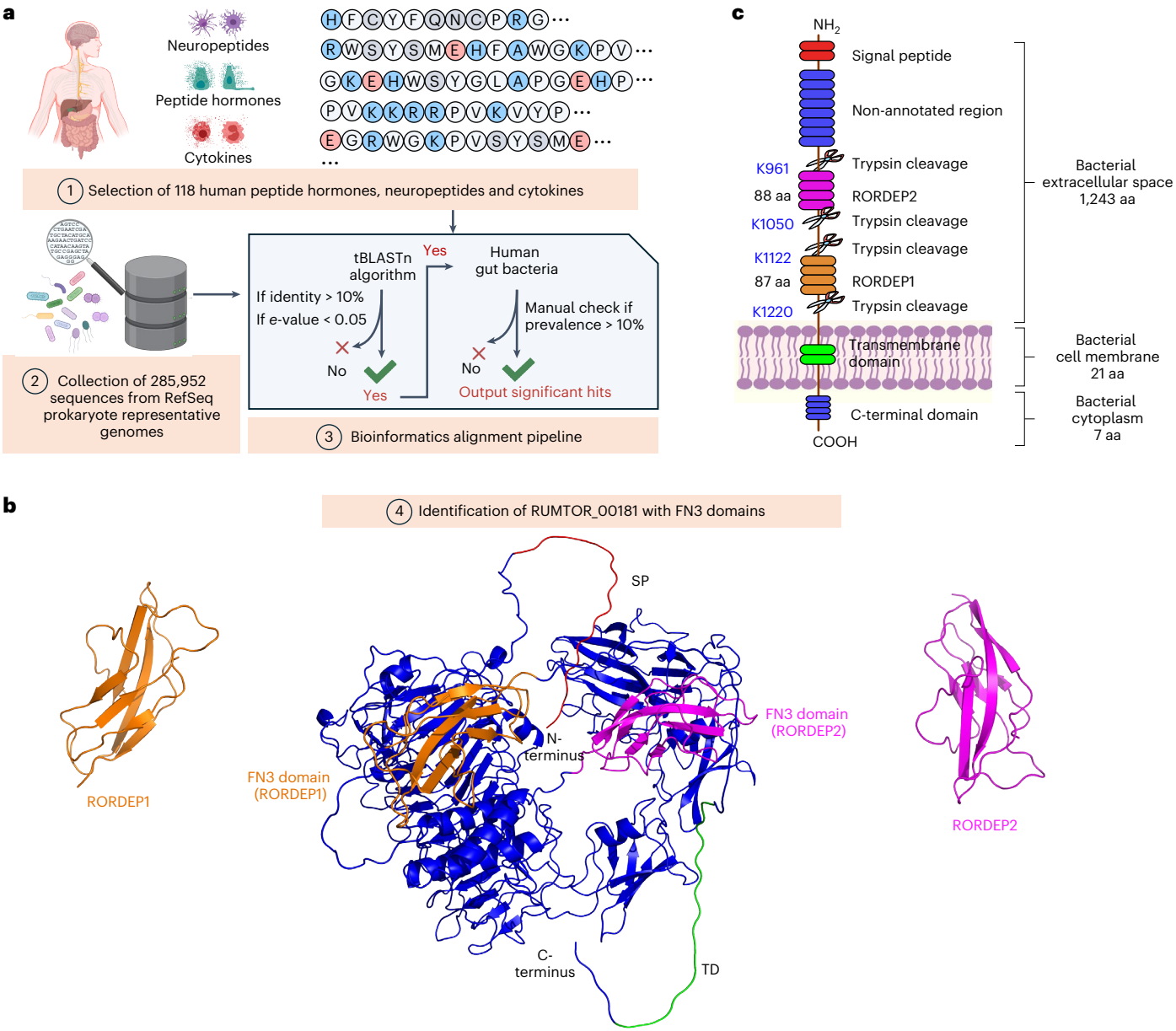

Fig. 1 | Identification of RUMTOR_00181 and RORDEPs. a, Utilization of a bioinformatics-driven genomic alignment approach revealed the presence of a RUMTOR_00181 protein in RT strains of human gut microbiota. The bacterial protein contains two FN3 protein domains with modest identity to the human FNDC5. **b**, Predictive modelling of the bacterial RUMTOR_00181 protein structure as performed in the AlphaFold Protein Structure Database (https://alphafold.ebi.ac.uk/entry/A5KIY5); this also holds for the structural prediction of RORDEPs. The AlphaFold-predicted 3D structure was visualized using Pymol (https://pymol.org/2/). SP, signal peptide; TD, transmembrane domain. **c**, A schematic representation of the topology of RUMTOR_00181 protein. aa, amino acids. The putative trypsin cleavage sites were predicted using PeptideCutter (https://web.expasy.org/peptide_cutter/). Panel **a** created with BioRender.com.

fast show means of 176 pM and 210 pM, respectively, exhibiting a three- to fourfold interindividual variation (Fig. 2e). Quantification of the two peptides shows acceptable intra-individual coefficients of variation (Extended Data Fig. 2b), and they show a tight positive correlation (Fig. 2f). Circulating levels of RORDEPs and host BMI or body fat percentage show no relationship (Supplementary Fig. 6).

An RT strain expressing both RORDEPs improves host metabolism

Following a feasibility study (Supplementary Fig. 7), we conducted interventions in high-fat-fed mice given oral gavage twice weekly with the RT ATCC 27756 strain expressing both RORDEPs, here named RT2 in a dose of 5×10^9 colony-forming units (CFU) or heat-killed RT2 in an equivalent amount or phosphate-buffered saline (PBS) containing 10% glycerol (Fig. 3a). At the end of the 8-week intervention, the engraftment was quantified by qPCR. Compared with the PBS group, the live-RT2-treated group showed a fivefold increase in faecal RT2 abundance (Extended Data Fig. 3a), while having a minimal impact on the overall gut microbiota composition (Extended Data Fig. 4).

The RT2 treatment results in an improved glucose tolerance and a lowering of body weight gain, fat tissue mass and fat cell size, but an increase in lean body mass (Fig. 3b–g and Extended Data Fig. 3b–d). In parallel, we find an upregulation of uncoupling protein 1 (UCP1) expression in the butterfly-shaped interscapular brown adipose tissue in the live-RT2-treated group (Extended Data Fig. 3e,f). Thermogenic gene markers, including *Ucp1*, *Cidea* and *Dio2*, show an enhanced expression

https://doi.org/10.1038/s41564-025-02064-x

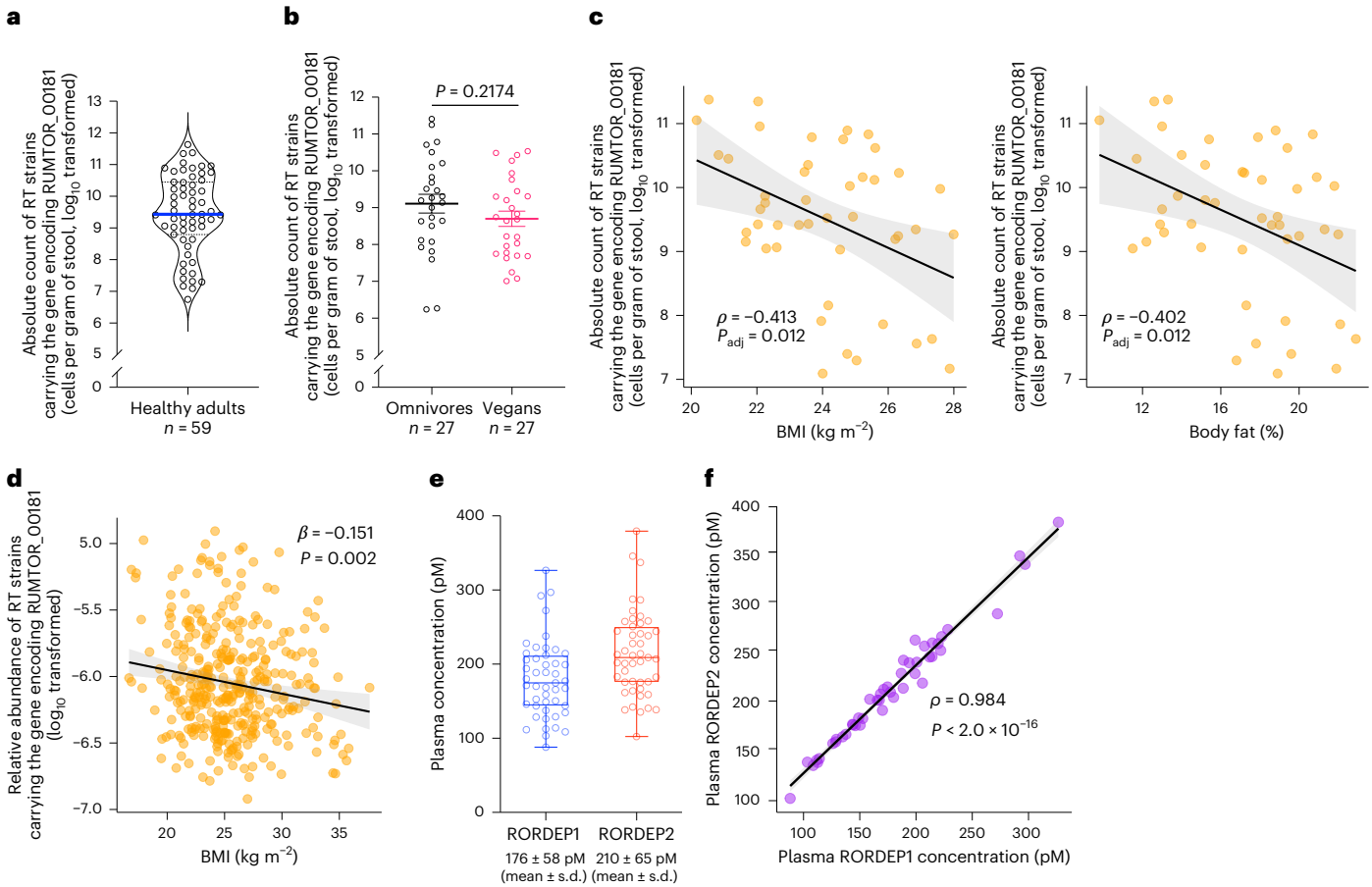

Fig. 2 | RT strain abundance and plasma RORDEPs and their host correlatives. a, Abundance of RT strains harbouring the RUMTOR_00181 gene in stools from healthy adults. The RORDEP1 nucleotide sequence was used as a marker of the RUMTOR_00181 gene. The data are normalized against the total bacterial cell count. The blue line indicates the median value. **b**, Abundance of RT strains carrying the RUMTOR_00181 gene in stools from omnivores (black) and vegans (pink), shown as jittered strip plots. The mean value and the standard error of the mean are overlaid on the individual dots. The *P* value was computed by Wilcoxon rank-sum test (unpaired, two sided). **c**, Inverse relationships between the abundance of RUMTOR_00181-positive strains of the RT species and BMI (left) and fat percentage (right), analysed after excluding 13 individuals with undetectable plasma RORDEP levels. **d**, Association between BMI and the abundance of the RUMTOR_00181 gene-carrying RT strains in the LifeLines DEEP 2016 cohort ($n = 1{,}135$)[28]. The relationship was assessed using a linear regression model, with BMI as the dependent variable and the relative abundance of the RUMTOR_00181 gene as the independent variable. β (beta) represents the regression coefficient from a linear regression model. Covariates include age, sex and sequencing read count. Only individuals with non-zero RUMTOR_00181 abundance (orange dots) are visualized. **e**, Plasma RORDEP1 and RORDEP2 peptides in 46 healthy Danish adults. Each data point represents an individual measurement. In the box-and-whisker plot, the box boundaries represent the 25th and 75th percentiles. The line in the middle denotes the median (50th) percentile. The whiskers span between the minimum and maximum values. **f**, Correlation between plasma concentrations of RORDEP1 and RORDEP2. For **c** and **f**, Pearson's two-sided correlation (ρ) tests were performed, and *P* values were adjusted for multiple comparisons using the Benjamini–Hochberg method in **c**. For **c**, **d** and **f**, error bands represent the linear regression line (black solid line) and the 95% confidence interval (grey shaded region).

in the live-RT2-treated mice, whereas expression of genes involved in lipogenesis, including *Fasn*, *Scd1* and *Acaca*, is reduced in inguinal white adipose tissue. Genes involved in lipolysis are upregulated while the expression of a key adipose inflammation marker, *Tnf*, is diminished (Fig. 3h). Finally, the cortical thickness of femoral bone is increased in the RT2-treated mice (Fig. 3i,j and Extended Data Fig. 3g). By contrast, mice treated with an RT ATCC 35915 strain (here called the RT3 strain) lacking RUMTOR_00181 show no change in glucose tolerance or weight development but exhibit increased expression of markers of lipogenesis and inflammation in adipose tissue (Supplementary Fig. 8), probably attributable to the presence of virulence factors[29].

An engineered *E. coli* strain expressing RORDEP1 improves host metabolism

To examine whether the metabolic benefits elicited by intervention with the RT2 strain are specifically attributable to RUMTOR_00181 and thereby expression of RORDEPs independent of the *R. torques* genomic background, we engineered *E. coli* Nissle 1917 (EcN) to express RORDEP1 (EcN-RORDEP1; Extended Data Fig. 5a–c). Diet-induced obese (DIO) mice on a high-fat diet received a daily oral gavage of 5×10^{10} CFU of either EcN-RORDEP1 or control EcN for 4 days, with streptomycin added to the drinking water to promote engraftment. Consistently across two sets of independent interventions with monitoring periods of 18–21 days, mice treated with EcN-RORDEP1 showed improved glucose tolerance and a more pronounced reduction in body weight compared with controls, with the weight difference persisting throughout the study periods (Extended Data Fig. 5d–m). In one of the experiments, engraftment levels were assessed and found to remain high, and the *E. coli* abundance in the ileum, caecum and colon was similar between groups (Extended Data Fig. 5h,i).

Differences in animal models (lean versus DIO mice), dosage regimens and administration routes used across the RT and *E. coli* experiments may potentially explain the observed differences in the onset and magnitude of the RORDEP-induced metabolic responses.

https://doi.org/10.1038/s41564-025-02064-x

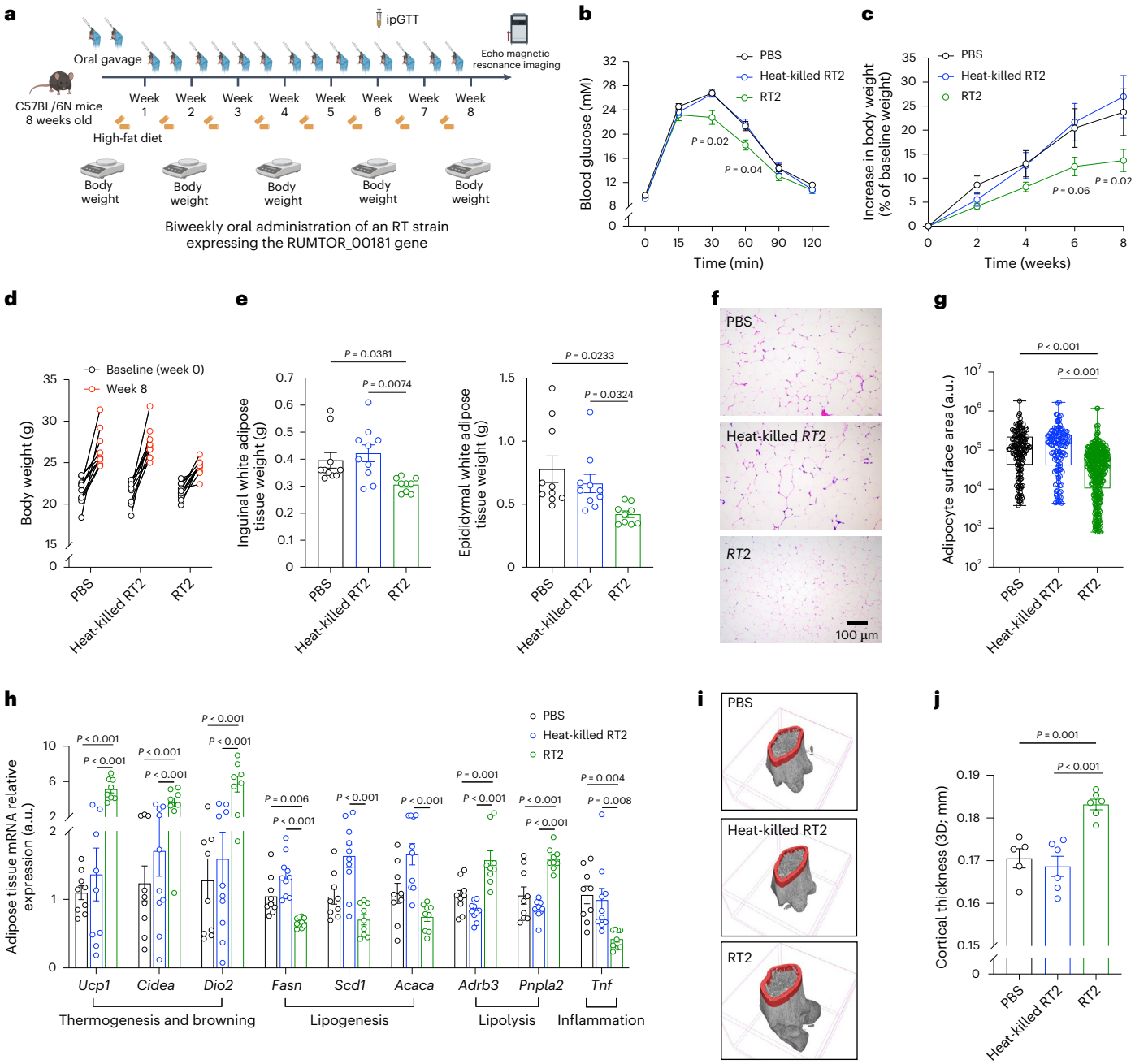

Fig. 3 | The RT2 strain expressing both RORDEPs improves mouse metabolism. **a**, Lean male C57BL/6N mice were given a high-fat diet for 8 weeks along with twice-weekly oral gavage of live RT2 at a dose of 5×10^9 CFU per 100 µl of sterile PBS containing 10% glycerol. Control groups received sterile PBS containing 10% glycerol or an equivalent dose of heat-killed RT2. **b**, An ipGTT was done at week 6. **c**, Relative body weight changes in mice following the intervention. Weight increase was normalized to baseline at week 0. **d**, Body weight changes between week 0 and 8 across the three groups of mice. **e**, Weights of inguinal and epididymal white adipose tissue (measured at termination). **f**, Representative H&E-stained sections of inguinal white adipose tissue from each group ($n = 9$ images per group). The scale bar in the bottom of **f** applies to all images in each panel. **g**, Surface areas of segmented adipocytes from representative H&E-stained sections of inguinal white adipose tissue in **f**. Box plot elements: the centre line represents the median; the box limits indicate the 25th and 75th percentiles; the whiskers extend from the minimum to the maximum values. **h**, mRNA expression levels of genes related to thermogenesis and browning, lipogenesis, lipolysis and inflammation in inguinal white adipose tissue. **i**, 3D cross-sectional micro-CT images of femoral bone, with red sections indicating regions selected for cortical thickness analysis. **j**, Cortical thickness measurements derived from 3D images ($n = 5$ or 6 mice per group). Data are presented as mean ± s.e.m. Unless otherwise stated, $n = 8$ or 9 mice per group. Statistical analysis used two-way ANOVA with Bonferroni post hoc correction for **b** and **c**, and one-way ANOVA with Dunnett's post hoc correction for **e**, **g**, **h** and **j**. Panel **a** created with BioRender.com.

RORDEP1 induces a rise of plasma GLP1, PYY and insulin but a decline of GIP

To further explore the metabolic roles of RORDEPs, both were recombinantly produced in an *E. coli* culture using standard protein expression protocols (Methods and Supplementary Fig. 9a,b). Small-angle X-ray scattering experiments show that RORDEP1 is a monomer (Methods and Supplementary Fig. 9c). However, thermal stability tests indicate that heat exposure induces dimerization of r-RORDEP1 aligning with some degree of thermal instability (Supplementary Fig. 9d).

As irisin was the lead protein in the discovery of RORDEPs, and as irisin is reported to bind to integrin receptors in adipocytes and osteocytes[30], we investigated the potential interaction of r-RORDEP1 with various integrin receptors. However, we observed no binding between r-RORDEP1 and any of the tested integrins (Supplementary Figs. 10–13).

Next we assessed the potential bioactivity of r-RORDEP1 in various human cell cultures, including white adipocytes, osteoblasts, skeletal muscle cells, the enteroendocrine NCI-H716 cell line and rat INS-1 cells. However, r-RORDEP1 in various supraphysiological concentrations does not per se elicit consistent effects in any of the cellular experiments (Extended Data Fig. 6).

Similarly, intravenous infusion of r-RORDEP1 in rats does not result in any alterations of blood glucose levels over a 3-h monitoring period (Supplementary Fig. 14). The latter finding together with the lack of direct cellular effects made us hypothesize that RORDEPs exert their metabolic effects through indirect mechanisms and primarily when administered via the intestinal or peritoneal route. Therefore, we explored the potential effects of r-RORDEP1 on the release of intestinal and pancreatic hormones following an oral glucose load in lean rats (Fig. 4a). We find that a single intraperitoneal dose of r-RORDEP1 induces a decline of blood glucose compared with a placebo (Fig. 4b). Notably, r-RORDEP1 causes a 50% decline in the plasma GIP concentration while the plasma concentration of GLP1, PYY and insulin is increased (Fig. 4c–f). Plasma glucagon remains unaltered (Fig. 4g).

To extend studies of the biological in vivo effects of r-RORDEP1 on a pathological condition, an intraperitoneal injection of r-RORDEP1 was given once daily for 10 days to high-fat-fed db/db mice. The r-RORDEP1 intervention resulted in an improved glucose tolerance compared with a placebo (Fig. 4h,i). To confirm that these metabolic effects were specifically attributable to r-RORDEP1 and not due to non-specific effects of peptide administration, additional experiments were performed in lean mice comparing bioactivities of r-RORDEP1 and a scrambled sequence of RORDEP1 (Extended Data Fig. 7a–d). Following an oral glucose load combined with a single intraperitoneal injection of peptide, mice treated with r-RORDEP1 show improved glucose tolerance, whereas mice treated with the scrambled peptide have unchanged glucose tolerance compared with a placebo (Extended Data Fig. 7e,f).

To further compare the in vivo potency of r-RORDEP1 and r-RORDEP2, we administered each peptide in a similar dose via intraperitoneal injection to lean normal chow-fed mice once daily for 7 days (Fig. 4j). Compared with the PBS injection, r-RORDEP1 and RORDEP2 show equal potency in enhancing the expression of thermogenesis- and browning-related genes (*Ucp1*, *Prdm16* and *Dio2)* in inguinal white adipose tissue (Fig. 4k).

RORDEP1 enhances insulin sensitivity of hepatic glucose production

To mimic the natural intestinal release of RORDEPs in humans and to further investigate the role of gut luminal r-RORDEP1 in glucose homeostasis, we infused r-RORDEP1 into the rat duodenum under a euglycaemic pancreatic clamp (Fig. 5a). Before these experiments, the stability of r-RORDEP1 was assessed in in vitro experiments with simulated intestinal fluid (SIF) showing a calculated half-life of approximately 3 h (Extended Data Fig. 8a). Further experiments using a gut-on-chip model, complemented by ultra-performance liquid chromatography (UPLC) that was validated for r-RORDEP1 specificity, showed that r-RORDEP1 traverses an intestinal epithelial monolayer without impairing cell viability or tight junction integrity (Extended Data Fig. 8b–g). Moreover, following intraperitoneal injection of r-RORDEP1 in lean mice, the relative abundance of r-RORDEP1 in peripheral blood circulation declines to 50% within 45 min (Extended Data Fig. 8h,i).

Intestinal administration of r-RORDEP1 in rats under a euglycaemic pancreatic clamp leads to a dose-dependent increase in glucose infusion rate. The infusion of r-RORDEP1 at the highest infusion rate of 200 pmol kg^{-1} min^{-1} increases the glucose infusion rate about fourfold (8.1 ± 0.7 mg kg^{-1} min^{-1} for r-RORDEP1 compared with 2.0 ± 0.1 mg kg^{-1} min^{-1} for PBS; $P < 0.0001$ (Fig. 5b,c). On the basis of these findings, an infusion rate of 200 pmol kg^{-1} min^{-1} of r-RORDEP1 was chosen for subsequent experiments.

Next we administered isotopically labelled glucose intravenously to rats under pancreatic clamp conditions, allowing us to concurrently monitor changes in both hepatic glucose production and peripheral glucose uptake (Fig. 5d). Following intestinal infusion of r-RORDEP1, we find that the hepatic glucose production (HGP) rate declines by about 40%, whereas glucose uptake into peripheral tissues remains unaltered (Fig. 5e–g).

To understand the underlying molecular mechanisms of the RORDEP-reduced HGP, another cohort of lean rats received intestinal infusion of r-RORDEP1 at 200 pmol kg^{-1} min^{-1} (Fig. 6a) for 3 h. Blood glucose levels decrease significantly (Fig. 6b) and liver transcriptome and proteome profiling show clear separation between r-RORDEP1- and control-treated rats (Fig. 6c and Extended Data Fig. 9a,b). Univariate statistical analysis returns 2,145 significantly differentially expressed genes between r-RORDEP1- and control-treated groups, of which 966 genes are upregulated and 1,179 are downregulated (Fig. 6d) that further annotate to 85 Kyoto Encyclopedia of Genes and Genomes (KEGG) pathways (Supplementary Fig. 15). Proteome analyses show that 379 liver proteins are differentially expressed between r-RORDEP1-treated and control groups (Extended Data Fig. 9c). Collectively, these transcriptome and proteome data, combined with phosphoproteomic and pathway analyses, show a downregulation of genes and proteins controlling liver gluconeogenesis, glycogenolysis and lipogenesis but an upregulation of key genes and proteins involved in insulin signalling, glycogenesis and glycolysis (Fig. 6e, Extended Data Fig. 10, Supplementary Table 9 and Supplementary Fig. 16).

Discussion

The human microbiome is hypothesized to be a potentially rich but untapped resource for the discovery of novel compounds that may have a regulatory impact on human biology[10,12–14,17]. Investigating this concept, we applied a genomic alignment approach to mine a public database for similarities between coding nucleotide sequences of 118 human ligands and their precursor proteins involved in metabolism and 285,952 representative reference genomes of prokaryotes. In some RT strains, we identified a gene that encodes the RUMTOR_00181 protein consisting of 1,271 amino acid residues including two FN3 domains and a signal peptide, the latter suggesting a secreted protein. The two FN3-domain-containing bacterial peptides, RORDEP1 and RORDEP2, with 24% and 25% amino acid identity, respectively, to the human hormone irisin, are predicted to be proteolytically cleaved and continuously released to the gut lumen.

The RORDEP-synthesizing bacteria are prevalent and abundant in the human intestinal microbiota, and the presented human epidemiological studies, as well as our preclinical studies, suggest that these bacterial strains may impact host metabolism. We find that the abundance of RORDEP-synthesizing RT strains correlates inversely with BMI and body fat. In addition, interventions in high-fat-fed mice with an RT strain synthesizing both RORDEPs or in DIO mice with an *E. coli* strain, engineered to express RORDEP1, elicit an improved glucose tolerance, a higher bone density and a less high-fat-diet-driven weight gain. The impact on weight reduction is related to an enhanced adipose tissue expression of genes involved in thermogenesis, browning and lipolysis, and a diminished expression of lipogenic and inflammatory genes.

Next, we focused on RORDEPs. Peritoneal administration of r-RORDEP1 in mice induces an improved glucose tolerance and an increase of thermogenesis markers while peritoneal injection in rats after an oral glucose load induces an increase in plasma GLP1, PYY and insulin but a decline in plasma GIP. On the basis of previous knowledge[31–35], the effects of r-RORDEP on the release of the mentioned

https://doi.org/10.1038/s41564-025-02064-x

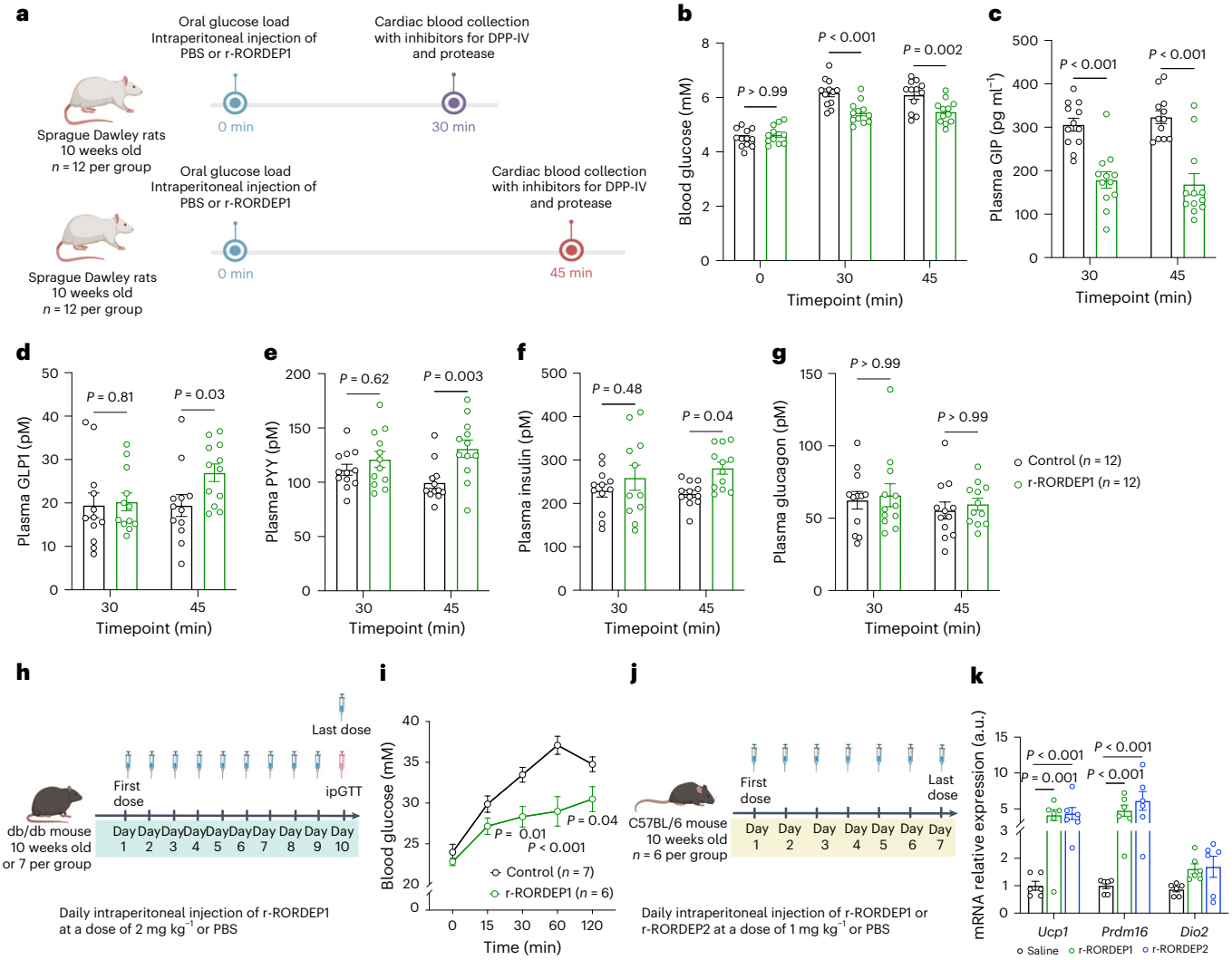

Fig. 4 | Peritoneal delivery of r-RORDEP1 improves the metabolism of rats and mice. a, Schematic representation of the experimental design evaluating the effects of an oral glucose load and intraperitoneal injection of r-RORDEP1 on plasma concentrations of glucose, GIP, GLP1, PYY, insulin and glucagon in rats. Lean Sprague Dawley male rats 10 weeks of age were administered an oral glucose load (1 g kg^{-1}) over 0–2 min, followed by an intraperitoneal injection of r-RORDEP1 (0.8 mg kg^{-1}) or PBS as control ($n = 12$ per group). **b**–**g**, Levels of blood glucose (**b**), plasma GIP (**c**), plasma GLP1 (**d**), plasma PYY (**e**), plasma insulin (**f**) and plasma glucagon (**g**) measured at designated timepoints after glucose load and r-RORDEP1 injection. **h**, Experimental workflow for testing the effect of r-RORDEP1 on glucose tolerance in db/db mice. High-fat-fed db/db mice were administered daily intraperitoneal injections of r-RORDEP1 (2 mg kg^{-1}) or PBS (control) for 10 days ($n = 6$ or 7 per group). **i**, Results of the ipGTT. Blood glucose levels were measured at baseline and at designated timepoints following glucose administration. **j**, Experimental design evaluating the effect of intraperitoneal injections of r-RORDEP1 in mice. Lean C57BL/6 male mice 10 weeks of age were daily administered with an intraperitoneal injection of r-RORDEP1 (1.0 mg kg^{-1}) or saline as control ($n = 6$ per group) for 7 days. **k**, Daily intraperitoneal injection of r-RORDEP1 or r-RORDEP2 in mice ($n = 6$ per group) for 7 days induces increased expression of genes involved in thermogenesis and browning of inguinal white adipose tissue. The mRNA levels of indicated genes were analysed by qRT-PCR. Data were analysed using Student's *t*-test. For **b**–**g**, **i** and **k**, data are expressed as mean ± s.e.m. Statistical significance was determined using two-way ANOVA with Bonferroni's post hoc test for **b**–**g** and **i** and one-way ANOVA with Dunnett's post hoc test for **k**. Panels **a**, **h** and **j** created with BioRender.com.

hormones are expected to result in a diminished food intake and a relative protection against obesity driven by a high-fat diet. Furthermore, intestinal infusion of r-RORDEP1 improves hepatic insulin sensitivity by a marked reduction in insulin-mediated inhibition of liver glucose production coupled with downregulation of genes and proteins controlling gluconeogenesis, glycogenolysis and lipogenesis, but an upregulation of key genes and proteins involved in glycogenesis, glycolysis and hepatic insulin signalling.

Irisin, the lead human peptide hormone in our discovery of RORDEPs, shares only modest amino acid residues with the two FN3-domain-containing bacterial polypeptides. Still, irisin and RORDEPs have in preclinical studies similar in vivo effects on adipose and bone tissues[22,30]. However, unlike irisin, RORDEPs do not interact with integrin receptors.

Our report comes with limitations. Effects of intestinal or intravenous delivery of r-RORDEP1 were tested only for a few hours and targeting rat liver and blood glucose homeostasis. Experiments with intestinal or parenteral infusion of r-RORDEPs for weeks are needed to explore the long-term effects of these peptides on multiple targets of rodents and non-human primates including adipose tissue, skeletal muscle, bone and brain. In addition, we have not explored whether RORDEPs being continuously secreted and released into both the intestines and the bloodstream primarily have their effects mediated via the enteric nervous system, via blood circulation or both.

https://doi.org/10.1038/s41564-025-02064-x

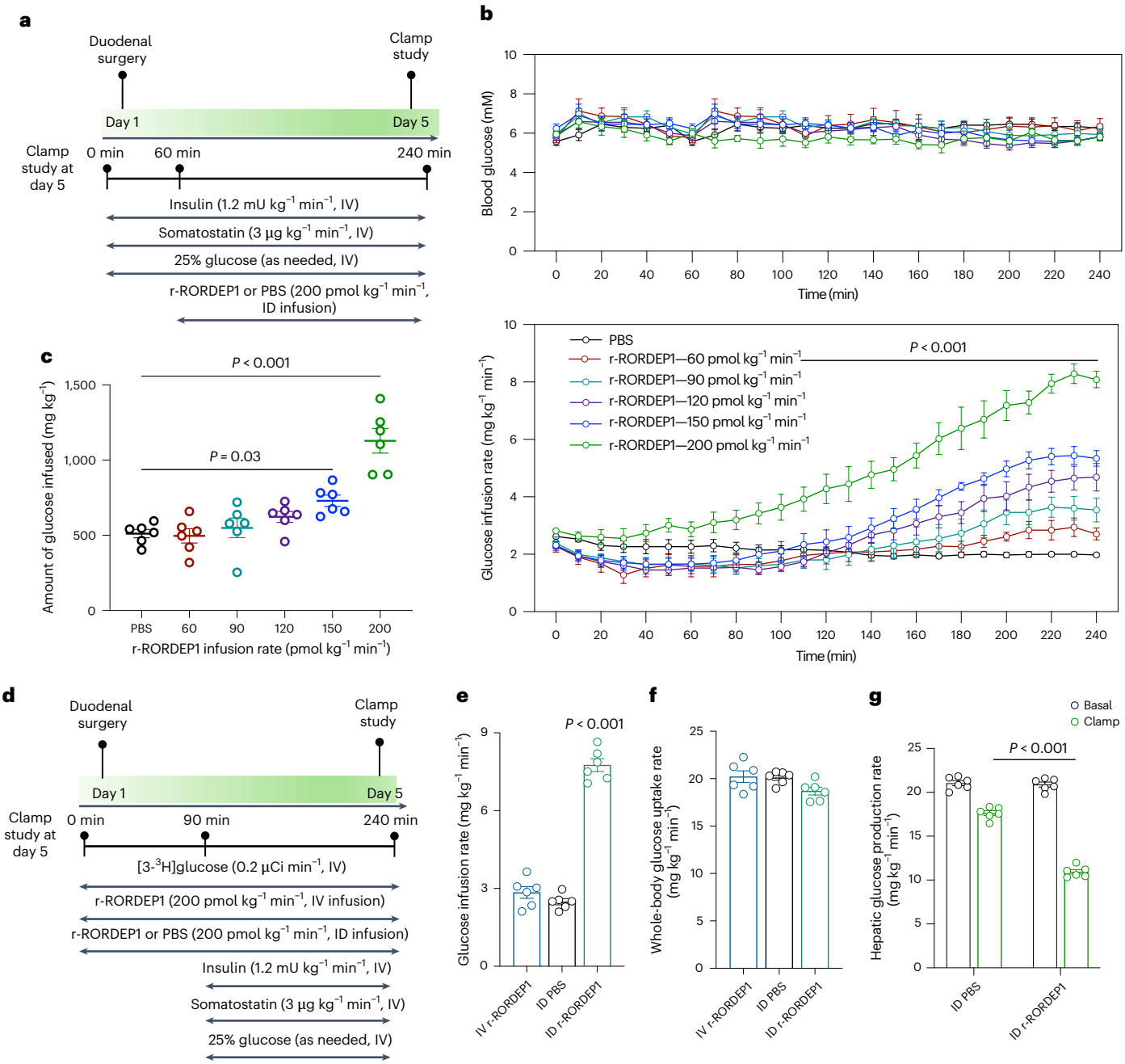

Fig. 5 | Intestinal delivery of r-RORDEP1 enhances the insulin sensitivity of hepatic glucose output in rats. a, Experimental schematic showing that lean male Sprague Dawley rats (8 weeks old) were cannulated on day 1 and subjected to a 4-h euglycaemic pancreatic clamp on day 5. From 60 min to 240 min, the rats received intraduodenal infusions of either PBS or r-RORDEP1 (60–200 pmol kg^{-1} min^{-1}), alongside constant duodenal infusion of insulin and somatostatin. Glucose was infused intravenously as needed to maintain euglycaemia. ID, intraduodenal. IV, intravenous. **b**, Blood glucose levels (top) and cumulative glucose infusion rates (bottom) over time during the clamp procedure; $P < 0.001$ indicates significant differences in at least one RORDEP1-treated group compared with PBS. **c**, A scatter plot depicting the AUC for the glucose infusion rates needed to sustain euglycaemia in rats ($n = 6$ per group) receiving varying concentrations of r-RORDEP1 during a euglycaemic pancreatic clamp. **d**, Experimental schematic of additional intervention arms comparing ID PBS, IV r-RORDEP1 and ID r-RORDEP1 delivery. [3-^{3}H]glucose was infused to monitor hepatic glucose production throughout the clamp procedure. **e**, Glucose infusion rates required to maintain euglycaemia during the clamp for the conditions shown in **d**. **f**, Bar graph showing glucose clearance rates across the study conditions described in **d**. **g**, Bar graph illustrating glucose production rates under the conditions outlined in **d**. Data are presented as mean ± s.e.m. Statistical significance was assessed using two-way ANOVA with Dunnett's post hoc test (**b**), one-way ANOVA with Dunnett's post hoc test (**c** and **f**) and two-sided unpaired Student's *t*-test (**g**). For **b**, **c** and **e**–**g**, $n = 6$ rats per group.

Furthermore, experiments are warranted to explore the mode of action of RORDEPs including the discovery of their receptor. Hypothetically, RORDEPs may exert permissive synergistic effects together with a variety of hormones and metabolites targeting organs such as enteroendocrine cells, liver, fat tissue, skeletal muscle, bones and brain, as well as enteric neuronal signalling directed at target tissues. Finally, randomized clinical trials are now awaited exploring the physiological role of RORDEPs in healthy individuals and the potential of RORDEPs in native or engineered forms for the prevention and treatment of common human metabolic disorders.

https://doi.org/10.1038/s41564-025-02064-x

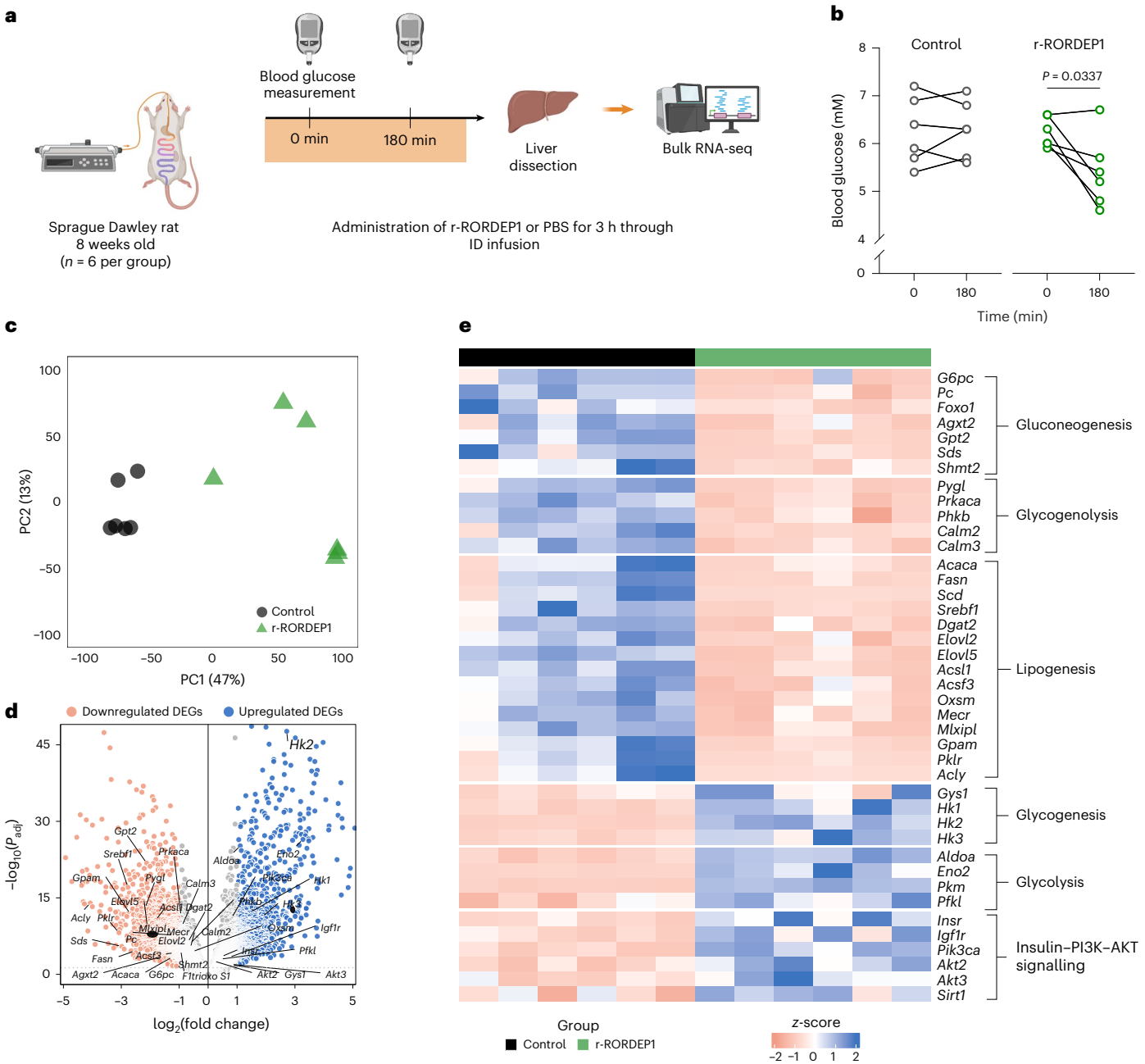

Fig. 6 | Intestinal delivery of r-RORDEP1 to rats changes the expression of key liver genes involved in metabolism and insulin signalling. a, A total of 12 8-week-old lean male Sprague Dawley rats fed standard chow were randomized to receive either intraduodenal infusion of r-RORDEP1 (200 pmol kg^{-1} min^{-1}) ($n = 6$ in the RORDEP1 group) or sterile PBS for 3 h ($n = 6$ in the control group). **b**, r-RORDEP1 administration resulted in a 13% reduction in blood glucose levels at 180 min relative to the baseline at timepoint 0 min. Significance was determined using paired Student's *t*-test. **c**, PCA score plot showing 12 rat liver RNA samples from r-RORDEP1 or control infusion groups, based on 13,453 normalized gene expressions after variance stabilizing transformation. The plot illustrates all genes projected onto the first and second principal components. **d**, Volcano plot illustrating the results of univariate analysis of differentially expressed genes (DEGs) in the liver. Each point represents one gene, plotted with its $\log_2$(fold change) on the *x*-axis and $-\log_{10}$-adjusted *P* value on the *y*-axis. Genes significantly upregulated ($P_{adj} < 0.05$ and $\log_2$(fold change) > 1) are shown in blue, significantly downregulated genes ($P_{adj} < 0.05$ and $\log_2$(fold change) < −1) are in orange, and non-significant genes or those not meeting the fold change criteria are in grey. **e**, Heatmap showing gene expression profiles (*z*-score of normalized expression levels) associated with gluconeogenesis, glycogenolysis, lipogenesis, glycogenesis, glycolysis and the insulin–PI3K–AKT signalling pathway. All genes shown are significantly differentially expressed between the two experimental groups. For **d** and **e**, the *P* values were adjusted using the Benjamini–Hochberg method for multiple corrections. Panel **a** created with BioRender.com.

Methods

Bioinformatics analyses

A database encompassing 118 human proteins and their precursors (Supplementary Table 1) related to human metabolism was curated through a manual search in the UniProt database (https://www.uniprot.org/) using the keywords 'human peptide hormones', 'human neuropeptides' and 'human cytokines'. The prokaryotic genome sequences downloaded from the NCBI database (ftp://ftp.ncbi.nlm.nih.gov/blast/db) were searched for the protein and peptide sequences reported in Supplementary Table 1 with a threshold *e*-value ≤ 0.05 and identity > 10% using tBLASTn (2.2.27+). Mapping results are provided in https://github.com/fjw536/RORDEP. An additional follow-up

bioinformatics alignment (Supplementary Table 2) was performed by tBLASTn to query the protein sequence of RUMTOR_00181 against 244 available metagenomic or culturomic *[Ruminococcus] torques* strain genomes (as of 4 June 2025; https://www.ncbi.nlm.nih.gov/datasets/genome/?taxon=33039).

Alignment between the amino acid sequences of RORDEP1 and RORDEP2 and 1,077 sequences of available human FN3-domain-containing proteins (https://github.com/fjw536/RORDEP) were performed using NCBI BLASTp (2.2.27+), and phylogenetic trees were built by BLAST pairwise alignments (Supplementary Fig. 2; tree method, neighbourhood joining; maximal sequence difference, 0.8; and distance, Grishin (amino acid)). The high-quality protein structures of RUMTOR_00181 were modelled using the artificial intelligence algorithm AlphaFold2 (ref. 36). Following AlphaFold modelling, the predicted structures were visualized using Pymol2.5 software (https://pymol.org/2/). Multiple sequence alignment was performed with Clustal Omega (available at https://www.ebi.ac.uk/Tools/msa/clustalo/) to identify the positions of cysteine residues and to count both identical and conserved residues. Protein sequence identity is calculated by dividing the number of identical positions within the alignment by the total length of the alignment region. Potential virulence-associated factors in the genomes of RT strains ATCC 27756 and ATCC 35915 were identified through homology mapping against the core dataset of the Virulence Factors of Pathogenic Bacteria (VFDB)[37], using NCBI BLASTn (version 2.12.0).

The search for potential proteases and peptidases in the genome of RT ATCC 27756 was carried out using the MEROPS database[38]. This database serves as a comprehensive resource for information on peptidases (also known as proteases, proteinases and proteolytic enzymes) and their inhibitors. The classification of peptidases in the MEROPS database is hierarchical and based on structural characteristics.

Bacterial strains and culture conditions

For use in mouse intervention studies, a RUMTOR_00181 gene-carrying RT strain (Holdeman and Moore 27756 with strain designation VPI B2-51 (ATCC) and in our study protocol named RT2) was purchased from ATCC Bacteriology Collection (https://www.atcc.org/). The bacterial strains were cultured under anaerobic conditions (95% N_2, 5% H_2) following handling instructions from ATCC. When the optical density at 600 nm (OD_{600}) of the bacterial culture reached 0.8, an aliquot of the culture was serially diluted and then plated onto brain heart infusion agar (BHI agar, Millipore, 70138) to determine the bacterial load. For oral gavage in mice, cultures of both strains were centrifuged at 6,000 *g* for 10 min, washed twice with PBS and concentrated with 20% (vol/vol) sterile glycerol anaerobically to 5×10^{10} CFU per 100 µl. Optionally, concentrated RT2 strains at 5×10^{10} CFU per 100 µl were diluted to 5×10^{9} CFU per 100 µl, autoclaved at 121 °C for 15 min and aliquoted to have 'heat-killed RT2'. Before oral administration to mice, live bacterial solution stocks were thawed and diluted to 5×10^{9} CFU per 100 µl.

In the genetically modified organism (GMO) study, we used engineered *E. coli* Nissle 1917 called the EcN (Mutaflor) strain, previously established as a chassis strain for advanced microbiome therapeutics[39]. This strain was modified to include a green fluorescent protein (GFP) gene at the transposon Tn7 attachment site and the *aadK* gene for streptomycin resistance, enhancing cultivation and engraftment in mouse models. The strain's native pMUT1 plasmid was removed and replaced with a re-engineered version of pMUT1, including the *kanR* gene for strain selection and expression of RORDEP1. For the expression and release of RORDEP1 by the Gram-negative chassis, the sequence of the OmpA secretion signal was fused downstream to the start codon in the open reading frame of RORDEP1 (ref. 40). For detection and semi-quantification of the secreted RORDEP1, a bioluminescence signal was introduced downstream of the secretion-tag OmpA (ref. 41). To clone the fragments on pMUT1, the gBlocks containing the secretion and bioluminescence signal upstream of the coding sequence of RORDEP1 were flanked with a 25–30-nucleotide sequence (Integrated DNA Technologies) complementary to the primer's tails designed to amplify the vector. For recombinant expression in the *E. coli* Nissle 1917 strain, the codon optimized gene fragments were cloned into the native cryptic plasmid pMUT1 under the control of previously characterized constitutive promoter MS8 (P_{MS8})[42]. A ribosomal binding site (RBS) library was generated in silico to tune the expression levels of the peptides using the EMOPEC software[43] (Empirical Model and Oligos for Protein Expression Changes; http://emopec.biosustain.dtu.dk). Four Shine–Dalgarno sequence variants (RBS1 to 4) were generated with different predicted expression levels. Thus, four different reverse primers were designed to amplify the backbone plasmid, each one flanked with a different RBS variant. PCRs for cloning were performed using the Phusion High-Fidelity PCR Master Mix with HF Buffer (Thermo Fisher Scientific, F531L). All PCR products were treated with DpnI (New England Biolabs, R0176S) and purified (GeneJET Gel Extraction Kit, Thermo Fisher Scientific, K0691) according to instructions from the vendors. Fragments were assembled using Gibson Assembly Master Mix (New England BioLabs, E2611L) as recommended by the vendor. A volume of 2 µl of the cloning mixture was transformed into 50 µl of NEB 10-beta competent *E. coli* cells (New England BioLabs, C3019H), by gentle mixing, followed by incubation for 30 min on ice and heat-shock for 30 s at 42 °C and subsequently on ice for 5 min. A total of 950 µl of super optimal broth with catabolite repression medium (NEB 10-beta/Stable Outgrowth Medium, B9035S) was added and incubated at 37 °C for 1 h at 250 rpm. A 100-µl aliquot was spread on pre-warmed LB agar plates supplemented with 50 µg ml^{-1} kanamycin, which were incubated at 37 °C overnight. Colony PCR to confirm positive clones was performed using OneTaq 2× Master Mix with Standard Buffer (New England BioLabs, M0482S). The cloning was verified by Sanger sequencing (Eurofins Genomics Europe Shared Services). Four different plasmid vectors were generated for recombinant expression of RORDEP1.

Plasmids were purified (NucleoSpin Plasmid EasyPure, MACHEREY-NAGEL, 740727.250) and transformed into electrocompetent cells of the EcN strain. Briefly, an overnight culture of wild-type EcN was 100-fold diluted in LB broth media and incubated at 37 °C, shaking until cells reached an OD_{600} of 0.4–0.6. Cells were washed (5 min, 4,000 *g*, 4 °C) with an equal volume of ice-cold 10% glycerol (Honeywell, 15523), three times in total, and concentrated 250× in ice-cold 10% glycerol. A 50-µl aliquot of EcN competent cells was mixed with 1 µl (50 ng $µl^{-1}$) of appropriate engineered plasmid, electroporated (MicroPulser Electroporator, Bio-Rad Laboratories) and recovered in 950 µl of super optimal broth with catabolite repression medium for at least 1 h. A 100-µl aliquot was spread on pre-warmed LB agar plates supplemented with 50 µg ml^{-1} kanamycin and 50 µg ml^{-1} streptomycin, which were incubated at 37 °C overnight. Engineered strains were saved in 25% glycerol at −80 °C until further analysis. Whole-plasmid nanopore sequencing (Unveil Bio ApS) was performed for all plasmids purified by the engineered EcN strains.

Growth profile analysis of all engineered strains was performed by kinetic studies on cell growth (temperature: 37 °C; run: 24 h; interval: 10 min; shake: linear (continuous); read: sfGFP (F) 485, 528 and optical density (A) 600) using an Epotech 2 microplate reader (BioTek, Agilent Technologies) under anaerobic conditions. Individual colonies of all strains were inoculated in pre-reduced 2×YT broth medium supplemented with 50 µg ml^{-1} streptomycin and 50 µg ml^{-1} kanamycin in a deep-well 96-well plate (Agilent Technologies, 204751) and incubated at 37 °C, shaking (250 rpm), anaerobically (BD GasPak EZ anaerobe pouch system, 260683), overnight. A Nunc Replication System (Thermo Fisher Scientific) was used to inoculate the strains in fresh pre-reduced 2×YT media with antibiotics. Growth curves were generated, and growth rates were estimated using Quantitative Growth Curve Evaluation software[43] (QurvE; https://www.qurveanalysis.com/app/qurve). All anaerobic procedures were performed in a Coy anaerobic chamber (Coy Laboratory Products), and all the reagents, media and

consumables used were pre-reduced for at least 24 h. All experiments were performed in three biological replicates. The fitness cost of peptide secretion on cell growth was calculated by dividing the growth rate of the control strain with the growth rate of the respective engineered strain. The experiment was performed in biological triplicates.

For the detection and semi-quantification of bioluminescent-tagged RORDEP1 in the spent bacterial fraction, individual colonies of the engineered strain and the negative control were inoculated in 2×YT broth medium supplemented with 50 μg ml^{-1} streptomycin and 50 μg ml^{-1} kanamycin and incubated at 37 °C, shaking (250 rpm), overnight. Cultures were diluted 100-fold in the same fresh media and incubated at 37 °C, shaking, overnight. The Nano-Glo HiBiT Extracellular Detection System (Promega, N2420) bioluminescent assay was performed on the bacterial spent fraction following the instructions provided by the vendor. Briefly, appropriate volumes of the LgBiT Protein and the Nano-Glo HiBiT Extracellular Substrate were diluted 100- and 50-fold, respectively. The detection mixture was added to the spent bacterial fraction in a 1:1 ratio. Luminescence (1 s integration time) was measured in an opaque 96-well plate after 5 min of incubation. A 20-μM HiBiT control protein (Promega, N3010) was used as positive control to generate the standard curve for semi-quantification of the secreted peptides in the spent media. An *E. coli* Nissle 1917 strain harbouring the empty pMUT1 vector was used as negative control. The experiment was performed in biological triplicates.

Preparation of bacterial supernatant filtrates and proteomics analysis

The supernatant was collected from a 150-ml culture of RT2 and filtered using filters with several differing pore sizes and molecular-mass cutoffs. Swing-bucket centrifugation (Eppendorf 5415R centrifuge; Eppendorf) was applied for all the procedures. The supernatants were centrifuged at 7,000 *g* for 10 min at 4 °C and then passed through polyethersulfone filters (0.22 μm; Merck Millipore) to remove the residual bacterial cells. The derived filtrates were passed through 100-kDa filters (Vivaspin 20 polyethersulfone ultrafiltration unit; Sartorius) at 6,000 *g* for 10 min. The 100-kDa filtrates were loaded onto 30-kDa filters (Sartorius) and centrifuged at 6,000 *g* for a further 10 min. The 30-kDa filtrates were then passed through 3 kDa (Pall Microsep Centrifugal Device; Pall) at 3,200 *g* for 10 min. The 3–30-kDa filtrate (500 μl) was frozen at −80 °C until it was assayed.

Methanol and chloroform precipitation of the crude protein extract was performed as follows: 100 μl of the protein extract was combined with 400 μl of methanol. Then, 100 μl of chloroform was added, and the mixture was vortexed. Subsequently, 300 μl of LC–MS-grade water was added, followed by another round of vortexing. The mixture was then centrifuged at the maximum speed for 1 min, after which the methanol and water layer was carefully removed. Next, 300 μl of methanol was added, and the mixture was vortexed to dislodge the protein pellet. After spinning at maximum speed for 5 min, the chloroform and methanol layer was cautiously removed without disturbing the pellet. The pellet was then allowed to dry in tubes with open lids for approximately 5 min at room temperature. Finally, the protein precipitates were redissolved in 100 μl of denaturation buffer, which contained 8 M urea in a 10-mM Tris buffer.

In the process of preparing for trypsin digestion and determining the required concentration of trypsin, several key steps were undertaken. Initially, the proteins in the sample were reduced using 5 mM dithiothreitol (DTT) for 1 h at room temperature. This was followed by the alkylation of the proteins with 10 mM iodoacetamide, also for an hour, but conducted in the dark to maintain the reactivity of iodoacetamide. Then the sample was first diluted to a concentration of less than 1 M urea using 900 μl of 20 mM ammonium bicarbonate. Subsequently, LC–MS-grade trypsin was added in a 1:50 weight/weight ratio. The sample was then left to digest overnight at 37 °C with slow shaking.

After the digestion process, the sample was dried down in a SpeedVac (Eppendorf, Concentrator Plus) under the 'V-HV' mode. This drying was conducted at room temperature without heating for 1 h, after which the liquid level was checked. The process continued under the 'V-AQ' setting until the sample was just dry. The protein extracts were resuspended by vortexing for 1 min in 0.1% formic acid (FA) before adding 0.1% trifluoroacetic acid (TFA) to a final volume of 25 μl.

The concentration of peptides was determined using a NanoDrop spectrophotometer. Following this, eluted peptides were desalted using C18 Stage Tips, as previously described[44]. C18 Empore disk membranes (3M) were packed into the bottom of 200-μl pipette tips. The purification process involved washing the peptides with 0.1% TFA and 5% methanol in Milli-Q water and repeating this step three times. This washing was performed by centrifugation at 1,500 *g* using a specially designed three-dimensional-printed centrifugal block. For elution, 60 μl of solution consisting of 0.1% TFA and 50% acetonitrile in Milli-Q water were used, and this step was repeated three times. The eluted peptides were subsequently dried at 60 °C in a SpeedVac centrifuge. The dried peptides were then reconstituted and sonicated in a solution of 5% acetonitrile and 0.1% FA. The peptide concentration was again measured using the NanoDrop, and a quantity of 500 ng of the purified peptides was prepared for injection into the LC–MS/MS system for analysis.

Desalted and normalized protein samples were analysed on Orbitrap Exprolis 480 MS (Thermo Fisher Scientific) coupled to a Evosep One LC system (Evosep Biosystems). In the analysis of each sample, peptides were first loaded onto a column with 15 cm × 150 μm inner diameter (ID) with 1.9-μm C18 beads (PepSep) heated at 60 °C coupled to a 20-μm-ID electrospray emitter (Bruker Daltonics). The elution of peptides was performed over a standard 21-min gradient, with buffer A (0.1% (v/v) FA in water) and buffer B (0.1% (v/v) FA in acetonitrile), at a flow rate of 1 μl min^{-1}. The Q-Exactive instrument (Thermo Fisher Scientific) was operated in a data-independent acquisition (DIA) method for this process. Full MS spectra were acquired at a resolution of 60,000 with either an automatic gain control (AGC) target of 300% or a maximum injection time of 100 ms, covering a scan range from 300 to 1,650 m/z. The collection of MS2 spectra was conducted at a resolution of 30,000. This process used an AGC target set to 300%; alternatively, it used a maximum injection time capped at 100 ms. In addition, these spectra incorporated the use of higher-energy collisional dissociation (HCD) fragmentation, which was calibrated to a normalized collision energy level of 30%.

The raw files were analysed using DIA-NN 1.8.1 in direct mode and visualized using Skyline (version 23.1, 64-bit). The spectra were matched against the UniProt database of RT ATCC 27756 (UP000003577). Cysteine carbamidomethyl was set as a static modification. The false-discovery rate was set to 0.01 for both proteins and peptides with a minimum length of six amino acids and was determined by searching a reverse database.

Human study participants

For quantification of RUMTOR_00181-carrying strains in human stools and estimation of the abundance of RORDEP1 and 2 in human plasma, respectively, 59 healthy adult men were phenotypically characterized (Supplementary Table 6). The study was approved by the Ethical Committees of the Capital Region of Denmark (H-16021787). Height was measured with the participants not wearing shoes, and weight was measured to the nearest 0.1 kg, with the participants in underwear. Plasma glucose was measured using a colourimetric slide test, and plasma insulin was measured using immunoassay. The homeostatic model of insulin resistance was calculated from fasting insulin and glucose concentrations as reported previously[45].

For the assessment of the potential impact of dietary habits on the abundance of RT strains releasing RORDEPs in faecal samples, the absolute cell counts of RUMTOR_00181-carrying strains were

measured in 27 healthy adults eating a vegan diet and in 27 healthy adults eating an omnivorous diet (Supplementary Table 7). The study was approved by the Ethical Committees of the Capital Region of Denmark (H 3 2012-145).

All human studies were performed in accordance with the principle of Helsinki Declaration II, and written informed consent was obtained from each participant before they could enter the study.

Microbial genomic DNA extraction

In human and mouse faecal samples, and in cultures of RT strains, metagenomic DNA extraction was performed using the NucleoSpin soil kit (Macherey-Nagel) according to the manufacturer's instructions. A NanoDrop 2000 spectrophotometer (Thermo Scientific) was used to measure DNA purity and concentration.

Quantification of the abundance of RUMTOR_00181-carrying strains in human faecal samples

This protocol consists of two parts: a measurement of the faecal bacterial load and a quantification of RUMTOR_00181-carrying strains. For microbial load determination, 80–120 mg of frozen (−80 °C) stool aliquots were used as reported[46,47].

For the quantitation of RUMTOR_00181-carrying strains in human stools, metagenomic DNA was extracted from 250 mg stool using the protocol described before[47]. Primer pairs targeting universal 16S rDNA or RORDEP1 gene sequence were applied for the detection of total amounts of bacteria and RUMTOR_00181-carrying strains, respectively, using qPCR assay conditions described in the above section (Supplementary Table 10). A standard curve ranging between 3×10^3 CFU and 3×10^7 CFU was included in the qPCR assay by diluting the standard DNA from a pure culture of RT2. Absolute abundance of RUMTOR_00181-carrying strains for each sample was estimated by normalizing the relative abundance of RUMTOR_00181-carrying strains to the bacterial cell load of the individual faecal sample.

In silico analysis of the RUMTOR_00181 gene in the human gut metagenomes of study participants in the LifeLines DEEP 2016 cohort

To elucidate the prevalence and abundance of the RUMTOR_00181 gene within the human gut microbiome, in silico sequencing analysis was performed using metagenomic data from the LifeLines DEEP 2016 cohort[28]. This analysis leveraged the curatedMetagenomicData[48] repository (version 3.6.2), which encompasses a comprehensive dataset of 7,772,785 UniProt Reference Clusters (UniRef) gene families derived from the cohort's metagenomic sequencing. The amino acid sequence of RUMTOR_00181 from *[Ruminococcus] torques*—also known as the FN3-domain-containing protein (NCBI accession number WP_004845365.1)—was used as the query for screening the metagenomic data. Protein-level searches were conducted against the UniRef90 gene family database using the BLASTP algorithm (version 2.7.1+) with stringent parameters: an *e*-value threshold of 1×10^{-5} and a minimum sequence identity of 40% over at least 90% of the query protein length. These criteria were selected to ensure high-confidence identification of homologous sequences corresponding to RUMTOR_00181 within the diverse and complex metagenomic landscape of the human gut. Following the BLASTP screening, we quantified the presence and relative abundance of sequences homologous to RUMTOR_00181 using the curated gene family abundance tables provided by curatedMetagenomicData.

Preparation of human plasma samples and proteomics-based absolute quantification of RORDEP1 and RORDEP2 concentrations

A total of 20 µl of plasma was diluted with three volumes of buffer A and filtered using 0.2-µm AcroPrep filter plates (Pall). The filtered plasma was loaded onto a Multiple Affinity Removal Column (4.6 × 50 mm, Hu-14, Agilent) coupled to a 1260 Infinity II bio-inert high-performance liquid chromatography (HPLC; Agilent) according to the manufacturer's instructions, and the flow-through fraction (500 µl) collected in a time-dependent manner. Subsequently, 50 µl of depleted plasma was mixed with 50 µl of 2× lysis buffer (100 mM Tris–HCl (pH = 8.5), 10 mM TCEP, 40 mM CAA), incubated for 10 min at 95 °C and digested with trypsin and Lys-C (0.5 µg each) at 37 °C overnight. The digest was inactivated by the addition of TFA (1% final concentration).

AQUA peptide stock solutions were prepared by dissolving isotopically labelled RORDEP peptides (Supplementary Table 9) in 5% acetonitrile (ACN) to a final concentration of 5 pmol μl^{-1}. These AQUA peptides contain a labelled amino acid, allowing them to behave like natural peptides during chromatography and electrophoresis while being easily distinguishable by mass spectrometry. For the measurement of RORDEP in plasma samples, AQUA peptides were each further diluted and combined in a mix of 5 fmol μl^{-1}. Then 6 µl of the peptide digest and 2 µl of the ACQUA peptide mix were loaded onto Evotips (Evosep) following the manufacturer's instructions.

For the absolute quantification of RORDEPs in the plasma pool of RORDEP-positive subjects, r-RORDEP1 and r-RORDEP2 were diluted in the depleted plasma digest derived from a pool of plasma RORDEP-negative subjects and measured alongside the negative- and positive-pooled plasma samples. The amounts of the spiked-in peptides were adjusted according to their ionization capacities: to 3 µl of peptide digest, 20 fmol of peptides 1, 2 and 5–8; 40 fmol of peptide 4; and 400 fmol of reduced and alkylated peptide 3 were added (Supplementary Table 9).

Peptides were then separated on a Pepsep 15-cm, 150-µM-ID column packed with C18 beads (1.5 µm) using an Evosep ONE HPLC system applying the default 30 samples per day method. The column temperature was maintained at 50 °C. Upon elution, peptides were injected via a NanoSpray source and 30 µm stainless steel emitter (Evosep) into an Orbitrap Ascend Tribrid mass spectrometer (Thermo) operated in SureQuant mode. Briefly, starting from the 'Users Custom Panel Sure Quant' template, built in Thermo Excalibur software (v.4.7), spray voltage was set to 2,200 V, MS data were collected over a 400–1,200 m/z range (120,000 resolution, 251 ms maximum injection time and AGC target 250%). MS/MS scans were triggered by a list of heavy labelled peptides of interest (Supplementary Table 1) and acquired using 15,000 resolution, 27 ms maximum injection time, AGC target 1,000%, 1.4 Th isolation window and 30 normalized collision energy. MS/MS spectra having a minimum of $n = 4$ expected target ion fragments (Supplementary Table 9), defined by unique peptide sequences that do not share more than a minimal degree of homology (typically less than 30% over any seven-amino acid stretch) with other proteins, were triggering a second MS/MS scan for the endogenous light peptide. Isolation offset was set to −4 Th or −2.67 Th, respectively, for a double- or triple-charge precursor. Other settings include Orbitrap resolution 60,000, 123 ms maximum injection time, AGC target 1,000% and HCD collision energy 30. The total fixed cycle time, switching between all 3 MS scan types, was set to 3 s.

A spectral library was generated with MaxQuant (v1.6.15.0). Peak lists were searched against the human UniProt FASTA database combined with RORDEP 1–2 sequences and 262 common contaminants by the integrated Andromeda search engine. The false discovery rate was set to 1% for both peptides (minimum length of seven amino acids) and proteins. Carbamidomethylation of cysteine was specified as fixed modification, heavy lysine (+8 Da), oxidation of methionine and acetylation at the protein N-terminus as variable modifications. 'Match between runs' was disabled.

SureQuant raw files were analysed using Skyline 23.1.0.268 software following developer tutorials and guidelines. Briefly, in 'Peptide Settings', heavy isotope modifications for lysine (+8 Da) were activated, while carboamidomethyl (C) was set as structural modifications. In 'Transition Settings', ion charges were set to +1 and +2 and ion types

to 'p, y, b'. Product ion selection was set from m/z >precursor to last ion-1. Ion match tolerance was 0.1 m/z, and up to eight product ions were allowed to be selected from the spectral library. The mass analyser was set to 'Orbitrap' and resolving power to 60.000 for MS1 filtering. In MS/MS filtering options, acquisition mode was set to 'SureQuant' and mass analyser to 'Centroided'. Only scans within 5 min of spectral library MS/MS retention time ID were selected. After an attentive visual inspection of the correct Skyline peptides integration, a matrix containing the light and heavy total area of fragments for each target peptide was exported and used for quantification. Peptide fragments used for quantification are listed in Supplementary Table 9.

Mouse gut microbial DNA extraction, 16S rRNA gene sequencing and bioinformatics analysis

Microbial DNA was extracted from approximately 250 mg of mouse stool samples using the NucleoSpin Soil Mini Kit (Macherey-Nagel) following the manufacturer's protocol. The extraction process began with the lysis of stool samples through a combination of chemical treatment and mechanical disruption, which involved adding lysis buffer to zirconium bead tubes containing the samples and performing bead beating with a specialized vortex adaptor. The crude lysate was subsequently treated to eliminate inhibitors, ensuring thorough sample purification. The purified lysate was then combined with a DNA-binding solution and passed through a silica-based spin filter. After a two-step washing procedure, the DNA bound to the membrane was eluted using 10 mM Tris buffer. The concentration of the extracted DNA was quantified using a Qubit Flex Fluorometer with the Qubit dsDNA HS Assay Kit (Thermo Fisher Scientific).

For sequencing, DNA libraries were constructed using the Quick-16S Plus NGS Library Prep Kit (Zymo Research). The V3 and V4 regions of the 16S rRNA gene were amplified via PCR using primers 341F (a mixture of CCTACGGGDGGCWGCAG and CCTAYGGGGYGCWGCAG) and 806R (GACTACNVGGGTMTCTAATCC). Dual eight-nucleotide indices compatible with Illumina sequencing were added in a subsequent PCR step. Following quantification with the Qubit fluorometer, the DNA libraries were circularized using the Element Adept Library Compatibility Workflow and sequenced on the Element AVITI platform using the AVITI 2 × 150 Cloudbreak Sequencing Kit.

Bioinformatics analysis commenced with the removal of primer sequences from the raw sequencing data using Cutadapt. Quality trimming was performed with DADA2, in which sequences were filtered based on a predefined Phred quality score threshold, and both forward and reverse reads were trimmed to uniform lengths according to their quality scores, retaining higher-quality reads for longer lengths. DADA2 used a machine learning-based parametric error model to estimate error rates for the reads, operating under the assumption that true sequences are more abundant than erroneous variants. The core sample inference algorithm was then applied to the filtered data, followed by the merging of paired-end reads that shared at least 12 bases of identical overlap. Chimeric sequences, identified as combinations of more abundant parent sequences, were removed. The cleaned and trimmed reads were subsequently clustered into amplicon sequence variants (ASVs) with 97–99% similarity.

Taxonomic classification of the ASVs was conducted using the naive Bayesian classifier of DADA2 in conjunction with the RDP trainset 18 database. To assess differences in gut microbial composition between baseline and follow-up samples, taxonomic abundances at the family level were visualized using stacked bar plots. Alpha diversity was evaluated using the Shannon index, and statistical comparisons were made using a two-sided Wilcoxon test. All data analyses were performed using R (version 4.3.2).

Expression of 6×His-tagged RORDEP1 or RORDEP2 in *E. coli*

Target DNA sequences of RORDEPs were codon optimized for *E. coli* strain BL21 (DE3). The synthesized DNA sequences were cloned into the pET-30a (+) vector for protein expression. The vector products were transformed into the *E. coli* strain BL21 Star (DE3). The *E. coli* containing RORDEPs in plasmids were cultured on an agar plate supplemented with ampicillin (50 μg ml^{-1}) at 37 °C overnight. A single colony was then inoculated into terrific broth medium containing the same antibiotic and incubated at 37 °C with shaking at 200 rpm. When OD_{600} reached 0.8, the bacterial culture was induced with isopropyl-β-D-1-thiogalactopyranoside (IPTG) at 37 °C for 4 h. Bacteria were collected by centrifugation and the resulting pellets resuspended in lysis buffer. After sonication, the supernatants containing the target protein were separated by centrifugation and purified using a one-step purification on a Ni column (GenScript Biotech). The final products were kept in 50 mM Tris–HCl, 150 mM NaCl and 10% glycerol, pH 8.0, followed by sterilization using a 0.22-μm filter, before being stored in aliquots. The concentration was determined using a bicinchoninic acid (BCA) protein assay. Protein purity and molecular weight were assessed using standard SDS–PAGE and intact mass spectrometry. An endotoxin test was performed using the ToxinSensor Chromogenic LAL Endotoxin Assay Kit (L00350C, GenScript Biotech), using a modified Limulus Amebocyte Lysate and a synthetic-colour-producing substrate to quantitatively detect endotoxin chromogenically in a broad range (0.01–1 EU ml^{-1}). The endotoxin levels of recombinant RORDEPs were <0.1 EU ml^{-1}.

Small-angle X-ray scattering analysis of r-RORDEP1

The r-RORDEP1 protein was dialysed against a 20-mM Tris buffer at pH 8.0, using Slide-A-Lyzer dialysis cassettes (G2, 3.5-kDa molecular weight cutoff). The protein solution was concentrated using Amicon Ultra-0.5 centrifugal filter units with a 3.5-kDa cutoff, to achieve final concentrations of 1.0, 2.0 and 6.6 mg ml^{-1}, respectively, for subsequent SAXS experiments.

SAXS data collection was conducted at the BM29 BIOSAXS beamline at the European Synchrotron Radiation Facility, on 15 April 2021. The instrument was equipped with a Pilatus 2M detector, set at 2.83 m from the sample, to cover a q-range of 0.044–5.205 nm^{-1}. The X-ray wavelength was fixed at 0.998 nm. A 500 × 100 mm^2 beam was used for all measurements. The samples were irradiated in a quartz glass capillary at 20 °C, and data were collected in 10-s exposures to minimize radiation damage, with frame-by-frame comparison for monitoring.

Two modes of SAXS analysis were used: batch mode and a flow cell that was connected to a size-exclusion column (SEC-SAXS) mode. For batch mode, protein concentrations of 1.0 g l^{-1} and 2.0 g l^{-1} were used. In SEC-SAXS, RORDEP1 was injected at a concentration of 6.6 mg ml^{-1} into an AdvanceBio SEC 130-Å column pre-equilibrated with buffer and run at a flow rate of 0.16 ml min^{-1}. Absolute scaling was achieved by comparing with scattering from sterile water, and normalization was based on transmitted intensity by beam-stop counter.

SAXS data reduction was performed using PRIMUSqt from the ATSAS package (2.8.32). Basic analyses to determine parameters such as Guinier, p(r), and Vp were also conducted within the same software environment. Molecular graphics were generated using PyMOL (version 1.8.2.3, Schrödinger), and figures were produced using the Spyder software within the Anaconda 3 environment. Theoretical scattering curves for a monomeric and dimeric human irisin structure (PDB entry: 4LSD), which shares 29% sequence identity with RORDEP1, were calculated using CRYSOL. Fits to the experimental data allowed for the determination of the oligomeric state of RORDEP1 in solution. The radius of gyration (R_g) and the maximum particle dimension (D_{max}) were calculated from the SAXS data. Molecular weights were estimated using the pair distribution function ($MW_{p(r)}$) and Porod's law (MW_{porod}). For batch SAXS, R_g values were determined as 1.53 nm and 1.51 nm for the 1.1 g l^{-1} and 2.0 g l^{-1} concentrations, respectively, both with a D_{max} of 5.0 nm. Molecular weight estimates were 12.1 kDa and 11.7 kDa ($MW_{p(r)}$), and 7.8 kDa and 8.3 kDa (MW_{porod}). For SEC-SAXS, at a protein concentration of 6.6 g l^{-1}, the R_g was measured at 1.50 nm, D_{max} at 5.0 nm and MW_{porod} at 8.5 kDa.

Thermostability characterization of r-RORDEP1 by SEC-MALS and nano differential scanning fluorimetry analysis

The oligomeric state of r-RORDEP1 after heat treatment was analysed using SEC with multi-angle static light scattering (SEC-MALS). The analysis was performed using an Agilent system equipped with a Wyatt Optilab µT-rEX refractive index detector and a Wyatt µDAWN TREOS MALS detector. Data acquisition and analysis were conducted with Astra software version 7.3.2.19. Each run used a 20-µl sample injection volume, with a protein load of 15–20 µg. Separation was achieved using an AdvancedBio SEC 300A column (2.7 µm, 4.6 × 150 mm), with 20 mM Hepes and 150 mM NaCl as the mobile phase. Nano differential scanning fluorimetry was conducted on a Panta system (NanoTemper) at a concentration of 3 mg ml^{-1} with a temperature ramp from 20 °C to 95 °C with a gradient of 1.5 °C min^{-1}. Unfolding was detected by monitoring the fluorescence at 330 nm, 350 nm and the 350:330 ratio.

Cell culture experiments

Human white preadipocytes (PromCell, C-12732, lot number 456Z005.1, isolated from human omentum) were cultured until 80% confluent in preadipocyte growth medium (PromCell, C-27410, basal medium supplemented with 0.05 ml ml^{-1} fetal calf serum, 0.004 ml ml^{-1} endothelial cell growth supplement, 10 ng ml^{-1} epidermal growth factor, 1 µg ml^{-1} hydrocortisone, 90 µg ml^{-1} heparin) and switched to preadipocyte differentiation medium (PromCell, C-27436, basal medium supplemented with 8 µg ml^{-1} D-biotin, 0.5 µg ml^{-1} insulin, 400 ng ml^{-1} dexamethasone, 44 µg ml^{-1} 3-isobutyl-1-methylxanthine (IBMX), 9 ng ml^{-1} L-thyroxine, 3 µg ml^{-1} ciglitazone). The differentiation process to mature adipocytes was considered completed after 12–14 days. The treatment of r-RORDEP1 and PBS started from the third day of differentiation to the end with refreshment at every other day. Cells were collected after 14 days of differentiation, and thermogenic and lipogenic genes were quantified by qPCR.

Human osteoblasts (Promocell, C-12720, lot number 445Z012.2, isolated from human femoral heads) were cultured in growth media (Promocell, C-27001, basal medium supplemented with 10% fetal calf serum) until 80% confluent and switched into differentiation media containing differentiation-promoting supplements of 10 mM β-glycerophosphate and 50 µg ml^{-1} ascorbic acid in α-MEM (Fisher Scientific, 15430584). On days 3, 6 and 9 of differentiation, cells were treated with r-RORDEP1 and PBS in the presence of β-glycerophosphate and ascorbic acid. Cells were collected on day 10. Transcription regulators and osteoblast differentiation marker genes were quantified by qPCR.

Human skeletal myoblasts (PromoCell, C-12530, lot number 451Z031.15, isolated from human musculus pectoralis major) were cultured in growth media (PromoCell, C-23060, basal medium supplemented with 5% fetal calf serum, 50 µg ml^{-1} fetuin, 10 ng ml^{-1} epidermal growth factor, 1 ng ml^{-1} basic fibroblast growth factor, 10 µg ml^{-1} insulin, 0.4 µg ml^{-1} dexamethasone) until 80% confluent and switched into differentiation media (PromoCell, C-23061, basal medium supplemented with 10 µg ml^{-1} insulin) developed to induce the fusion of myoblasts to form myotubes with typical multinucleated syncytia. After 4 days, extensive formation of multinucleated syncytia was observed. For a stable differentiation of skeletal muscle cells, after 5 days of incubation in differentiation medium, cells were switched back to growth medium. Treatment of r-RORDEP1 and PBS started from the third day of differentiation. Cells were collected after 10 days of differentiation and myogenesis genes were quantified by qPCR.

GLP1-secreting human cell line NCI-H716 (ATCC, CCL-251) cells were seeded at a concentration of 1×10^5 cells per well onto a poly-D-lysin-coated plate (Sigma-Aldrich, P8920). The cells were cultured in RPMI1640 medium (Thermo Fisher, 11875093) supplemented with 10% (v/v) heat-inactivated newborn calf serum (Thermo Fisher, 16010167), with the medium being refreshed every other day until the cells reached 80–85% confluence. After reaching confluence, the cells were incubated for 2 h in KRH buffer for baseline secretion or KRH buffer supplemented with either (1) 10 mM glucose and 10 µM forskolin (Sigma-Aldrich, F6886)/IBMX (Sigma-Aldrich, I5879) as positive stimulants or (2) r-RORDEP1 at concentrations of 1.5 nM, 15 nM and 150 nM. The KRH buffer was made in house, consisting of 138 mM NaCl, 4.5 mM KCl, 4.2 mM $NaHCO_3$, 1.2 mM NaH_2PO_4, 2.5 mM $CaCl_2$, 1.2 mM $MgCl_2$ and 10 mM HEPES, supplemented with 0.1% (wt/vol) fatty-acid-free BSA (Sigma-Aldrich, catalogue number A-603-10G), adjusted to pH 7. Supernatants were collected and centrifuged at 1,500 *g* for 5 min at 4 °C to remove any floating cells or debris. GLP1 levels in the supernatants were then quantified using a GLP1 EIA Kit (Sigma-Aldrich, RAB0201), following the manufacturer's instructions.

Rat insulin-secreting INS-1E 832/13 cells (a gift from B. Emanuelli, Novo Nordisk Foundation Center for Basic Metabolic Research, Faculty of Health and Medical Sciences, University of Copenhagen) were grown in a monolayer at 37 °C in a humidified incubator gassed with 5% CO_2, in RPMI1640 medium containing 2 mM glutamine supplemented with 10% heat-inactivated fetal bovine serum, 100 IU ml^{-1} penicillin, 100 µg ml^{-1} streptomycin, nonessential amino acids (all from Life Technologies, Invitrogen), 10 mM HEPES (pH 7.4), 1 mM sodium pyruvate and 50 µM of 2-mercaptoethanol. At 70% confluence, the cells were treated with r-RORDEP1 and PBS for 24 h. After the treatments, the supernatant media were collected for enzyme-linked immunosorbent assay (ELISA) measurement (Sigma-Aldrich, RAB0904) of secreted insulin levels at 1 h and 24 h.

In all listed cell culture experiments, r-RORDEP1 was added at concentrations listed in Extended Data Fig. 6.

Assessment of the binding between r-RORDEP1 and integrin receptors using SPR assay

In the surface plasmon resonance (SPR) assay on a Biacore 8K instrument (Cytiva) assessing the binding interactions between Fc-tagged RORDEP1 (Fc-RORDEP1) and various human integrin receptors, Fc-RORDEP1 was diluted to 10 µg ml^{-1} in running buffer containing 10 mM HEPES, 150 mM NaCl, 3 mM EDTA and 0.005% Tween-20 at pH 7.4. Each of the 24 human integrin subunits was prepared at 1,000 nM in the same buffer. At 25 °C, Fc-RORDEP1 was captured onto a Series S Sensor Chip Protein A by injecting it at 10 µl min^{-1} until approximately 1,000 response units (RU) were achieved. Integrin analytes were then injected over the immobilized Fc-RORDEP1 at 1,000 nM, with an association phase of 60 s and a dissociation phase of 150 s at a flow rate of 30 µl min^{-1}. The sensor surface was regenerated after each cycle using 10 mM glycine–HCl (pH 1.5) at 20 µl min^{-1} for 30 s. Binding interactions were monitored in real time and processed by referencing against a blank flow cell to correct for non-specific binding. Interactions were evaluated qualitatively based on response units during the association and dissociation phases. Negative controls included injections of running buffer over the Fc-RORDEP1 surface and integrin analytes over a reference surface without immobilized Fc-RORDEP1. All experiments were conducted in duplicate.

In the SPR assay assessing affinity between r-His-RORDEP1, echistatin TFA and biotinylated human ITGAV&ITGB5 heterodimer protein in the presence of three running buffer solutions, the biotinylated integrin αVβ5 heterodimer was immobilized onto a streptavidin (SA) sensor chip by injecting 20 µg ml^{-1} of the protein in running buffer at 10 µl min^{-1} until approximately 4,000 RU were achieved. Four running buffers were prepared: buffer A: 1× HBS-N (10 mM HEPES, 150 mM NaCl) and 0.05% Tween-20, pH 7.4, supplemented with 1 mM $CaCl_2$ and 1 mM $MgCl_2$; buffer B: buffer A with 1 nM Hsp90aa1; buffer C: buffer A with 1 mM $MnCl_2$; and buffer D: buffer B with 1 mM $MnCl_2$. Analytes (r-His-RORDEP1 and echistatin TFA) were prepared in each running buffer immediately before injection. The analytes were injected over the immobilized integrin at a flow rate of 30 µl min^{-1}, with an association phase of 60 s and a dissociation phase of 150 s. The sensor surface was regenerated between runs as needed using appropriate

regeneration conditions. Binding interactions were monitored in real time and processed using the Biacore control software, referencing against a blank flow cell to correct for non-specific binding. Responses were evaluated based on the magnitude of RU during association and dissociation phases. All experiments were performed in duplicate to ensure reproducibility.

ELISA-based evaluation of binding affinity between r-RORDEP1 and integrin heterodimers

An ELISA-based assay was conducted to evaluate the binding affinity between RORDEP1 and various integrin heterodimers. In the first setup, ELISA plates were coated with recombinant His-tagged RORDEP1 or His-tagged fibronectin at a concentration of 5 μg ml^{-1} (100 μl per well) and incubated overnight at 4 °C. Gradient dilutions (0.001–10 μg ml^{-1}) of integrin heterodimers (Acro Biosystems)—including αVβ1 (IT1-H82W6), α4β1 (IT1-H82W1), α5β1 (IT1-H82Wa), α8β1 (IT1-H82Wb), αVβ3 (IT3-H82W9), αVβ5 (IT5-H82Wa), αVβ6 (IT6-H82E4) and αVβ8 (IT8-H82W5)—were added to the wells and incubated for 2 h at room temperature. Bound integrins were detected using a streptavidin–horseradish peroxidase conjugate (Thermo Fisher, 21126) diluted 1:10,000. In the second setup, ELISA plates were coated with the integrin heterodimers at 5 μg ml^{-1}, and gradient dilutions of Fc-tagged RORDEP1 (0.001–10 μg ml^{-1}) were added to the wells. Detection was performed using an anti-human IgG, Fcγ fragment-specific antibody diluted 1:10,000. After incubation with detection antibodies in both assays, 3,3′,5,5′-tetramethylbenzidine substrate was added for colour development, and the reaction was stopped with 2 N sulfuric acid. Absorbance was measured at 450 nm, and binding affinities were determined by plotting absorbance values against protein concentrations to generate binding curves and calculate EC_{50} values.

Fluorescence polarization assay for recombinant RORDEP1–integrin binding

To assess the binding of r-RORDEP1 to integrins, a fluorescence polarization (FPOL) assay was used. r-RORDEP1 was first labelled with either TAMRA-NHS ester or sulfo-Cy5-NHS ester (Lumiprobe). For this, 100 μl of r-RORDEP1 at a concentration of 130 μM was incubated with a 1.5× molar excess of the respective dye for 4 h at room temperature, targeting preferential labelling at the N-terminus. The labelled protein was then subjected to buffer exchange with 20 mM HEPES and 150 mM NaCl, pH 7.4, to remove unreacted dye. The final protein concentration was 70 μM, with a degree of labelling estimated at 0.6.

The FPOL assay was performed with an r-RORDEP1 tracer concentration of 70 nM in a buffer containing 20 mM HEPES, 150 mM NaCl, 0.05% Tween-20 and 2 mM $MnCl_2$, at pH 7.4. Integrin αVβ3 was used at a concentration of 340 nM, and integrin αVβ5 at 500 nM. Samples were incubated for up to 3 h at 22 °C, making sure that equilibrium was attained. FPOL was measured on a Tecan Spark fluorescence plate reader in a 384-well plate (Greiner 784900). For detecting TAMRA fluorescence, a 535/25 nm excitation filter and a 595/35 emission filter were used; for detecting Cy5 fluorescence, a 620/20 nm excitation filter and a 680/30 nm emission filter were used. The data were not corrected for different detection efficiencies of the parallel and perpendicular detectors (G-factor 1), which is justified as the focus is on relative changes.

Stability assessment of r- RORDEP1 in simulated intestinal fluid

SIF was prepared as recommended[49]. In brief, 25 mg of pancreatin (8× United States Pharmacopeia activity) was dissolved in 20 ml of KH_2PO_4 (6.8 mg ml^{-1}, pH 6.8) to afford 1× UPS activity SIF. The resulting mixture was vortexed for 1 min, followed by sonication for 15 min at 25 °C. The final suspension (pancreatin does not dissolve fully) was centrifuged and syringe filtered before use.

A total of 520 μl of freshly prepared SIF was preincubated at 37 °C for 15 min. The r-RORDEP1 stock solution (80 μl of 375 μM) was added to the fluid, and the mixture was gently stirred by pipetting and incubated at 37 °C (600 μl total volume; 30 μM final r-RORDEP1 concentration). Control experiments were performed in parallel in a KH_2PO_4 buffer (520 μl) by spiking it with 80 μl of RORDEP1 and incubating at 37 °C (30 μM final r-RORDEP1 concentration). A total of 75 μl of sample was drawn at 0, 15, 30, 60, 120, 240 and 480 min and quenched by ice-cold 5% TFA in H_2O solution (75 μl). All samples were centrifuged, filtered and analysed with UPLC (to determine the amount of ligand left) and LC–MS (to identify cleavage products of r-RORDEP1).

Transport of r-RORDEP1 across a monolayer of epithelial cells using a gut-on-chip model

Caco-2 cells (ATCC, HTB-37) were cultured in Dulbecco's modified Eagle medium (DMEM, Gibco) supplemented with 20% fetal bovine serum (Gibco) and 1% penicillin–streptomycin (Gibco) to prepare the Caco-2 culture medium. The cells were maintained in T25 culture flasks within a humidified incubator at 37 °C with 5% CO_2, and 5 mL of the culture medium was replaced every 2 days. Once the cells reached over 85% confluence, they were passaged at a 1:2 ratio using standard trypsinization techniques.

For the construction of the gut-on-chip model, high-throughput membrane barrier chips (Avatarget) were transferred into a laminar flow hood to ensure sterility. Caco-2 cells at ≥85% confluence was detached using 1 ml trypsin (Gibco) and resuspended in 1 ml of Caco-2 culture medium, followed by cell counting. A suspension containing 2×10^5 cells per cm^2 was prepared by adding 200 μl of the resuspended Caco-2 cells to the upper channel of each chip. The chips were then placed in a cell culture incubator at 37 °C with 5% CO_2 and allowed to adhere for 2 h. After the adhesion period, microscopic examination confirmed that the majority of Caco-2 cells had firmly attached to the membrane. Subsequently, 600 μl of Caco-2 culture medium was added to both the upper and lower channels of each chip, and the chips were returned to the incubator. The culture medium was refreshed every 48 h. After 7 days of incubation, the integrity of the epithelial monolayer was verified by measuring the transepithelial and transendothelial electrical resistance (TEER)[50], with values ≥ 500 Ω cm^{-2} indicating successful construction of the gut-on-chip model, suitable for subsequent peptide permeability assays.

TEER measurements were conducted using a WPI EVOM2 STX2 meter. The chopstick electrodes were first equilibrated in PBS for 15 min until the instrument stabilized at 0 Ω. The electrodes were then carefully inserted into the designated detection wells of the membrane barrier chip and the upper channel, ensuring that both electrodes were submerged in the culture medium. Once the readings stabilized, the TEER value was recorded and calculated using the formula TEER = T (Ω) × A (cm^2), where T represents the measured resistance and A is the area of the model.

For the peptide permeability assay, r-RORDEP1 was prepared in DMEM at final concentrations of 75 μM, 150 μM and 300 μM. FITC-Dextran 4000 (Biotiny) at 1 mg ml^{-1} was used as a positive control. The experimental setup included four groups: 75 μM for 12 h, 150 μM for 12 h, 300 μM for 12 h and a positive control with FITC-Dextran 4000 for 12 h, each with triplicate wells. For each experiment, 200 μl of the respective peptide or positive control solution was added to the upper channel, and 500 μl of DMEM culture medium was added to the lower channel. The chips were incubated under the specified conditions, and after the incubation periods of 12 h, the culture medium from the lower channel was collected and stored at −80 °C for subsequent chromatographic analysis.

Cell viability was assessed using the CellTiter-Glo 2.0 Assay (Promega). The assay reagent was equilibrated to room temperature and mixed with Caco-2 culture medium in a 1:1 ratio. After aspirating the culture medium from both channels of the chip, 200 μl of the mixed reagent was added to the upper channel. The chip was then placed on a shaker plate and gently agitated for 5 min to ensure thorough mixing, followed by a 20-min incubation at room temperature. Subsequently,

100 µl of the luminescent solution from the upper channel was transferred to a 96-well plate with transparent bottoms (Corning) and measured using a Tecan PRO M200 microplate reader. Cell viability was expressed as a percentage relative to control samples, calculated by comparing the OD values.

Chromatographic detection of peptide samples was performed using an HPLC system (Agilent 1260) equipped with a NanoChrom BioCore SEC-150 column (7.8 × 300 mm, 5 µm). The mobile phase consisted of 50 mM phosphate buffer and 300 mM sodium chloride in 10% acetonitrile, with isocratic elution at a flow rate of 1 ml min^{-1}. The column temperature was maintained at 30 °C, and detection was carried out using a variable wavelength absorbance detector set to 209 nm. Samples were injected in volumes of 10 µl using an autosampler. In addition, analysis of the positive control was conducted using an ultra-high-performance liquid chromatography system (Agilent 1290) with the same type of column. The mobile phase and column temperature were identical to the peptide analysis, but the flow rate was adjusted to 0.7 ml min^{-1}. Fluorescence detection was performed with an excitation wavelength of 492 nm and an emission wavelength of 520 nm, and samples were similarly injected at 10 µl using an autosampler. To validate the specificity of the UPLC detection peak corresponding to r-RORDEP1, PBS alone was analysed as a negative control, followed by analysis of PBS spiked with increasing concentrations of purified r-RORDEP1. Dose-dependent changes in peak intensity and consistency in retention times were monitored to confirm signal specificity.

Experiments in mice

Male mice with a C57BL/6 background (specific pathogen-free grade) and with varying ages as detailed below were purchased from Janvier Labs. All experiments in mice were conducted in accordance with approved protocols. The intervention study involving the RT strain and the GMO1 study were approved by the Danish Animal Experiments Inspectorate (license numbers 2018-15-0201-01491 and 2020-15-0201-00568, respectively) and by the University of Copenhagen (project numbers P20-392 and P23-145, respectively). The comparative study assessing the effects of r-RORDEP1 and scrambled r-RORDEP1 on glucose tolerance, conducted at WuXi AppTec, was approved under ethical approval ID GP01-QD112-2024v1.2 (https://www.wuxiapptec.com). All mouse experiments were performed in accordance with Institutional Animal Care and Use Committee (IACUC) guidelines and in compliance with the Animal Welfare Act, the Guide for the Care and Use of Laboratory Animals and the Office of Laboratory Animal Welfare.

All mice were housed at 23 ± 1 °C on a 12-h light and 12-h dark cycle with ad libitum access to food and purified water. Mice were allowed to acclimatize on the different diet as described for 7–14 days before the experiments. Group assignments were based on their baseline body weights, and mice were typically housed in groups, except otherwise specified. In the mouse studies, no typical side effects such as vomiting, diarrhoea, constipation or physical activity behaviour were noted.

In an 8-week feasibility study, we investigated the potential impact of two doses of RT strain on glucose tolerance in mice, all of which were 8 weeks old at the start of the intervention. The mice that were fed with normal chow diet (63.9% kcal% carbohydrate, 20.3% kcal% protein and 15.8% kcal% fat) were randomized into groups of 3 or 4 mice. They were administered oral gavage twice weekly (3–4 days apart), with sterile PBS containing 10% glycerol, live RT2 at doses of 5×10^7 (low dose) and 5×10^8 (high dose) CFU per 100 µl in sterile PBS containing 10% glycerol and heat-killed RT2 at a dose of 5×10^8 CFU per 100 µl in sterile PBS containing 10% glycerol, respectively. At week 7 of the experiment, an intraperitoneal glucose tolerance test (ipGTT) was performed. The mice were fasted for 4 h followed by an intraperitoneal injection of glucose (2 g kg^{-1} body weight) dissolved in sterile PBS. Blood samples from the tail vein were taken at $t = 0, 30, 60, 90$ and 120 min for measurement of blood glucose applying glucose strips (Bayer, 84167836) and a CONTOUR NEXT EZ meter. All measures were performed on the regular laboratory bench to avoid noise and additional stress to the mice.

In the intervention testing the effect of the RT strain at 5×10^9 CFU per 100 µl in sterile PBS containing 10% glycerol, 8-week-old mice were randomized to groups of 8–10 mice. The mice were then fed a high-fat diet (HFD, 45% kcal% fat, 35% kcal% carbohydrate and 20% kcal% protein; Research Diet D12451i) and provided purified water ad libitum. For 8 weeks, the animals received oral gavage twice weekly (3–4 days apart) with either sterile PBS containing 10% glycerol, live RT2 or heat-killed RT2 at 5×10^9 CFU per 100 µl in sterile PBS with 10% glycerol. At week 7 of the experiment, an ipGTT was performed. Faecal samples were collected before gavage and at the end of the experiment, then immediately stored at −80 °C until further analysis. Body weights were recorded using Analytical Balance Kern ADB 200-4 weight scales. Lean and fat mass were determined by quantitative magnetic resonance using Echo-MRI 4-in-1 Body Composition Analyser (EchoMRI) at week 6.

At the end of each mouse study, the animals were fasted for 4 h and euthanized with cervical dislocation. Depending on the specific study objective, various tissues (liver, brown adipose tissue, inguinal white adipose tissue and epididymal white adipose tissue) were immediately dissected on ice. The mass of the freshly dissected inguinal or epididymal fat tissues was recorded using Analytical Balance Kern ADB 200-4 weight scales. Inguinal white adipose tissue depots were fixed in 4% paraformaldehyde and 1× PBS overnight at 4 °C, followed by immersion into ethanol (100% w/v) for 24 h before paraffin embedding. The remaining tissues were stored at −80 °C for further analysis. For the determination of adipocyte size, adipose tissue paraffin sections were stained with haematoxylin and eosin (H&E staining; $n = 3$ in each of the three groups). Images were obtained under bright-field microscopy with ×100 magnification. A representative image for each group was shown in our study. Fat cell size was quantified and compared in the three intervention groups using AdipoCount[51], which is an automated system for counting adipocytes, using image processing algorithms to greatly enhance the efficiency of adipocyte quantification. Femurs were precisely dissected and fixed in 4% paraformaldehyde and 1× PBS at 4 °C before the microcomputed tomography (micro-CT) analysis. Faecal samples from the mice were collected before they were killed. Microbial DNA extraction and qPCR assay were performed as previously described using primer pairs specifically targeting the RORDEP1 gene (Supplementary Table 10) for the assessment of the engraftment of RT2 after the intervention.

For mRNA expression analysis by qPCR of thermogenesis, browning and inflammation markers, tissue samples were homogenized with a steel bead (Qiagen, 69989) and 500 µl of QIAzol Lysis Reagent (Qiagen, 79306) per 50 mg of frozen tissue. Post-homogenization, the samples were centrifuged at 12,000 *g* for 15 min at 4 °C, and the supernatant was collected. RNA was extracted according to the instructions provided by the manufacturer of the RNeasy mini kit (Qiagen, 74106), followed by measurements of RNA purities and concentrations by NanoDrop 2000/2000c spectrophotometers (Thermo Fisher, ND2000CLAPTOP). Reverse transcription was done on RNA (1 µg) from last step using the High-Capacity RNA-to-cDNA Kit (Thermo Fisher Scientific, 10704217), following the provided protocol and heating process. The resulting cDNA was then analysed by real-time PCR using the LightCycler 480 System (Roche Diagnostics), combined with Precision PLUS Master Mix (Primer Design, PPLUS- Roche Diagnostics). For each gene of interest, the PCR was performed in white 384-well plates, using the ΔΔCt method to quantify RNA expression levels. Primer sequences for the qPCR are listed in Supplementary Table 10.

Proteins were extracted from 50–100 mg of brown adipose tissue using RIPA lysis buffer (Millipore, 20-188) with added protease inhibitor (Thermo Fisher Scientific, A32953). Protein concentrations were quantified using the Pierce BCA Protein Assay kit (Thermo Fisher Scientific, A55864). The proteins were then diluted with 4× Laemmli protein sample buffer (Bio-Rad, 1610747), heated at 95 °C for 5 min and

separated on a 4–15% Criterion TGX Precast Midi Protein Gel (Bio-Rad, 5671084). For immunoblotting, anti-UCP1 (Abcam, ab10983) and anti-β-actin antibodies (Abcam, ab115777) were used, the latter serving as the housekeeping control. The Gel Doc XR+ System (Bio-Rad) was used to visualize the membranes according to the guides from Bio-Rad.

High-resolution desktop microcomputed tomography imaging (Bruker, Skyscan 1172) was applied for micro-CT analysis of mouse distal femurs of HFD-fed mice. The parameters for the scan are as follows: X-ray voltage of 50 kV, X-ray current of 200 µA, filter of 0.5 mm aluminium, image pixel size of 4–5 µm, camera resolution of 1,280 pixel field width, tomographic rotation of 180°/360°, rotation step of 0.3–0.5°, frame averaging of 1–2 and scan duration of 30–50 min. The cortical boundaries (metaphyseal–diaphyseal) were selected with reference to the growth plate. A cross-sectional slice was selected as a growth plate reference slice, in the following way: moving slice by slice towards the growth plate from the metaphysis–diaphysis, a point is reached where a clear 'bridge' of low-density cartilage (chondrocyte seam) becomes established from one corner of the cross-section to another. This bridge is established by the disappearance of the last band of fine primary spongiosa bone interrupting the chondrocyte seam. This landmark allows a reference level to be defined for the growth plate: cortical volumes of interest are then defined relative to this reference level. The cortical region commenced about 2.15 mm (500 image slices) from the growth plate level in the direction of the metaphysis and extended from this position for a further 0.43 mm (100 image slices). Three-dimensional (3D) morphometric parameters were calculated for the cortical selected regions of interest. The 3D parameters were based on the analysis of a marching-cubes-type model with a rendered surface. Structure thickness in 3D was calculated using the local thickness or 'sphere-fitting' method, and the structure model index (an indicator of the relative prevalence of plates and rods) was derived according to the method of Hildebrand and Ruegsegger. The degree of anisotropy was calculated by the mean intercept method. Rendered 3D models were constructed for 3D viewing of cortical analysed regions. Model construction was by the 'double time cubes' method, a modification of the marching cubes method. The 3D cortical thicknesses (Ct.Th, mm) of the femurs collected from the HFD-fed mice were compared in this study.

The intervention testing the effects of the engineered EcN strains included 24 HFD-fed DIO mice, aged 20 weeks (initial 8 weeks of age plus 12 weeks on the HFD). Each mouse was single housed. From acclimatization to the end of the intervention, the mice were fed a HFD (60% kcal% fat, 20% kcal% carbohydrate and 20% kcal% protein; Research Diets, D12492i) and provided purified water ad libitum. Body weight was recorded in the morning of every third day on a Precision Scale KERN EMB weight scale. On day −4 of the study (the 13th day of acclimatization), regular water was replaced with streptomycin water (5 g l^{-1}). On day 0 of the study, faecal samples were collected from each mouse. This marked the beginning of a 4-day oral gavage intervention (days 0–3 of the study, 100 µl of the engineered strains (5×10^{10} CFU per 100 µl)) with freshly prepared EcN strains administered daily. On day 4, post-gavage, additional faecal samples were collected and analysed to confirm stable colonization. To monitor the engraftment during and at the end of the study, faeces and intestinal contents were collected and dissolved in a pre-weighted 1.5 ml Dulbecco's PBS solution (pH 7.0–7.3, Gibco, 14190144) on ice and manually homogenized. The weight of faecal sample was recorded. Solids were spun down at 500 *g* and the supernatants (in two technical replicates) were serially diluted (10^8 dilution) in the same solvent. Dilutions were spotted on lysogeny broth agar supplemented with 50 µg ml^{-1} streptomycin and 50 µg ml^{-1} kanamycin. After an overnight incubation at 37 °C, engraftment was estimated as CFU ml^{-1} per gram of faeces. On day 20, the mice underwent an ipGTT. On day 21 of the study, the mice were euthanized in a 4–6-h fasted state. Blood, tissue and intestinal contents were collected for further analysis.

Effects on expression thermogenesis marker genes (inguinal white adipose tissue) following daily intraperitoneal injections of r-RORDEP1, r-RORDEP2 (both at 1 mg kg^{-1} body weight) or physiological saline for 7 days were explored in mice fed with chow diet at the age of 8 weeks ($n = 6$ mice per group). Tissues were collected on ice at the time of death of the mice and stored at −80 °C until analyses. The mRNA levels of indicated genes were analysed by qPCR as described in the gene expression analysis above.

To investigate the impact of r-RORDEP1 in regulating blood glucose in the diabetic mouse model, male BKS-Leprdb/db/JOrlRj mice (*Mus musculus*) were obtained from Janvier Laboratories at 8 weeks of age, with initial body weights ranging from 30 g to 45 g. Upon arrival, the mice were singly housed to meet scientific requirements and were maintained on a Purina 5008 (FormuLab Diet) regimen. After a 2-week acclimation period, the study commenced when the mice reached 10 weeks of age. All animals were kept under a controlled 12:12-h light–dark cycle, with lights turned off at 3 pm daily. Before treatment, mice underwent randomization based on their 4-h fasted blood glucose levels measured 3 days before the study (day −3). Only mice showing fasting blood glucose concentrations exceeding 10 mM were included. These mice were then assigned to receive daily intraperitoneal injections of r-RORDEP1 at a dosage of 2 mg kg^{-1} or PBS as a control for a duration of 10 days ($n = 6$ or 7 per group). Throughout the treatment period, body weights and blood glucose levels were monitored to assess metabolic changes. On day 11, an IPGTT was performed to evaluate glucose tolerance.

In the comparative study of the effects of r-RORDEP1 and scrambled r-RORDEP1 on glucose tolerance, the scrambled r-RORDEP1 sequence was generated using GenScript's peptide screening tools (https://www.genscript.com/peptide_screening_tools.html), in which permutations of the original RORDEP1 amino acid sequence were performed to create multiple scrambled variants. The final scrambled sequence, illustrated in Extended Data Fig. 7a, was selected based on its maintained similarity in identity, secondary structure, hydrophobicity and water solubility to the native r-RORDEP1, as shown in Extended Data Fig. 7b. The scrambled RORDEP1 was recombinantly synthesized using the pET30a expression vector with NdeI (CATATG) and HindIII (AAGCTT) restriction sites, without biotinylation, using an identical expression protocol as used for r-RORDEP1. A total of 45 male C57BL/6J mice at 8 weeks of age were obtained from Gempharmatech. Upon arrival, the mice were singly housed in cages with unique cage numbers for identification. The housing environment was maintained under specific pathogen-free conditions with controlled temperature (20–24 °C) and relative humidity (30–70%), monitored daily. An electronic lighting system provided a 12-h light and 12-h dark cycle. Enrichment toys were supplied to promote well-being. Mice had ad libitum access to a standard chow diet and fresh water. The animals were acclimated in the testing facility for 2 weeks before the study. After acclimation, 36 mice were selected based on body weight and fasting blood glucose levels and randomly assigned to 3 groups of 12 mice each. The groups included a vehicle control group receiving PBS, a group receiving r-RORDEP1 at a dose of 1 mg kg^{-1} and a group receiving scrambled RORDEP1 at the same dose. On day 1, following a 6-h fasting period, each mouse received an oral glucose load of 2 g kg^{-1} body weight. Immediately thereafter, the mice were administered their respective treatments via intraperitoneal injection according to the dosing protocol. Tail vein blood glucose levels were measured at 0 (baseline), 30, 60 and 120 min post-glucose load using a hand-held glucometer (Lifescan, Johnson & Johnson Medical Equipment). Measurements were performed in duplicate at each timepoint for each mouse to ensure accuracy, and the mean value was used for further analysis.

In the assessment of the plasma half-life of r-RORDEP1, 8-week-old chow-diet-fed lean male C57BL/6J mice ($n = 4$ per group) were intraperitoneally injected with either r-RORDEP1 (1 mg kg^{-1}) or sterilized PBS, and blood was collected from the tail vein at indicated timepoints.

The r-RORDEP1 in plasma was measured by immunoblotting, using an anti-His-Tag Antibody (Cell Signal Technology, 2365) to detect the 6×His-tag on r-RORDEP1. The pixel intensity of the immunoblotting bands of 6×His-tag RORDEP1 and the adjacent background were measured using ImageJ[52].

Experiments in rats

All rat experiments were conducted in accordance with national and international guidelines for the care and use of laboratory animals and were approved by the relevant regulatory authorities. Studies involving intravenous infusion (approval ID: 2023-15-0201-01508) and assessment of r-RORDEP1 effects on incretin release (approval ID: 2023-15-0201-01393) in rats were approved by the Danish Animal Experimentation Council. The intraduodenal infusion study was reviewed and approved by the Animal Ethics Committee of Chongqing Medical University (approval ID: IACUC-CQMU-2024-0036).

In the intravenous infusion study testing the effect of r-RORDEP1 on glucose homeostasis in rats, 12 male lean chow-fed 8-week-old Sprague Dawley rats were randomized based on body weight (measured on study day −7). In study week −1, intravenous (IV) catheters were implanted in the jugular vein (for infusion) and carotid artery (for blood sampling). On study day 1, the rats were infused with either vehicle (PBS) or r-RORDEP1 (200 pmol kg^{-1} min^{-1}) at a flow rate of 0.25 ml h^{-1}. Blood glucose concentration was measured at t = 0, 15, 30, 60, 90, 120 and 180 min.

To assess the impact of r-RORDEP1 on rat incretin release, 48 8-week-old lean male Sprague Dawley rats were randomly assigned to 4 groups, with 12 rats per group. Each rat received an oral glucose load of 1 g kg^{-1}, administered over a 2-min period. Immediately following glucose administration, rats in the two experimental groups were intraperitoneally injected with r-RORDEP1 at a dosage of 0.8 mg kg^{-1}. By contrast, rats in the two control groups received an equivalent volume of PBS as a vehicle control. Blood glucose levels were measured at baseline, 30 min and 45 min post-glucose administration to evaluate the glycaemic response. At designated timepoints of either 30 min or 45 min after glucose administration, rats were humanely killed. Cardiac blood was collected using a syringe and transferred into Microvette/Vacuette tubes containing an anticoagulant. To preserve the integrity of the analytes, dipeptidyl peptidase-4 and protease inhibitors were added to the blood samples immediately upon collection. The tubes were then inverted five times to ensure thorough mixing and kept at 4 °C until centrifugation at 3,000 g for 10 min. Following centrifugation, plasma supernatants were carefully transferred to new tubes and promptly frozen on dry ice. The plasma samples were subsequently stored at −70 °C until further analysis. Incretin hormones, including GIP, GLP1 and PYY, insulin, and glucagon were quantified using ELISA-based methods. Specifically, rat plasma GIP levels were measured following the manufacturer's protocol using the Rat/Mouse GIP (Total) ELISA kit (EZRMGIP-55K; Merck Millipore), while the plasma GLP1 levels were quantified using the MSD V-PLEX Plus GLP1 Total Kit (catalogue number K1503PG). PYY concentrations were determined using a commercially available ELISA kit (Alpco, Mouse/Rat PYY ELISA, catalogue number 48-PYYRT-E01.1). Rat insulin levels were measured using a homogeneous LOCI/AlphaLISA assay. This assay involved the formation of a concentration-dependent bead–analyte–immune complex, resulting in luminescent output measured using a PerkinElmer Envision reader. The assay used anti-rat insulin monoclonal antibody D3E7-conjugated acceptor beads and biotinylated monoclonal antibody D6C4, both specific to rat insulin, in conjunction with generic streptavidin-coated donor beads. Rat glucagon levels were assessed using LOCI/AlphaLISA technology, similarly forming bead–analyte–immune complexes that emit luminescence measured by the PerkinElmer Envision reader. The assay used in-house-produced anti-glucagon monoclonal antibody GLU 1F20-conjugated acceptor beads and biotinylated monoclonal antibody GLU 2F7, both targeting glucagon, along with generic streptavidin-coated donor beads.

In the duodenal infusion study, we applied the following protocol: male Sprague Dawley rats, 9 weeks old and weighing around 300 g, were purchased from the Experimental Animal Center of Chongqing Medical University. During the experiments, rats were housed on a 12-h light and 12-h dark cycle with ad libitum access to purified water and a rodent chow diet (63.9% kcal% carbohydrate, 20.3% kcal% protein and 15.8% kcal% fat). All rats were acclimatized to the environment for 7 days before any designated surgical procedures.

On day 1, duodenal cannulations were performed in rats as previously reported[53]. In brief, a catheter was inserted into the proximal duodenum (approximately 1.5–2 cm downstream of the pyloric sphincter) and indwelling catheters were placed into the internal jugular vein for duodenum infusion, and intravenous infusion, respectively. Recovery from surgery was estimated by monitoring a normalization of food intake and body weight stabilization to pre-surgery levels. To ensure similar nutritional status, rats were restricted to 20 g of food on the night preceding the euglycaemic pancreatic clamp experiments. Rats were randomized into six different intervention groups, each consisting of six animals. On day 5 after surgery, a euglycaemic pancreatic clamp was performed for 4 h. In the euglycaemic pancreatic clamp, endogenous secretion of insulin and glucagon is suppressed by intravenous infusion of somatostatin while blood glucose is maintained at euglycaemia and plasma insulin is kept constant at study basal level by continuous infusion of exogenous insulin. An infusion of concentrated glucose is given intravenously, the infusion rate being dynamically regulated according to frequent monitoring of blood glucose. Thus, continuous intravenous infusions of somatostatin (at 3 μg kg^{-1} min^{-1}, Kunming Jida Pharmaceutical) and short-acting human insulin (at 1.2 mU kg^{-1} min^{-1}, Novolin R, Novo Nordisk) via the right internal jugular vein were given from t = 0–240 min. r-RORDEP1 was administered through duodenal infusion with infusion rates of 0, 60, 90, 120, 150 and 200 pmol kg^{-1} min^{-1}, respectively at t = 60–240 min of the euglycaemic pancreatic clamp. Blood samples from the tail vein were taken every 10 min for measurement of blood glucose using a portable glucometer. To maintain blood glucose at normoglycaemia, 25% (w/v) glucose solution was infused at the dynamic infusion rate of t = 0–240 min.

To explore the impact of r-RORDEP1 on blood glucose control and liver transcriptomic and proteomic alterations under physiological conditions, we administered r-RORDEP1 via intraduodenal infusion at a rate of 200 pmol kg^{-1} min^{-1} for 3 h. Blood glucose levels were measured before and after infusion (t = 0 and 180 min). Following the infusion, rats were euthanized, and liver tissues were harvested for bulk RNA sequencing analysis, bulk proteomics and phosphoproteomics analyses.

Total RNA was extracted from tissues using Trizol (Invitrogen) according to manual instructions. Subsequently, total RNA was qualified and quantified using a NanoDrop and Agilent 2100 bioanalyzer (Thermo Fisher Scientific). The RNA library construction and subsequent RNA sequencing were performed by BGI-Shenzhen, China. First-strand cDNA was generated using random hexamer-primed reverse transcription, followed by a second-strand cDNA synthesis. Afterwards, A-Tailing Mix and RNA Index Adapters were added by incubating to end repair. The cDNA fragments obtained from the previous step were amplified by PCR, and products were purified by Ampure XP Beads, then dissolved in EB solution. The product was validated on the Agilent Technologies 2100 bioanalyzer for quality control. The double-stranded PCR products from the previous step were heated, denatured and circularized by the splint oligo sequence to get the final library. The single-strand circle DNA (ssCir DNA) was formatted as the final library. The final library was amplified with phi29 to make DNA nanoballs, which had more than 300 copies of one molecule, DNA nanoballs were loaded into the patterned nanoarray, and single-end 50-base reads were generated on the BGIseq500 platform (BGI).

The sequencing data were filtered with SOAPnuke (v1.5.2), and the clean reads were mapped to the reference genome of the

GCF_000001895.5_Rnor_6.0 genome using HISAT2 (v2.0.4). Bowtie2 (v2.2.5) was applied to align the clean reads to the reference coding gene set, then expression level of gene was calculated by RSEM (v1.2.12).

Downstream analysis of RNA sequencing data was executed using an in-house-developed script in Rstudio (v4.3.0). In multivariate statistical analysis, dimensionality reduction was conducted via principal component analysis (PCA) using the 'prcomp' function in R (v4.3.0). This facilitated the discrimination of sample clusters and identification of outliers. Prior to PCA, a variance stabilizing transformation was applied to normalize count data distribution across samples, ensuring PCA outputs more accurately reflected biological rather than extreme values introduced by technical variance. Univariate statistical differential analysis was quantified using DESeq2 (v1.40.2). The 'lfcShrink' function of DESeq2 invoked the adaptive shrinkage method to mitigate the impact of low counts and high variance on $\log_2$(fold change) estimates. All reported fold changes were thus shrunken $\log_2$ values, with differentially expressed genes defined by an adjusted $P \leq 0.05$ and an absolute $\log_2$(fold change) over 1. For the data processing and visualization, packaged including dplyr (v1.1.4) and tidyr (v1.3.0) and ggplot2 (v3.4.4) were used.

In the sample preparation for bulk proteomics and phosphoproteomics analyses, rat liver tissues were collected following a 3-h intraduodenal infusion of r-RORDEP1. Approximately 10–25 mg of liver tissue was used for each sample. The tissues were transferred into 2-ml centrifuge tubes containing two steel beads. For proteomics samples, 10 mg of tissue was homogenized in an appropriate volume of SDS L3 lysis buffer supplemented with a 1× protease inhibitor cocktail containing EDTA. For phosphoproteomics samples, 25 mg of tissue was homogenized in 300 µl of Milli-Q water. Homogenization was performed using a grinder.

For proteomics samples, the homogenate was centrifuged at 25,000 *g* for 15 min at 4 °C to collect the supernatant. DTT was added to the supernatant to a final concentration of 10 mM, and the samples were incubated in a water bath at 37 °C for 30 min. For phosphoproteomics samples, 50 µl of 10% SDS was added to the homogenate, followed by DTT, to a final concentration of 10 mM. The samples were incubated at 95 °C in a metal bath for 10 min.

Subsequent steps were identical for both sample types. Iodoacetamide was added to each sample to a final concentration of 55 mM, and the mixtures were incubated in the dark for 45 min. Proteins were precipitated by adding cold acetone at a ratio of 1:5 (protein solution) and incubating at −20 °C for 2 h. The precipitated proteins were collected by centrifugation at 25,000 *g* for 15 min at 4 °C, and the supernatant was discarded. The protein pellets were air-dried and resuspended in an appropriate volume of SDS-free lysis buffer L3. The samples were homogenized again using a grinder to promote protein solubilization. Finally, the samples were centrifuged at 25,000 *g* for 15 min at 4 °C, and the supernatants containing the protein solutions were collected. Protein concentrations were measured using the Bradford assay.

For each sample, 100 µg of protein solution was diluted fourfold with 50 mM ammonium bicarbonate (NH_4HCO_3). Trypsin was added at a protein-to-enzyme ratio of 40:1 (2.5 µg of trypsin per 100 µg of protein), and the mixtures were incubated for digestion at 37 °C for 4 h. The resulting peptides were desalted using Strata X columns and vacuum dried.

For library generation, a high-pH reverse-phase fractionation was performed. Equal amounts of peptides from all samples were pooled and diluted with mobile phase A (5% ACN, pH 9.8). The pooled sample was subjected to high-pH reverse-phase chromatography using a Shimadzu LC-20AB HPLC system coupled with a Gemini C18 column (5 µm, 4.6 × 250 mm). Peptide separation was performed at a flow rate of 1 ml min^{-1} using the following gradient: 5% mobile phase B (95% ACN, pH 9.8) for 10 min; 5% to 35% B over 40 min; 35% to 95% B over 1 min; maintained at 95% B for 3 min; and equilibrated at 5% B for 10 min. The elution was monitored at 214 nm, and fractions were collected every minute. Ten fractions were combined and freeze-dried.

The LC–MS/MS analysis involved two main steps: data-dependent acquisition (DDA) for spectral library construction and DIA for peptide quantification. The nano-LC protocol used for both DDA and DIA modes was identical. Dried peptide samples were reconstituted in mobile phase A (2% acetonitrile, 0.1% FA) and centrifuged. The supernatants were injected into an ultra-high-performance liquid chromatography system for separation. Peptides were first trapped and desalted on a pre-column, then separated on an analytical column at a flow rate of 500 nL/min using a specified gradient.

For DDA library construction in bulk proteomics analysis, peptides were ionized using a nano-electrospray ionization source and analysed on an Orbitrap Exploris 480 mass spectrometer operated in DDA mode. Mass spectrometry parameters were optimized to enhance peptide identification. For DIA quantification, the mass spectrometer was operated in DIA mode to acquire comprehensive peptide ion data across the mass range. Instrument settings were adjusted to achieve high-resolution MS/MS scans suitable for accurate quantification.

In the phosphoproteomics analysis, the separated peptides were analysed using a timsTOF Pro mass spectrometer (Bruker Daltonics) operated in DDA mode for spectral library construction. This instrument combines trapped ion mobility spectrometry with time-of-flight mass spectrometry, providing enhanced separation and identification of phosphopeptides due to its high-resolution and ion mobility capabilities. Specific acquisition parameters were optimized to maximize the detection and characterization of phosphorylated peptides.

DDA data were processed using the Andromeda search engine within MaxQuant software to identify peptides and proteins, constructing spectral libraries for both bulk proteomics and phosphoproteomics analyses. DIA data were analysed using retention time calibration with indexed retention time peptides. A target–decoy approach was used to control the false discovery rate at 1%, ensuring reliable identification and quantification.

For phosphoproteomics data, phosphorylation sites were filtered based on the localization probability reported by MaxQuant, retaining only those sites with a localization probability of at least 0.75 to ensure confidence in site-specific phosphorylation analysis.

Differential expression analysis was conducted using the MSstats package in R, which applies a linear mixed-effects model to evaluate significant differences in protein or phosphoprotein abundance between samples. Data were preprocessed according to predefined comparison groups, and significance testing was performed based on the model. Proteins and phosphoproteins with an adjusted *P* value of less than 0.05 were considered significantly differentially expressed.

Lastly, to further evaluate the effect of r-RORDEP1 on glucose metabolism in vivo, titrated glucose was used as a tracer to observe alterations in hepatic glucose production and peripheral glucose disposal in a separate experiment under euglycaemic pancreatic clamp. [3-H^3]-glucose was administered with a primary intravenous bolus of 6 µCi at time 0 min followed by a continuous intravenous infusion of 0.2 µCi min^{-1} throughout the experiment of 240 min via the right internal jugular vein. Recombinant RORDEP1 at a rate of 200 pmol kg^{-1} min^{-1} or PBS was infused into the duodenum from 0 to 240 min. Blood sampling was performed from the carotid artery at $t = 60–90$ and $t = 220–240$ min. These samples were subsequently centrifuged to separate plasma and stored at −80 °C for the analysis of [3-H^3]-glucose specific activity. Hepatic glucose production rate and whole-body glucose uptake rate were calculated using specific activity of the [3-H^3]-glucose and the recordings of the dynamic 25% glucose infusion rates[54].

The tracer dilution principle is central to the isotope calculations. When introducing a known quantity of a labelled tracer (in case, [3-H^3]-glucose) into the bloodstream, it mixes with the body's existing glucose. As the body produces glucose (endogenous glucose production) plus exogenous infusion of glucose, these glucose compartments dilute the concentration of the labelled tracer in the blood. In the steady

phase of a euglycaemic pancreatic clamp, the rate of this dilution reflects the rate of endogenous glucose production plus exogenous infusion of glucose. The equal removal of labelled and unlabelled glucose from the bloodstream by tissue uptake minimally affected the dilution of the labelled tracer.

Thus, the calculation of hepatic gluconeogenesis was based on three formulas: formula 1, calculation of the glucose appearance rate as the sum of endogenous glucose production and glucose infusion rate; formula 2, equation of the glucose appearance rate to the glucose disappearance rate, equal to the glucose uptake rate; and formula 3, estimation of the tracer infusion rate ÷ glucose appearance rate = specific activity of the tracer in blood. In formula 3, the tracer infusion rate is the known component at which we infused the isotope-labelled glucose into the bloodstream. Specific activity is defined as the ratio of the labelled glucose ([3-H^3]-glucose) to the total amount of the glucose (both labelled and unlabelled glucose) in the blood.

Finally, the following two formulas were used in the calculation of the whole-body glucose uptake rate and hepatic glucose production: (1) the whole-body glucose uptake rate was calculated as tracer infusion rate ÷ specific activity of [3-H^3]-glucose in blood and (2) the HGP rate was calculated as whole-body glucose uptake rate ÷ glucose infusion rate.

Statistical analysis

All the presented data were obtained from biologically independent samples. Graphing and statistical analysis were performed using GraphPad Prism (version 10.1.0). Area under the curve (AUC) was calculated using the composite trapezoidal method as described previously[55]. Full descriptions of statistical tests were provided in the figure legends. For two-group comparisons, two-tailed Student's *t*-test was applied. For multiple group comparisons, one-way ANOVA was performed. For comparisons at each timepoint, two-way ANOVA was used, followed by correction for multiple testing. Data were presented as mean ± s.e.m. unless otherwise stated. *P* values less than 0.05 were considered statistically significant.

Reporting summary

Further information on research design is available in the Nature Portfolio Reporting Summary linked to this article.

Data availability

Anonymized clinical data of participants included in this study are provided in Supplementary Tables 6 and 7. Raw proteomics data that support the findings of this study have been deposited in the ProteomeXchange Consortium with the dataset identifier PXD057146 (human plasma) and MassIVE database (https://massive.ucsd.edu) with identifiers MSV000093785 (bacterial supernatants) and MSV000097951 (rat liver). The raw RNA-seq reads of rat liver tissue are available at the European Nucleotide Archive with accession number PRJEB89704. The predicted protein structure of RUMTOR_00181 is available at AlphaFold Protein Structure Database via identifier A5KIY5. Source data are provided with this paper.

Code availability

Code associated with the data analysis and visualization is available via GitHub at https://github.com/fjw536/RORDEP.

References

1. Ley, R. E., Peterson, D. A. & Gordon, J. I. Ecological and evolutionary forces shaping microbial diversity in the human intestine. *Cell* **124**, 837–848 (2006).
2. Gilbert, J. A. et al. Current understanding of the human microbiome. *Nat. Med.* **24**, 392–400 (2018).
3. Fischbach, M. A. Microbiome: focus on causation and mechanism. *Cell* **174**, 785–790 (2018).
4. Sberro, H. et al. Large-scale analyses of human microbiomes reveal thousands of small, novel genes. *Cell* **178**, 1245–1259.e14 (2019).
5. Minot, S. et al. The human gut virome: inter-individual variation and dynamic response to diet. *Genome Res.* **21**, 1616–1625 (2011).
6. Zou, Y. et al. 1,520 reference genomes from cultivated human gut bacteria enable functional microbiome analyses. *Nat. Biotechnol.* **37**, 179–185 (2019).
7. Almeida, A. et al. A new genomic blueprint of the human gut microbiota. *Nature* **568**, 499–504 (2019).
8. Ma, Y. et al. Identification of antimicrobial peptides from the human gut microbiome using deep learning. *Nat. Biotechnol.* **40**, 921–931 (2022).
9. Donia, M. S. et al. A systematic analysis of biosynthetic gene clusters in the human microbiome reveals a common family of antibiotics. *Cell* **158**, 1402–1414 (2014).
10. Cohen, L. J. et al. Commensal bacteria make GPCR ligands that mimic human signalling molecules. *Nature* **549**, 48–53 (2017).
11. Pujo, J. et al. Bacteria-derived long chain fatty acid exhibits anti-inflammatory properties in colitis. *Gut* **70**, 1088–1097 (2021).
12. Bae, M. et al. *Akkermansia muciniphila* phospholipid induces homeostatic immune responses. *Nature* **608**, 168–173 (2022).
13. Yoon, H. S. et al. *Akkermansia muciniphila* secretes a glucagon-like peptide-1-inducing protein that improves glucose homeostasis and ameliorates metabolic disease in mice. *Nat. Microbiol.* **6**, 563–573 (2021).
14. Plovier, H. et al. A purified membrane protein from *Akkermansia muciniphila* or the pasteurized bacterium improves metabolism in obese and diabetic mice. *Nat. Med.* **23**, 107–113 (2017).
15. Altindis, E. et al. Viral insulin-like peptides activate human insulin and IGF-1 receptor signaling: a paradigm shift for host–microbe interactions. *Proc. Natl Acad. Sci. USA* **115**, 2461–2466 (2018).
16. Qiang, X. et al. New melanocortin-like peptide of *E. coli* can suppress inflammation via the mammalian melanocortin-1 receptor (MC1R): possible endocrine-like function for microbes of the gut. *NPJ Biofilms Microbiomes* **3**, 31 (2017).
17. Quévrain, E. et al. Identification of an anti-inflammatory protein from *Faecalibacterium prausnitzii*, a commensal bacterium deficient in Crohn's disease. *Gut* **65**, 415–425 (2016).
18. Fan, Y. & Pedersen, O. Gut microbiota in human metabolic health and disease. *Nat. Rev. Microbiol.* **19**, 55–71 (2021).
19. Valentino, V., De Filippis, F., Marotta, R., Pasolli, E. & Ercolini, D. Genomic features and prevalence of *Ruminococcus* species in humans are associated with age, lifestyle, and disease. *Cell Rep.* **43**, 115018 (2024).
20. Vidal-Veuthey, B., González, D. & Cárdenas, J. P. Role of microbial secreted proteins in gut microbiota–host interactions. *Front. Cell Infect. Microbiol.* **12**, 964710 (2022).
21. Visconti, A. et al. Interplay between the human gut microbiome and host metabolism. *Nat. Commun.* **10**, 4505 (2019).
22. Boström, P. et al. A PGC1-α-dependent myokine that drives brown-fat-like development of white fat and thermogenesis. *Nature* **481**, 463–468 (2012).
23. O'Leary, N. A. et al. Reference sequence (RefSeq) database at NCBI: current status, taxonomic expansion, and functional annotation. *Nucleic Acids Res.* **44**, D733–D745 (2016).
24. Kraal, L., Abubucker, S., Kota, K., Fischbach, M. A. & Mitreva, M. The prevalence of species and strains in the human microbiome: a resource for experimental efforts. *PLoS ONE* **9**, e97279 (2014).
25. Yachida, S. et al. Metagenomic and metabolomic analyses reveal distinct stage-specific phenotypes of the gut microbiota in colorectal cancer. *Nat. Med.* **25**, 968–976 (2019).
26. Wirbel, J. et al. Meta-analysis of fecal metagenomes reveals global microbial signatures that are specific for colorectal cancer. *Nat. Med.* **25**, 679–689 (2019).

27. Hansen, T. H. et al. Impact of a vegan diet on the human salivary microbiota. *Sci. Rep.* **8**, 5847 (2018).
28. Zhernakova, A. et al. Population-based metagenomics analysis reveals markers for gut microbiome composition and diversity. *Science* **352**, 565–569 (2016).
29. Fan, Y. RORDEP: virulence factor mapping results. *GitHub* https://github.com/fjw536/RORDEP/tree/main/Virulence_factor_mapping_results (2025).
30. Kim, H. et al. Irisin mediates effects on bone and fat via αV integrin receptors. *Cell* **175**, 1756–1768.e17 (2018).
31. Turton, M. D. et al. A role for glucagon-like peptide-1 in the central regulation of feeding. *Nature* **379**, 69–72 (1996).
32. Shi, Y.-C. et al. Adult-onset PYY overexpression in mice reduces food intake and increases lipogenic capacity. *Neuropeptides* **46**, 173–182 (2012).
33. Miyawaki, K. et al. Inhibition of gastric inhibitory polypeptide signaling prevents obesity. *Nat. Med.* **8**, 738–742 (2002).
34. Gabe, M. B. N. et al. Human GIP(3-30)NH2 inhibits G protein-dependent as well as G protein-independent signaling and is selective for the GIP receptor with high-affinity binding to primate but not rodent GIP receptors. *Biochem. Pharmacol.* **150**, 97–107 (2018).
35. Véniant, M. M. et al. A GIPR antagonist conjugated to GLP-1 analogues promotes weight loss with improved metabolic parameters in preclinical and phase 1 settings. *Nat. Metab.* **6**, 290–303 (2024).
36. Jumper, J. et al. Highly accurate protein structure prediction with AlphaFold. *Nature* **596**, 583–589 (2021).
37. Chen, L. et al. VFDB: a reference database for bacterial virulence factors. *Nucleic Acids Res.* **33**, D325–D328 (2005).
38. Rawlings, N. D. et al. The MEROPS database of proteolytic enzymes, their substrates and inhibitors in 2017 and a comparison with peptidases in the PANTHER database. *Nucleic Acids Res.* **46**, D624–D632 (2018).
39. Armetta, J. et al. *Escherichia coli* promoters with consistent expression throughout the murine gut. *ACS Synth. Biol.* **10**, 3359–3368 (2021).
40. Tumas, S. et al. Engineered *E. coli* Nissle 1917 for delivery of bioactive IL-2 for cancer immunotherapy. *Sci. Rep.* **13**, 12506 (2023).
41. Dixon, A. S. et al. NanoLuc complementation reporter optimized for accurate measurement of protein interactions in cells. *ACS Chem. Biol.* **11**, 400–408 (2016).
42. Bonde, M. T. et al. Predictable tuning of protein expression in bacteria. *Nat. Methods* **13**, 233–236 (2016).
43. Wirth, N. T., Funk, J., Donati, S. & Nikel, P. I. QurvE: user-friendly software for the analysis of biological growth and fluorescence data. *Nat. Protoc.* **18**, 2401–2403 (2023).
44. Rappsilber, J., Mann, M. & Ishihama, Y. Protocol for micro-purification, enrichment, pre-fractionation and storage of peptides for proteomics using StageTips. *Nat. Protoc.* **2**, 1896–1906 (2007).
45. Matthews, D. R. et al. Homeostasis model assessment: insulin resistance and beta-cell function from fasting plasma glucose and insulin concentrations in man. *Diabetologia* **28**, 412–419 (1985).
46. Thirion, F. et al. The gut microbiota in multiple sclerosis varies with disease activity. *Genome Med.* **15**, 1 (2023).
47. Fan, Y. et al. The gut microbiota contributes to the pathogenesis of anorexia nervosa in humans and mice. *Nat. Microbiol.* **8**, 787–802 (2023).
48. Pasolli, E. et al. Accessible, curated metagenomic data through ExperimentHub. *Nat. Methods* **14**, 1023–1024 (2017).
49. Kremsmayr, T. et al. On the utility of chemical strategies to improve peptide gut stability. *J. Med. Chem.* **65**, 6191–6206 (2022).
50. Srinivasan, B. et al. TEER measurement techniques for in vitro barrier model systems. *J. Lab. Autom.* **20**, 107–126 (2015).
51. Zhi, X. et al. AdipoCount: a new software for automatic adipocyte counting. *Front. Physiol.* **9**, 85 (2018).
52. Schneider, C. A., Rasband, W. S. & Eliceiri, K. W. NIH Image to ImageJ: 25 years of image analysis. *Nat. Methods* **9**, 671–675 (2012).
53. Yang, M. et al. Duodenal GLP-1 signaling regulates hepatic glucose production through a PKC-δ-dependent neurocircuitry. *Cell Death Dis.* **8**, e2609 (2017).
54. Steele, R. Influences of glucose loading and of injected insulin on hepatic glucose output. *Ann. N. Y. Acad. Sci.* **82**, 420–430 (1959).
55. Allison, D. B., Paultre, F., Maggio, C., Mezzitis, N. & Pi-Sunyer, F. X. The use of areas under curves in diabetes research. *Diabetes Care* **18**, 245–250 (1995).

Acknowledgements

The study was supported by Independent Research Fund Denmark with grant number 1030-00123B and Novo Nordisk Foundation (NNF) with grant RUCILP F-19235-01-64-NNF21SA0070428. The Proteomics Research Infrastructure at the University of Copenhagen was supported by the NNF (grant agreement number NNF19SA0059305). The NNF Center for Basic Metabolic Research is an independent research institution at the University of Copenhagen, partially funded by an unrestricted donation from the NNF (NNF18CC0034900). The NNF Center for Biosustainability, Technical University of Denmark, was supported by the NNF under grant number NNF20CC0035580 and the NNF Challenge Programme, CaMiT, under grant agreement NNF17CO0028232. We acknowledge the European Synchrotron Radiation Facility (ESRF) for providing synchrotron radiation facilities, and we thank P. Pernot for assistance and support in using beamline BM29, A. Forman for help in the preparation of various laboratory experiments, O. K. C. Nielsen and N. A. N. Knight for help in performing the bacterial cell culture and microbial genomic DNA extraction, and J. Fels, M. Al Rubai and L. Eriksen from Novo Nordisk A/S for performing ELISA analyses.

Author contributions

O.P.: conceptualization, study design and devices, data interpretation and integration, overall supervision and paper writing. Y.F. and L. Lyu.: computational analyses, most wet laboratory experiments, development of the proteomics assay, all interventions on mice, all data analyses, interpretation and integration, including figure drawings and paper writing. W.Z.: conduction and analyses of all rat experiments. F.Z.: biophysical characterization of RORDEP1 and evaluation of RORDEP1–integrin bindings. C.D.D.C. and L.S.: supervision of hepatocyte studies and plasma incretin measurements. G.Y., L. Li and M.Y.: supervision of experiments on rats and derived data analyses. M.O.A.S.: supervision of GMO experiments. R.V.-U. and A. Koulouktsis: development and conduction of GMO experiments. M.B.: engineering of a GMO. M.W.: supervision and analyses of plasma proteomics data. A. Kulakova and P.H.: small-angle X-ray scattering analysis. T.H.H. and T.N.: phenotyping of human study participants. F.K.K., J.G., T.H.P. and P.R.: analyses and interpretation of preclinical and clinical results. K.S. and V.S.-B.: analyses of preclinical effects of RORDEP1. T.A.: assistance in mouse intervention. E.S.: bacterial cell counting in human faecal samples. All co-authors contributed to the data analyses and contributed substantially in the editing of the final paper.

Competing interests

O.P. and Y.F. are founders of GutCRINE. Currently, L.S., C.D.D.C. and F.Z. are scientists at Novo Nordisk. The other authors declare no competing interests.

Additional information

Extended data is available for this paper at https://doi.org/10.1038/s41564-025-02064-x.

Supplementary information The online version contains supplementary material available at https://doi.org/10.1038/s41564-025-02064-x.

Correspondence and requests for materials should be addressed to Oluf Pedersen.

Peer review information *Nature Microbiology* thanks Patrice Cani and the other, anonymous, reviewer(s) for their contribution to the peer review of this work.

[1]Novo Nordisk Foundation Center for Basic Metabolic Research, Faculty of Health and Medical Science, University of Copenhagen, Copenhagen, Denmark. [2]Department of Medicine, Copenhagen University Hospital—Herlev and Gentofte, Hellerup, Denmark. [3]Novo Nordisk Foundation Center for Biosustainability, Technical University of Denmark, Lyngby, Denmark. [4]Department of Clinical Biochemistry and the Key Laboratory of Laboratory Medical Diagnostics in the Ministry of Education, Chongqing Medical University, Chongqing, China. [5]Department of Endocrinology, the Second Affiliated Hospital, Chongqing Medical University, Chongqing, China. [6]Department of Drug Design and Pharmacology, Faculty of Health and Medical Sciences, University of Copenhagen, Copenhagen, Denmark. [7]Novo Nordisk A/S, Måløv, Denmark. [8]Department of Chemistry, Faculty of Science, University of Copenhagen, Copenhagen, Denmark. [9]Proteomics Research Infrastructure, University of Copenhagen, Copenhagen, Denmark. [10]Center for Clinical Metabolic Research, Copenhagen University Hospital—Herlev and Gentofte, Hellerup, Denmark. [11]Steno Diabetes Center Copenhagen, Herlev, Denmark. [12]Department of Clinical Medicine, Faculty of Health and Medical Sciences, University of Copenhagen, Copenhagen, Denmark. [13]Department of Medicine, Zealand University Hospital, Køge, Denmark. [14]These authors contributed equally: Yong Fan, Liwei Lyu. ✉e-mail: oluf@sund.ku.dk

https://doi.org/10.1038/s41564-025-02064-x

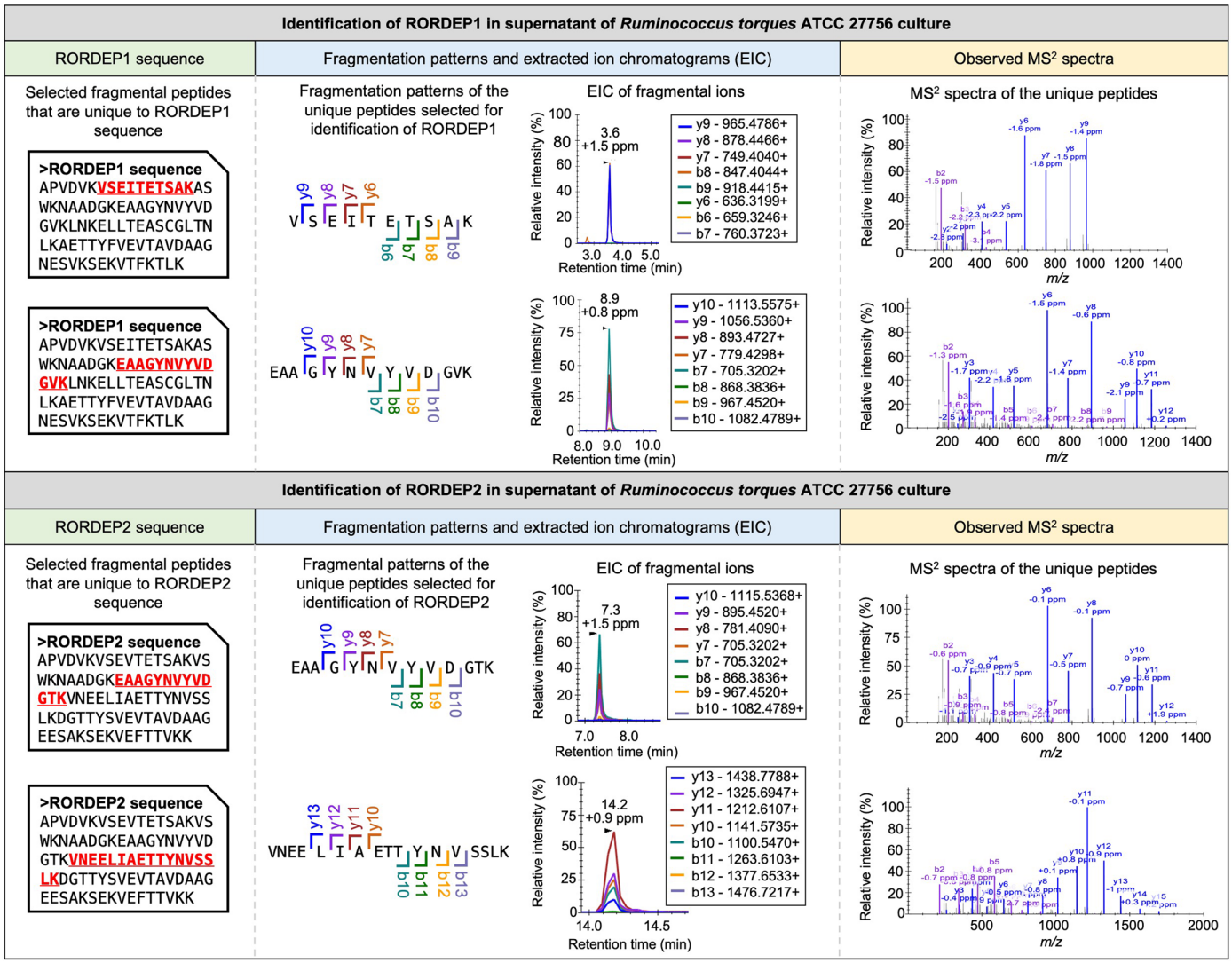

Extended Data Fig. 1 | Proteomics identification of selected proteotypic peptides that are unique to RORDEPs in supernatants of bacterial cultures using liquid chromatography-mass spectrometry (LC-MS). In each panel, the left section displays the selected proteotypic peptides (underscored and highlighted in red) that are unique to sequences of RORDEPs. In the central section, the left graph displays the fragmentation patterns for the unique peptides in the identification of RORDEPs, with b- and y- ions indicating that the fragmentation occurs in a way that the charge is retained on the N-terminus and C-terminus, respectively, of the respective peptide. The b-ions contain the amino-terminal end of the peptides and are numbered starting from the N-terminus (the beginning of the peptide chain). The y-ions contain the carboxyl-terminal end of the peptide and are numbered starting from the C-terminus (the end of the peptide chain). The right graph shows the extracted ion chromatograms (EIC) for b- and y-ions and the retention time for the selected proteotypic peptides in the 3-30 kDa fractions collected from cultural supernatants of RT ATCC 27756 containing RUMTOR_00181. The EICs of b- and y-ions are labeled according to the fragmentation patterns shown in the left section. In the right section, observed tandem mass spectrometry (MS^2) spectra are depicted. The illustrations detail their MS^2 with mass accuracy expressed in parts per million (ppm).

https://doi.org/10.1038/s41564-025-02064-x

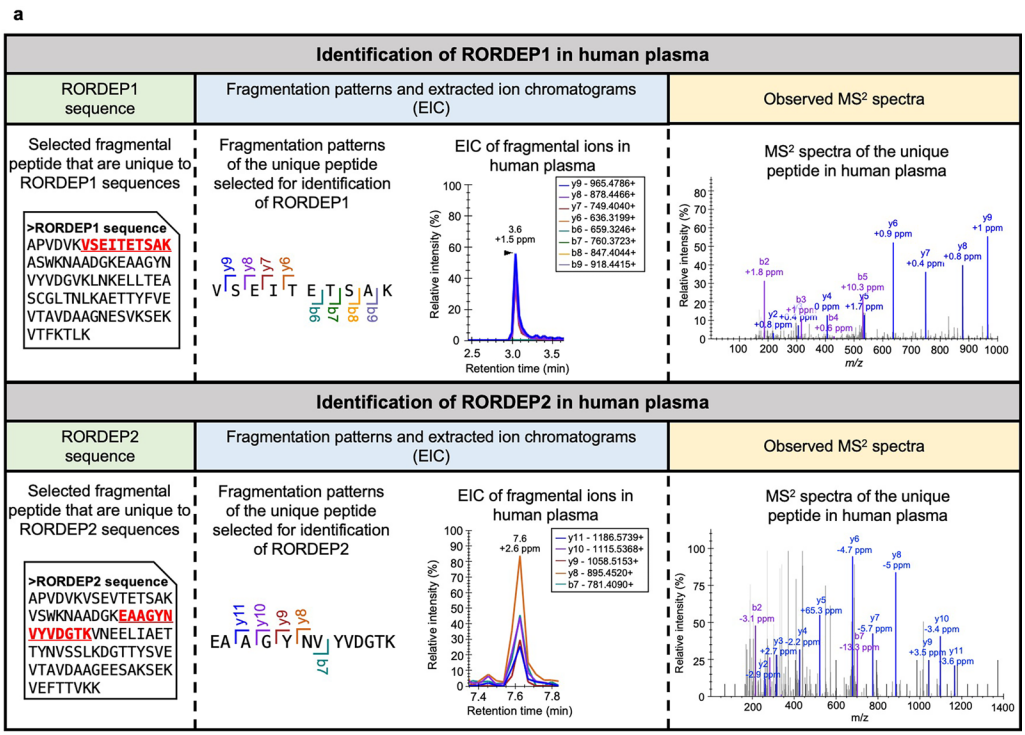

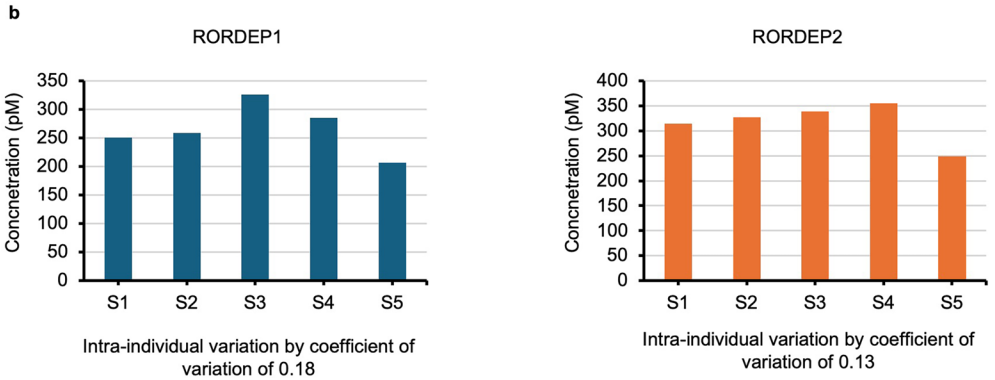

Extended Data Fig. 2 | Absolute quantification of RORDEP1 and RORDEP2 peptides in human plasma samples applying liquid chromatography tandem mass spectrometry (LC-MS). In panel **(a)**, the left section shows the selected proteotypic peptides (underscored and highlighted in red) that are unique to the sequences of RORDEP1 or RORDEP2. In the central section, the left graph displays the fragmentation patterns for the unique peptides in the identification of RORDEPs. b- and y- ions indicate that the fragmentation occurs in a way that the charge is retained on the N-terminus and C-terminus, respectively, of the peptide. The b-ions contain the amino-terminal end of the peptide and are numbered from the N-terminus (the beginning of the peptide chain) and the y-ions contain the carboxyl-terminal end of the peptide and are numbered from the C-terminus (the end of the peptide chain). The middle graph shows the extracted ion chromatograms for b- and y-ions, and the retention time for the selected proteotypic peptides in human plasma. The extracted ion chromatograms (EICs) of b- and y- ions are labeled according to the fragmentation patterns that are shown in the left graph. In the right section, observed tandem mass spectrometry (MS^2) spectra using a Q Exactive mass spectrometer is depicted. The section details their MS 2 with mass accuracy expressed in parts per million (ppm). **(b)** Bar graphs representing the coefficient of variation for intra- individual variability in signal intensity of RORDEP1 (blue) and RORDEP2 (orange). Each bar represents one individual sample out of five independently examined samples from the same plasma pool.

https://doi.org/10.1038/s41564-025-02064-x

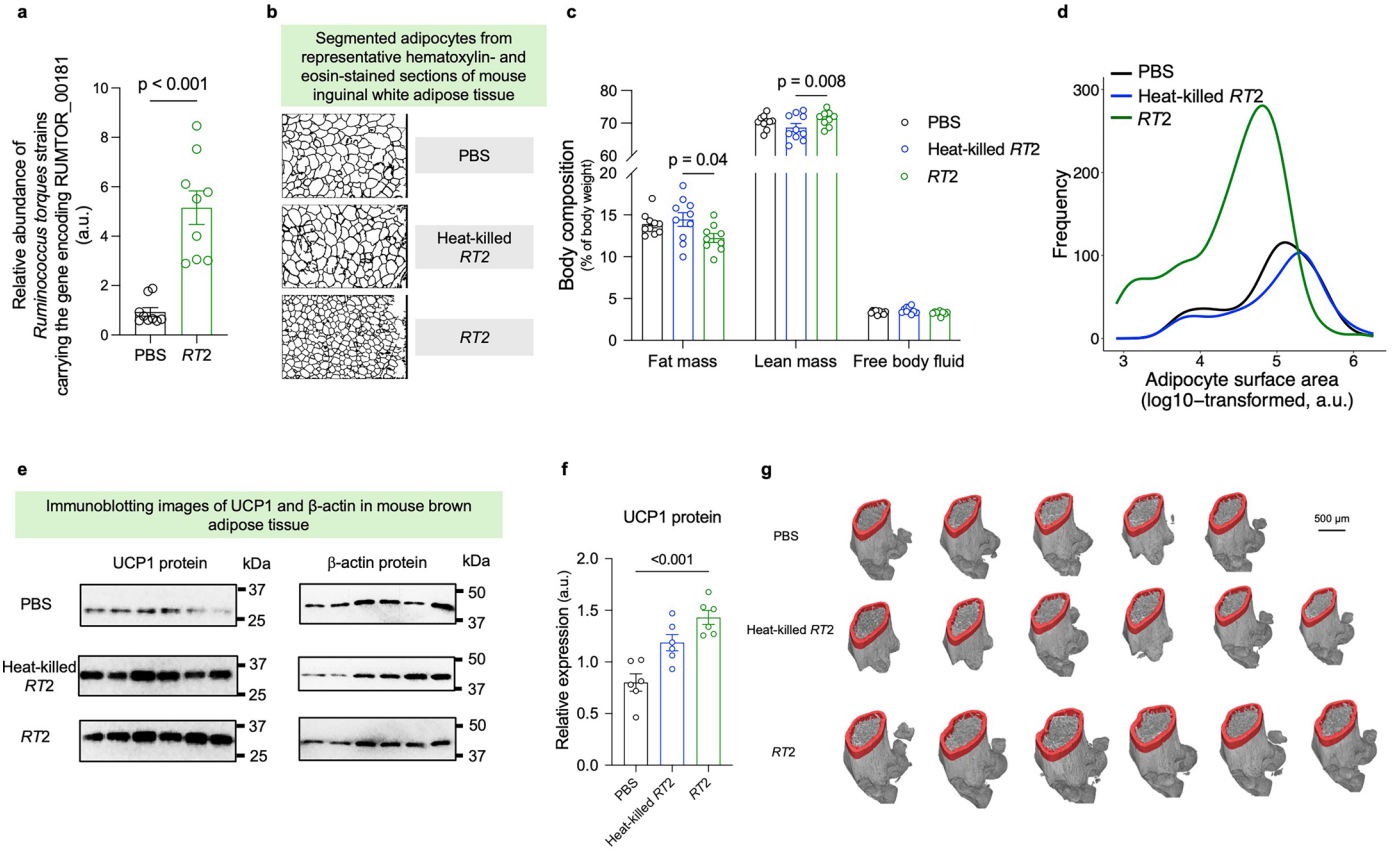

Extended Data Fig. 3 | Intestinal engraftment, body composition, brown adipose tissue expression of uncoupling 1 (UCP1) protein, and femoral cortical thickness in mice following eight weeks of oral gavage twice weekly of RT ATCC 27756 strain (RT2) expressing the RUMTOR_00181 gene. C57BL/6N mice were eight weeks old at start of intervention and were given a high-fat diet for a further eight weeks. The dose of RT2 was 5×10^9 in 100 µl of sterile phosphate-buffered saline (PBS) with with 10% glycerol or heat-killed RT2. **(a)** Engraftment testing at end of intervention at week eight (n = 9 per group). Abundance of RT strains expressing the RUMTOR_00181 gene was measured by quantitative PCR-normalized 16S rDNA in faecal DNA from mice treated with PBS or the live RT2 strain. **(b)** Segmented adipocytes from representative hematoxylin- and eosin-stained sections of inguinal white adipose tissue are depicted in Fig. 3f and analyzed using AdipoCount[51]. **(c)** Magnetic resonance imaging scanning of mouse body composition (n = 10 for PBS and heat-killed RT2 groups, and n = 9 for RT2 group). **(d)** The frequency distribution of adipocyte cell surface area (in arbitrary units, a.u.) in inguinal white adipose tissue across the three specified groups. **(e)** Immunoblotting result of UCP1- and housekeeping β-actin proteins in interscapular brown adipose tissue (n= six mice in each of four groups). **(f)** Quantifications of the immunoblottings of UCP1 and β-actin in panel c are given as ratios (n = 6 per group). **(g)** High-resolution 3D reconstructions of femoral bones (5–6 mice per group), with red sections indicating the regions selected for cortical thickness analysis. In panel **a**, significance was obtained by Student's t-test (two-sided). In panels **c** and **f**, statistical analysis was performed using one-way ANOVA with Dunnett's *post hoc* correction for multiple comparisons. For panels **a**, **c**, and **f**, data are presented as mean ± SEM.

https://doi.org/10.1038/s41564-025-02064-x

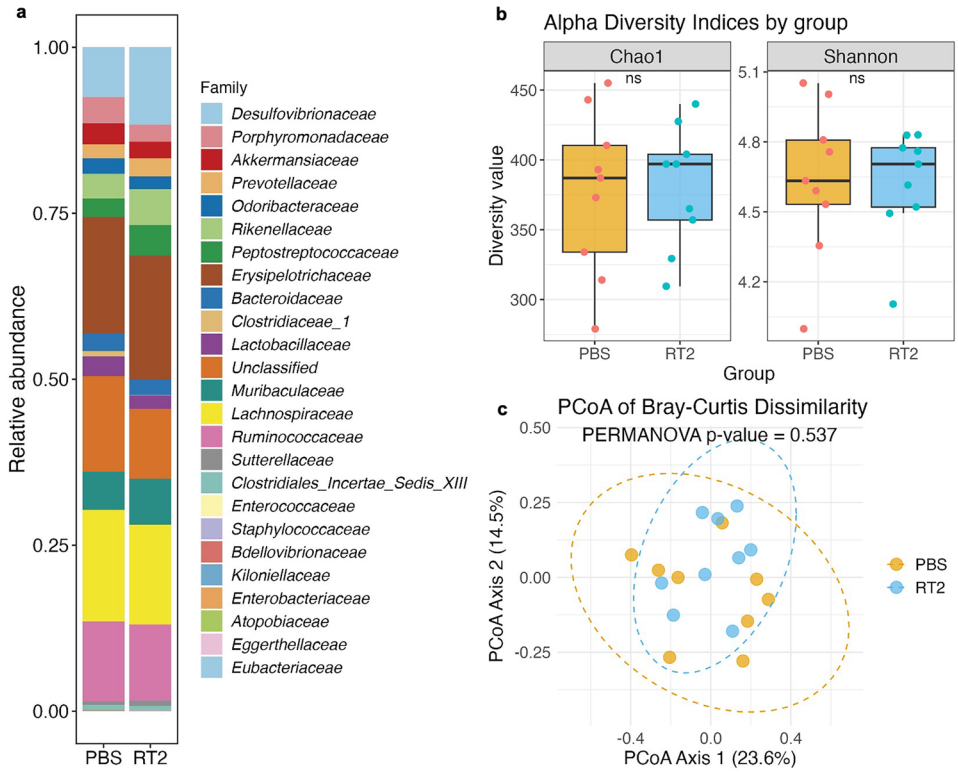

Extended Data Fig. 4 | Impact of *R. torques* ATCC 27756 (RT2) intervention on the 16S rRNA gut microbiota profile of mice. (a) Bar plots representing the relative abundance of bacterial families in the gut microbiota of mice treated with RT2 (n = 9) and control mice receiving sterile phosphate-buffered saline (PBS) containing 10% glycerol (n = 9) over an 8-week period *via* oral gavage. **(b)** Box plots illustrating the Chao1 richness estimator and Shannon diversity index for the gut microbiota of RT2-treated and control mice (n = 9 per group). Statistical significance was calculated using the two-sided Wilcoxon test; ns denotes non-significant. Box plot elements: centre line represents the median; box limits indicate the 25th and 75th percentiles; whiskers extend from the minimum to the maximum values. **(c)** Principal coordinate analysis (PCoA) plot visualizing the Bray-Curtis dissimilarity at the amplicon sequencing variants (ASVs) level, comparing the gut microbial communities of RT2-treated and control mice. PERMANOVA analysis (two-tailed) based on Bray-Curtis dissimilarity was conducted to assess differences between groups.

https://doi.org/10.1038/s41564-025-02064-x

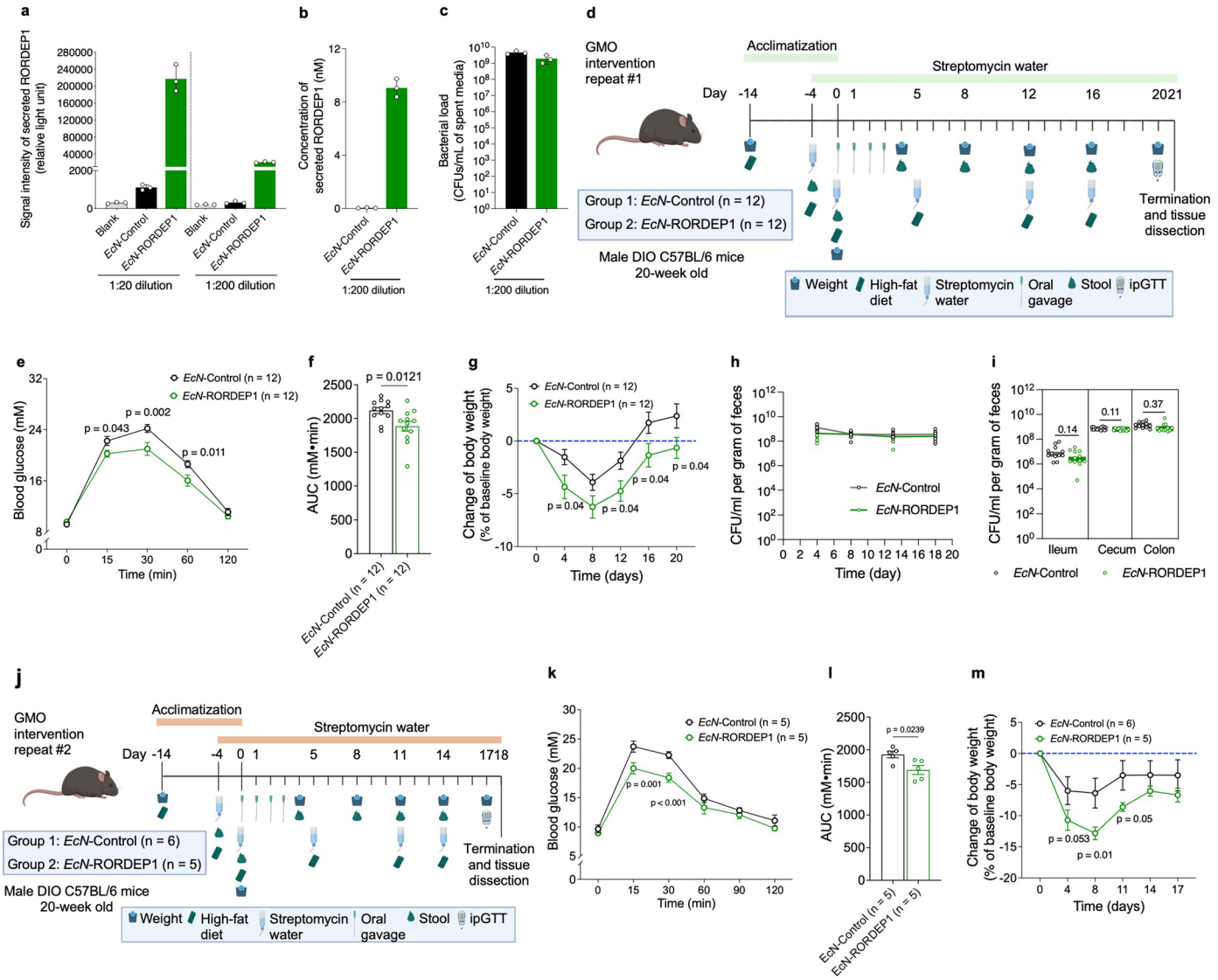

Extended Data Fig. 5 | Mouse interventions with *Escherichia coli Nissle* 1917 (EcN) engineered to express RORDEP1. (a) Luciferase reporter assay showing the signal intensity of secreted RORDEP1 in the spent culture supernatant of the engineered EcN strain and the negative control. Analyzed at 20-fold and 200-fold dilutions. Culture medium alone (lank; 2 × YT) was included to assess background signal. Bars represent the mean luciferase signal from three biological replicates. **(b)** Quantification of secreted RORDEP1 from the engineered strain using a standard curve generated with a HibiT-tagged control protein. **(c)** Bacterial load of the engineered EcN strains expressed as colony-forming units per milliliter (CFU/mL) of diluted culture media. **(d)** In independent experiment #1, twenty-four 20-week-old C57BL/6 N male mice, which had been on a high-fat diet for 12 weeks prior to the start of interventions, were assigned to each group receiving either 5×10^{10} CFU of live EcN-RORDEP1/100 µl of sterile phosphate-buffered saline (PBS) or 5×10^{10} CFU of live EcN-Control /100 µl of sterile PBS for four consecutive days. The timeline details the protocol for mice acclimatization and subsequent administration of EcN strains. From day minus four and until termination (day 21), streptomycin was added to drinking water to ensure a consistently high level of bacteria engraftment. **(e** and **k)** Blood glucose levels measured during intraperitoneal glucose tolerance test (ipGTT) in two independent experiments. **(f** and **l)** The area under the curve (AUC) for the ipGTT in two independent experiments. **(g** and **m)** Graphs illustrating the body weight alterations over time for both groups in two independent experiments. **(h)** This plot displays the engraftment profiles in mouse stools of the two different EcN strains; analyses were done at day 4, 8, 12 and 18, respectively, during a 20-day period in the independent experiment #1 as shown in panel **a**. The CFU per gram of feces are plotted on a logarithmic scale. Two groups are compared: the control group (EcN-Control, black circles) and the group treated with EcN- RORDEP1 (green circles). Data points represent mean CFU values, and error bars indicate standard deviations. **(i)** Distribution of *E. coli* expressed in CFU per gram of intestinal contents from various regions of the intestinal tract (ileum, cecum, and colon) on day 20 (termination) in the independent experiment #1 as shown in panel **(d)**. Each data point represents an individual sample from either EcN-Control (black) or EcN- RORDEP1 group (green), with the mean values indicated by the horizontal lines. **(j)** Overview of the second experiment lasting for 18 days. Statistical assessments for blood glucose levels and body weight changes were conducted using two-way ANOVA with Bonferroni *post hoc* adjustments. The significance of differences in AUC (panels **f** and **l**) and colonization (panel **i**) was determined with a two-sided unpaired Student's t-test. Panels **d** and **j** created with BioRender.com.

https://doi.org/10.1038/s41564-025-02064-x

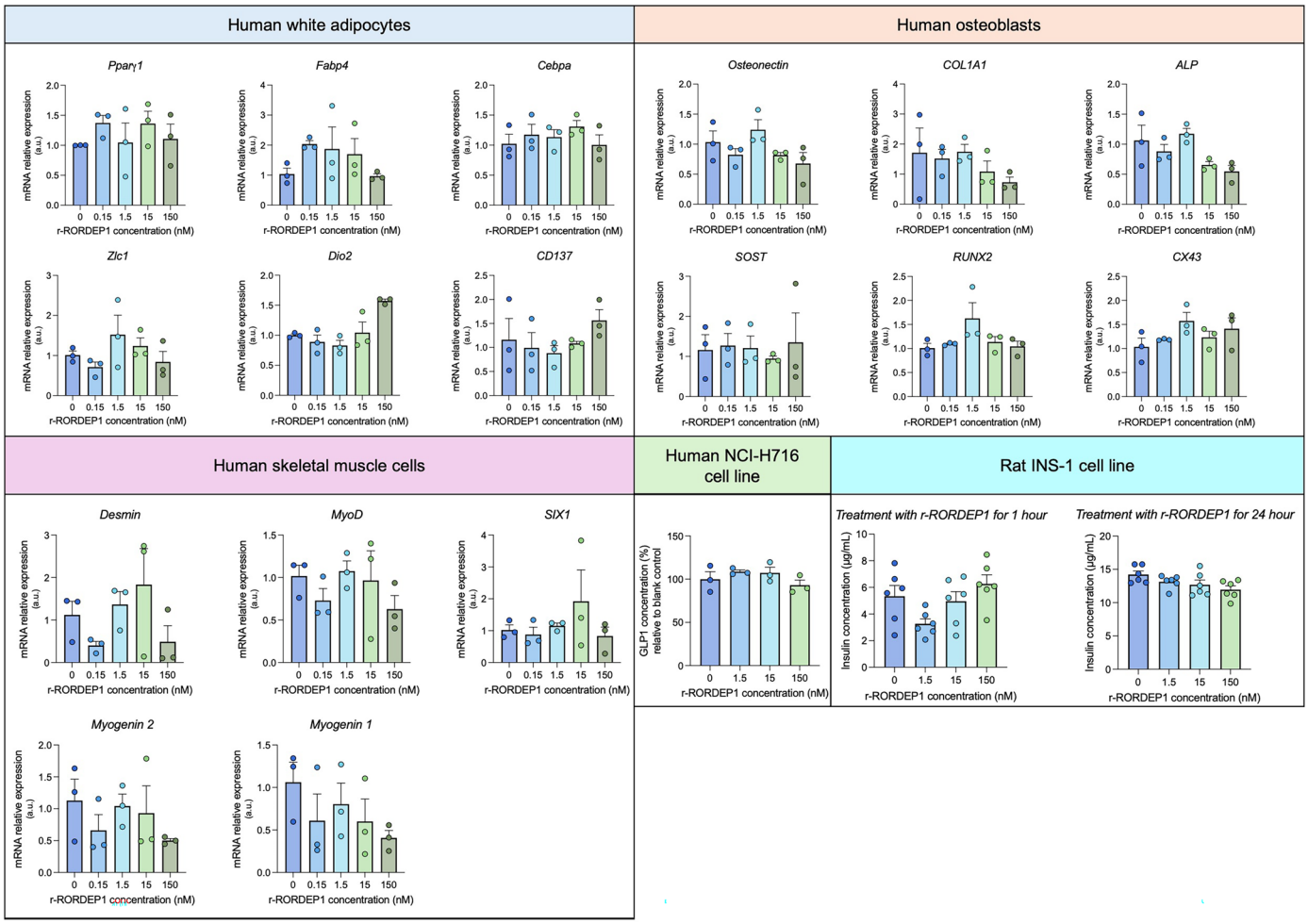

Extended Data Fig. 6 | Assessments of *in vitro* effects of recombinant RORDEP1 in human and mammalian cellular models applying gene expression profiling. In human white adipocytes, the expression of key adipogenic genes, including *Pparγ* (peroxisome proliferator-activated receptor gamma), *Hsl* (hormone-sensitive lipase), *Gpat3* (glycerol-3-phosphate acyltransferase 3), *Zbtb7* (zinc finger and BTB domain-containing protein 7A), *Dgat2* (diacylglycerol O-acyltransferase 2), and *Cd137* (tumor necrosis factor receptor superfamily member 9), was measured. In human osteoblasts, markers of osteogenic differentiation were assessed, including *Osterix* (transcription factor Sp7), *ALP* (alkaline phosphatase), *CCL1*(α) (chemokine ligand 1), *SOST* (sclerostin), *RUNX2* (runt-related transcription factor 2), and *COL1A1* (collagen type I alpha 1 chain). In human skeletal muscle cells, the expression of genes related to muscle differentiation and growth, such as *Desmin* (intermediate filament protein), *MyoD* (myogenic differentiation 1), *SX1* (Sarcobox), *MyoG1*, and *MyoG2* (myogenin isoforms), were evaluated. For human NCI-H716 enteroendocrine cells, the response to r-RORDEP1 treatment did not result in any significant transcriptional changes in the GLP-1 release. Similarly, in rat INS-1 pancreatic beta cells, a model commonly used for studying insulin secretion, r-RORDEP1 exposure for one hour at varying concentrations showed no significant effects. rat INS-1 cell line, n = 6 biological replicates; for the remaing, n = 3 replicates per condition. Error bars are the SEM of 3-6 independent replicates.

https://doi.org/10.1038/s41564-025-02064-x

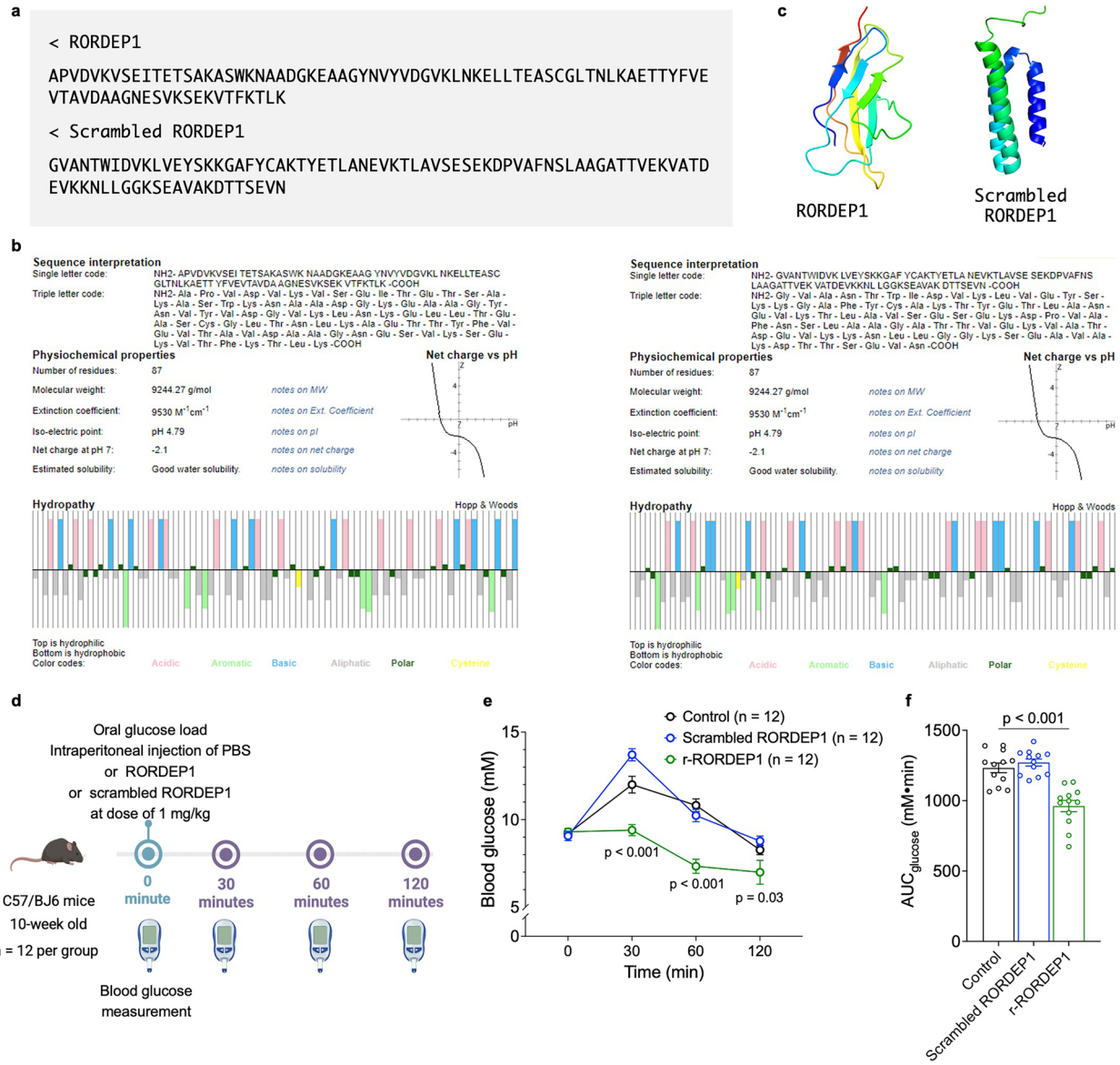

Extended Data Fig. 7 | Synthesis of scrambled recombinant RORDEP1 and testing of its potential effect on blood glucose over two hours in lean male C57BL/6J mice. (a) Amino acid sequences of r-RORDEP1 and scrambled r-RORDEP1. **(b)** Comparison of predicted physicochemical properties of native RORDEP1 and scrambled RORDEP1. **(c)** AlphaFold2-predicted 3-dimentional structure of the two RORDEP1 peptides. **(d)** Experimental workflow of mouse experiment evaluating effects of the two RORDEP1 peptides on blood glucose in mice (n = 12 mice per group) for two hours. An initial oral glucose load (2 g/kg) was given in the fasting state immediately followed by an intraperitoneal injection of either PBS, r-RORDEP1 or scrambled r-RORDEP1; the two peptides were given at a dose of 1 mg/kg. **(e)** Curves of the glucose tolerance test at the indicated time points for the two peptides showing no effect of scrambled r-RORDEP1. **(f)** Area under the curve (AUC) analysis of glucose tolerance test (n = 12 per group). PBS denotes phosphate-buffered saline. Data are expressed as mean ± SEM. Statistical significance was determined using two-way ANOVA with Dunnett's *post hoc* test for panel **e** and one-way ANOVA with Dunnett's correction for panel **f**. Panel **d** created with BioRender.com.

https://doi.org/10.1038/s41564-025-02064-x

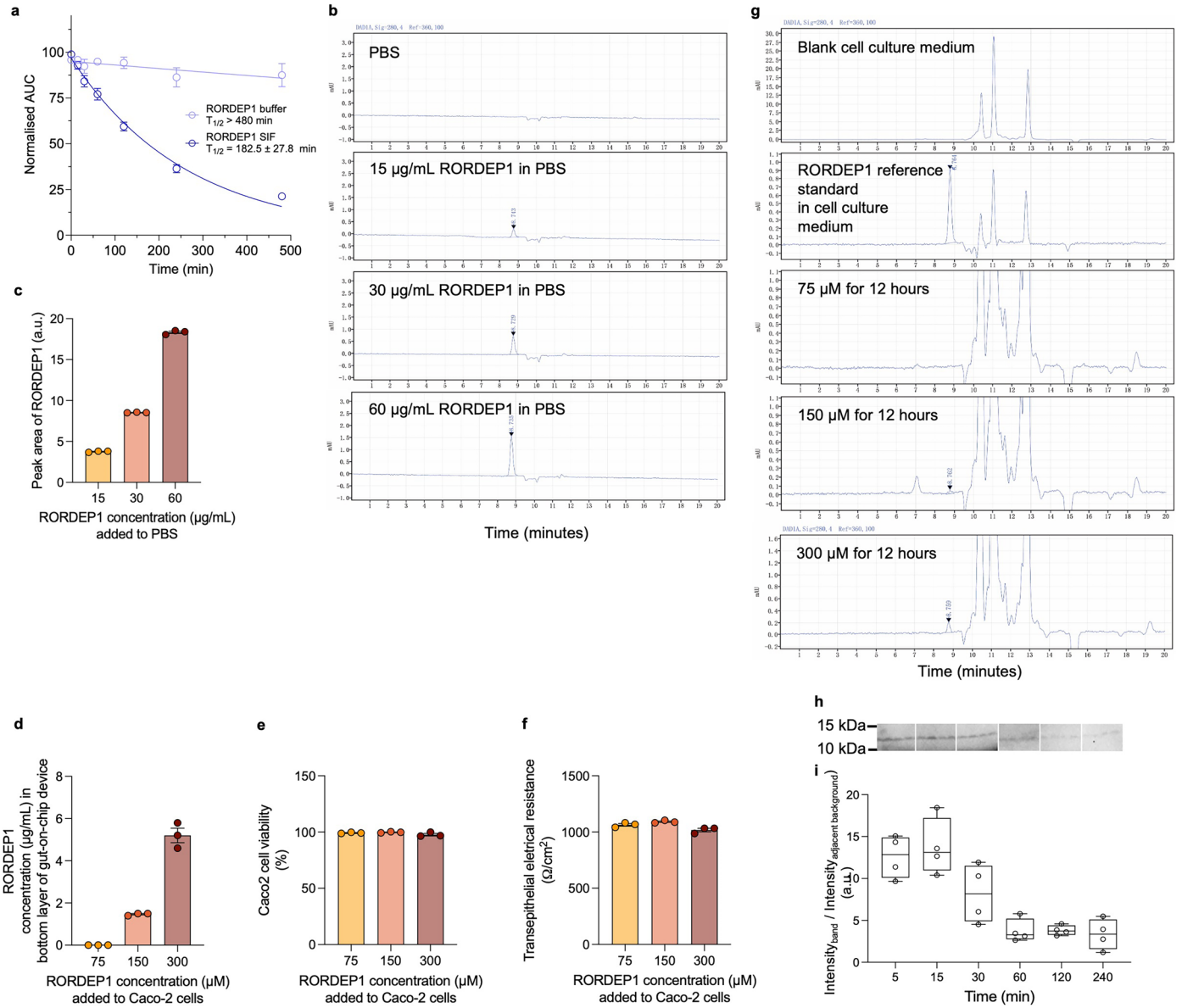

Extended Data Fig. 8 | Stability of recombinant RORDEP1 in intestinal fluid, gut epithelial permeability of r-RORDEP1, and *in vivo half*-life of r-RORDEP1. **(a)** *In vitro* stability of r-RORDEP1 (dark blue) in simulated intestinal fluid (SIF) including buffer control (light blue). Absorption that were measured at 214 nm illustrates r-RORDEP1 degradation upon exposure to SIF; data were recorded at various time points. Amount of left r-RORDEP1 upon the exposure to SIF or buffer were expressed as normalized area under the curves (AUCs) relative to 0 min. **(b)** Representative UPLC chromatograms of purified r-RORDEP1 spiked into phosphate-buffered saline (PBS) at increasing concentrations, demonstrating consistent retention time and concentration-dependent signal. **(c)** Quantification of r-RORDEP1 peak areas at increasing concentrations, expressed in arbitrary units (a.u.). **(d)** Quantitative analysis of r-RORDEP1 in the basolateral compartment following apical application of r-RORDEP1 at various concentrations during an incubation for 12 h. A dose-dependent increase in r-RORDEP1 concentration was observed. **(e)** Assessment of Caco-2 cell viability by 3-(4,5-dimethylthiazolyl-2)-2,5-diphenyltetrazolium bromide (MTT) viability assay after exposure to varying concentrations of r-RORDEP1. No significant impact on cell viability was observed compared to control. **(f)** Measurements of transepithelial electrical resistance (TEER) in Caco-2 monolayers following r-RORDEP1 exposure, indicating that tight junction integrity remained intact. **(g)** Representative chromatograms illustrating the presence and abundance of r-RORDEP1 in the basolateral compartment after transepithelial transport. The blank control in the chromatogram represents basolateral cell culture medium without r-RORDEP1 treatment, while the other chromatograms display either r-RORDEP1 reference standards or penetrated r-RORDEP1 detected in the basolateral medium. **(h)** Immunoblot analysis showing the presence 6×His-tagged-RORDEP1 polypeptide in plasma samples collected from four chow-fed lean eight weeks-old C57BL/6N mice at 5, 15, 30, 60, 120 and 240 min after intraperitoneal injection of r-RORDEP1 at a dose of 1 mg/kg. The expected size of the r-RORDEP1 protein (~12.5 kilodalton (kDa)) is indicated on the left. The blot lanes correspond to time points after administration by immunoblotting assay using anti-His-Tag Antibody (Cell Signal Technology, #2365). The experiment was performed once. **(i)** The relative abundance of plasma RORDEP1 was quantified by calculating the ratio of the pixel intensity for each band to the intensity of the adjacent background at various time points following the injection of 6×His-tagged r-RORDEP1 (n = 4 per group). This measurement was conducted using ImageJ software. Each data point represents an individual measurement from one mouse. Box-and-whisker plots display the median, quartiles, and range of protein abundance for each time point, with individual data points overlaid. For panels **a**, and **c**-**f**, data are presented as mean ± SEM, and n = 3 per group.

https://doi.org/10.1038/s41564-025-02064-x

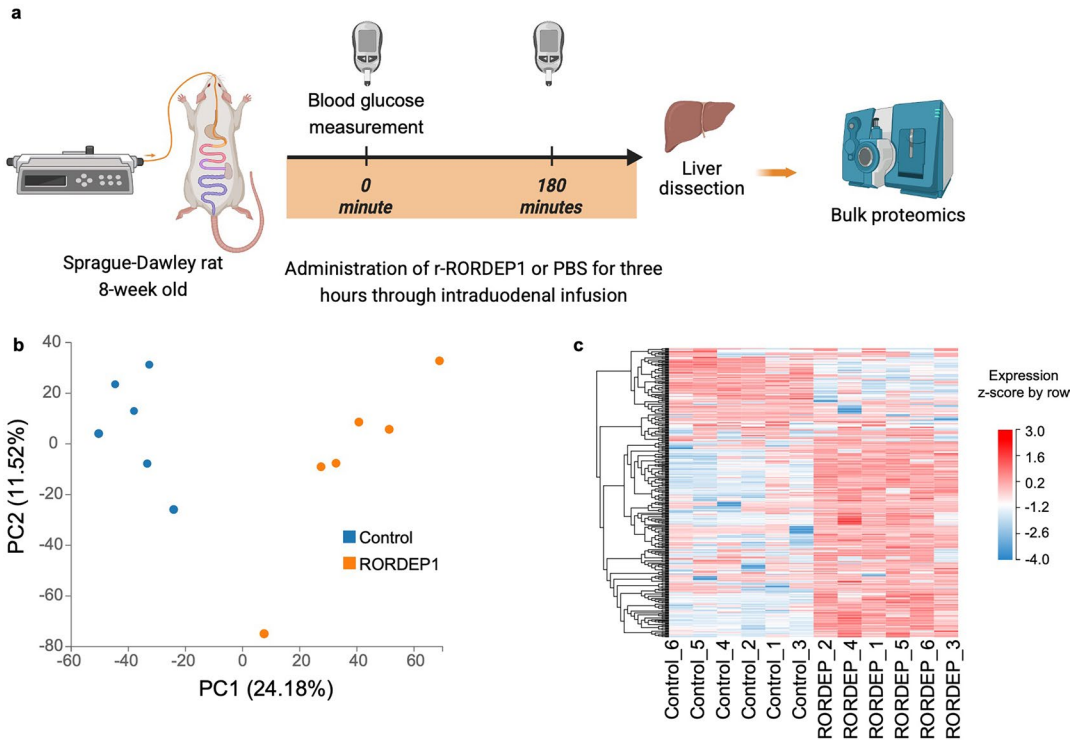

Extended Data Fig. 9 | Changes of the rat liver proteome following intestinal infusion of recombinant RORDEP1. (a) Twelve 8-week-old lean male Sprague-Dawley rats (six after r-RORDEP1 and six after infusion of phosphate buffered saline (PBS)) were included. r-RORDEP1 was infused into duodenum with a rate of 200 pmol/kg/min for three hours. The analysis involved profiling a total of 7,678 proteins from the rat liver. **(b)** Principal Component Analysis (PCA) plot displays the distribution of samples based on the first and second principal components (PC1 and PC2), capturing 24.2 % and 17.3 % of the total variance, respectively. Each point represents an individual sample, categorized by treatment group (r-RORDEP1 or PBS). **(c)** Heatmap visualizes 379 proteins that exhibit significant differential expression (277 up- and 109 down regulated) between the control and r-RORDEP1-treated groups. Differential expression was determined using a threshold q-value < 0.05. Expression of the differential proteome was z-score transformed for data visualization. Panel **a** created with BioRender.com.

https://doi.org/10.1038/s41564-025-02064-x

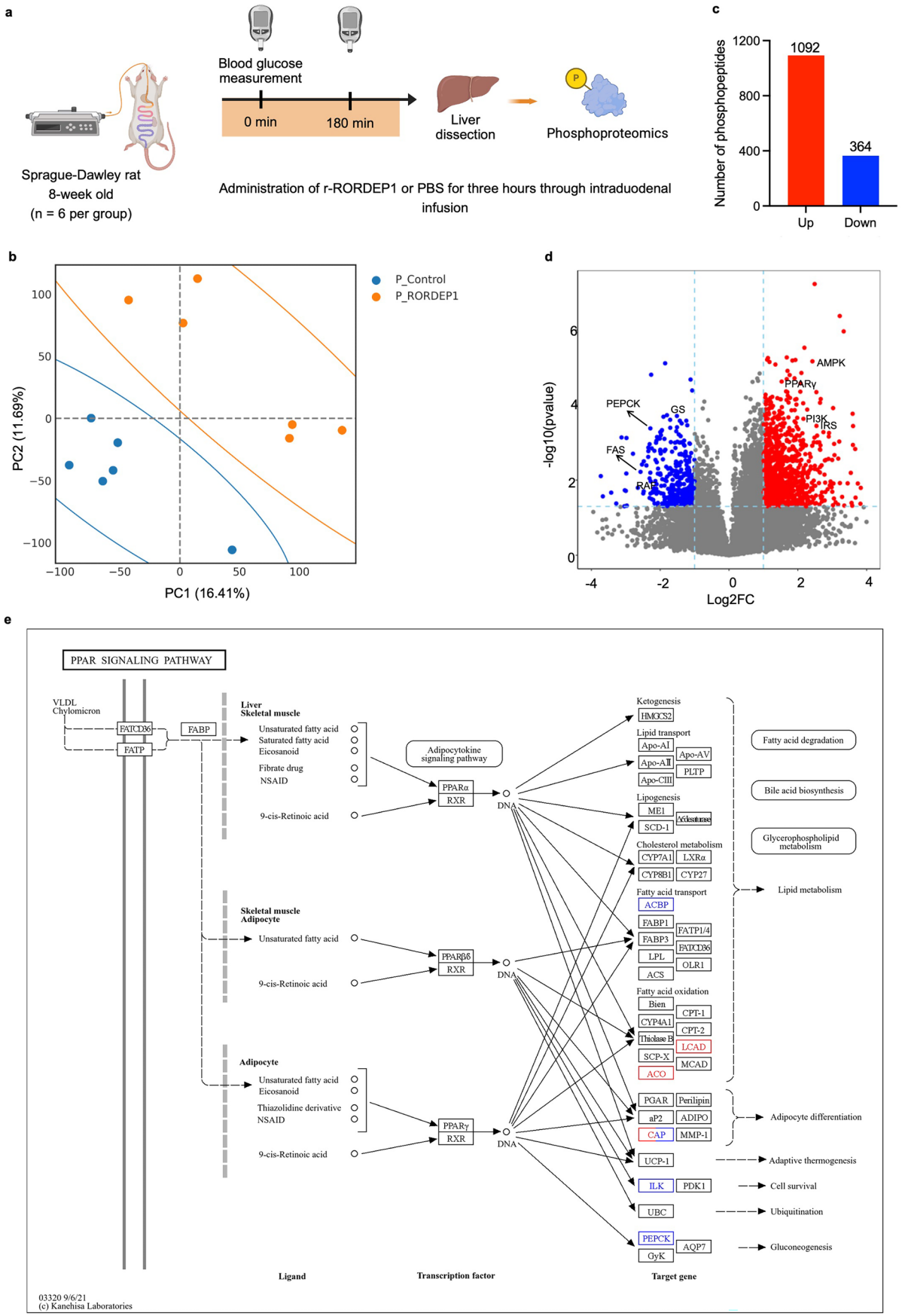

Extended Data Fig. 10 | See next page for caption.

https://doi.org/10.1038/s41564-025-02064-x

Extended Data Fig. 10 | Phosphoproteomics analysis of rat liver following intestinal infusion of recombinant RORDEP1. (a) Twelve 8-week-old lean male Sprague-Dawley rats (six after r-RORDEP1 and six after infusion of phosphate buffered saline (PBS)) were included. r-RORDEP1 was infused into duodenum with a rate of 200 pmol/kg/min for three hours. The analysis involved profiling a total of 4,877 phosphoproteins. **(b)** Principal Component Analysis (PCA) plot displays the distribution of samples based on the phosphoryl proteome in the group treated with PBS (P_Control) and the group treated with r-RORDEP1 (P_RORDEP1). **(c)** Visualization of the number of significantly differential (log2 fold change (log2FC) > 1 and adjusted $p < 0.05$) phosphoryl proteins between the two groups; up- and down-regulated features were colored with red and blue, respectively. **(d)** Volcano plot visualizing the changed phosphoryl proteins in panel b; proteins involved in hepatic glucose- and lipid metabolism are labeled. **(e)** Differential pathway enrichment analysis showing that phosphorylation of PPAR pathway was activated following *in vivo* exposure to r-RORDEP1. Up- and down-regulated phosphoryl proteins are marked with red and blue boxes, respectively. For panels c and d, the significance was determined using two-sided Student's *t*-test, with *post hoc* correction using the Benjamini-Hochberg method. Panel **a** created with BioRender.com.

nature portfolio

Corresponding author(s): Oluf Pedersen

Last updated by author(s): Jun 18, 2025

Reporting Summary

Nature Portfolio wishes to improve the reproducibility of the work that we publish. This form provides structure for consistency and transparency in reporting. For further information on Nature Portfolio policies, see our Editorial Policies and the Editorial Policy Checklist.

Statistics

For all statistical analyses, confirm that the following items are present in the figure legend, table legend, main text, or Methods section.

n/a	Confirmed
☐	☒ The exact sample size (*n*) for each experimental group/condition, given as a discrete number and unit of measurement
☐	☒ A statement on whether measurements were taken from distinct samples or whether the same sample was measured repeatedly
☐	☒ The statistical test(s) used AND whether they are one- or two-sided *Only common tests should be described solely by name; describe more complex techniques in the Methods section.*
☐	☒ A description of all covariates tested
☐	☒ A description of any assumptions or corrections, such as tests of normality and adjustment for multiple comparisons
☐	☒ A full description of the statistical parameters including central tendency (e.g. means) or other basic estimates (e.g. regression coefficient) AND variation (e.g. standard deviation) or associated estimates of uncertainty (e.g. confidence intervals)
☐	☒ For null hypothesis testing, the test statistic (e.g. *F*, *t*, *r*) with confidence intervals, effect sizes, degrees of freedom and *P* value noted *Give P values as exact values whenever suitable.*
☒	☐ For Bayesian analysis, information on the choice of priors and Markov chain Monte Carlo settings
☒	☐ For hierarchical and complex designs, identification of the appropriate level for tests and full reporting of outcomes
☐	☒ Estimates of effect sizes (e.g. Cohen's *d*, Pearson's *r*), indicating how they were calculated

Our web collection on statistics for biologists contains articles on many of the points above.

Software and code

Policy information about availability of computer code

Data collection	No specific software was used for the data collection.
Data analysis	All analyses in this study were conducted using tools that are publicly accessible. Specifically, GraphPad Prism (version 10.1.0) was utilized for both graphical representation and statistical evaluation of data derived from animal experiments. For the Small-Angle X-ray Scattering data reduction, PRIMUSqt from the ATSAS package (version 2.8.32) was used. For processing RNA sequencing data, a suite of software including SOAPnuke (version 1.5.2), HISAT2 (version 2.0.4), Bowtie2 (version 2.2.5), and RSEM (version 1.2.12) was employed. Additionally, analysis was performed with the use of R (version 4.3.0) and several of its packages: ggplot2 (version 3.4.4) for data visualization, dplyr (version 1.1.4) and tidyr (version 1.3.0) for data processing, along with DESeq2 (version 1.40.2) for differential expression analysis.

For manuscripts utilizing custom algorithms or software that are central to the research but not yet described in published literature, software must be made available to editors and reviewers. We strongly encourage code deposition in a community repository (e.g. GitHub). See the Nature Portfolio guidelines for submitting code & software for further information.

Data

Policy information about availability of data

All manuscripts must include a data availability statement. This statement should provide the following information, where applicable:

- Accession codes, unique identifiers, or web links for publicly available datasets
- A description of any restrictions on data availability
- For clinical datasets or third party data, please ensure that the statement adheres to our policy

Anonymized clinical data of participants included in this study are provided in Supplementary Tables 6 and 7. Raw proteomics data that support the findings of this study have been deposited to the ProteomeXchange Consortium with the dataset identifier PXD057146 (human plasma) and MassIVE database (massive.ucsd.edu) with identifiers MSV000093785 (bacterial supernatants) and MSV000097951 (rat liver). The raw RNA-seq reads of rat liver tissue are available at the European Nucleotide Archive with accession number PRJEB89704. The predicted protein structure of RUMTOR_00181 is available at AlphaFold Protein Structure Database via identifier A5KIY5. Source data are provided with this paper.

Research involving human participants, their data, or biological material

Policy information about studies with human participants or human data. See also policy information about sex, gender (identity/presentation), and sexual orientation and race, ethnicity and racism.

Reporting on sex and gender	This study includes two cohorts of human participants. Cohort 1: For quantification of RUMTOR_00181-carrying strains in human stools and estimation of the abundance of RORDEP1 and 2 in human plasma, respectively, 59 healthy adult men were recruited. Cohort 2: For the assessment of a potential impact of dietary habits on abundance of RT strains releasing RORDEPs in stool samples, the absolute cell counts of RUMTOR_00181-carrying strains were measured in 54 healthy adults (35 females and 19 males) following vegan or omnivorous diet.
Reporting on race, ethnicity, or other socially relevant groupings	For Cohorts 1 and 2, participants are Danish Caucasian.
Population characteristics	In Cohort 1, all participants are males (age 25 ± 4.0 years, body mass index (BMI) 23.8 ± 2.0 kg/m2) In Cohort 2, participants following vegan diet are aged 29.7 ± 1.7 years with BMI of 20.7 ± 5.3 kg/m2; participants following omnivorous diet are aged 30.4 ± 6.9 years with BMI of 21.6 ± 2.6 kg/m2.
Recruitment	For Cohort 1, participants were recruited in Denmark by advertisement in local newspapers, social media, and other online resources between 2016 and 2017. Inclusion criteria for the study were being male of about 18 to 35 years in good health, with stable weight, normal glucose metabolism, normal kidney and liver functions and normal blood pressure. Exclusion criteria from the study included all the people allergic to glucocorticoids, smokers, people that where prescribed oral medication in the previous 4 months, that consumed probiotics daily for the previous 4 months, with relevant dietary changes in the previous 2 months, that suffered either chronic or acute illness the previous 2 months as well, previous GI operation, mental disorders or individuals who were unable to give informed consent. Finally, all the individuals that required medical treatment during the study were also excluded from the study. For Cohort 2, participants were recruited from urban areas in Denmark by advertisement in local newspapers, social media, and other online resources from November 2013 to November 2014. Volunteers were eligible for inclusion if they were between 18 – 65 years of age and weight-stable (±1 kg, assessed by interview) for a minimum of 2 months. Vegan volunteers were eligible for inclusion in the study if they had been adherent to a vegan diet for a minimum of 1 year. Volunteers who received antibiotic treatment within 3 months, had known gastrointestinal disease or reported gastrointestinal symptoms at the time of the study, or followed a medically prescribed diet were ineligible for inclusion. Pregnant and lactating women were also ineligible. For both cohorts, there were no specific inclusion criteria that would introduce self-selection bias beyond standard voluntary participation in observational studies.
Ethics oversight	For Cohort 1, the study was approved by the Ethical Committees of the Capital Region of Denmark (H-16021787). For Cohort 2, the study was approved by the Ethical Committee of the Capital Region of Denmark (H 3 2012-145).

Note that full information on the approval of the study protocol must also be provided in the manuscript.

Field-specific reporting

Please select the one below that is the best fit for your research. If you are not sure, read the appropriate sections before making your selection.

☒ Life sciences ☐ Behavioural & social sciences ☐ Ecological, evolutionary & environmental sciences

For a reference copy of the document with all sections, see nature.com/documents/nr-reporting-summary-flat.pdf

Life sciences study design

All studies must disclose on these points even when the disclosure is negative.

Sample size	No formal sample size calculation was performed, as this is an observational study. The sample sizes were determined by the number of eligible participants available during the study period. The sample sizes are considered as sufficient for exploratory analysis and to detect relevant associations, in line with similar observational studies (PMID: 30425247 and 30397356).
Data exclusions	No data was excluded.
Replication	As a hypothesis generating study, no explicit replication attempts were made. As for the mouse study, all experiments were at least duplicated and all attempts at replication were successful and supported the conclusions in the manuscript.
Randomization	As the studies in humans were observational, there was no allocation or randomization. The experiments in rodents employed a methodological approach where animals were assigned to groups in a random manner, with assignments based on their body weights prior to the initiation of the experimental interventions.
Blinding	Blinding was not performed in the human sample analysis; however, all human samples were labeled with unique, non-identifying codes and were not linked to any personal participant information, minimizing potential bias. For all other experiments, investigators were blinded to group allocation during both data collection and analysis to ensure objectivity and reduce potential observer bias.

Reporting for specific materials, systems and methods

We require information from authors about some types of materials, experimental systems and methods used in many studies. Here, indicate whether each material, system or method listed is relevant to your study. If you are not sure if a list item applies to your research, read the appropriate section before selecting a response.

Materials & experimental systems

n/a	Involved in the study
☐	☒ Antibodies
☐	☒ Eukaryotic cell lines
☒	☐ Palaeontology and archaeology
☐	☒ Animals and other organisms
☒	☐ Clinical data
☒	☐ Dual use research of concern
☒	☐ Plants

Methods

n/a	Involved in the study
☒	☐ ChIP-seq
☒	☐ Flow cytometry
☒	☐ MRI-based neuroimaging

Antibodies

Antibodies used	Polycolonal: Rabbit anti-UCP1 (Abcam, ab10983) Rabbit anti-His-Tag Antibody (Cell Signal Technology, #2365) Monoclonal: Rabbit anti-beta-actin antibodies (Abcam, ab115777)[SP124]
Validation	Rabbit anti-UCP1 (Abcam, ab10983) has been validated in previous report PMID: 26772600. Rabbit anti-His-Tag Antibody (Cell Signal Technology, #2365) has been validated in PMID: 37674080. Rabbit anti-beta-actin antibodies (Abcam, ab115777) has been validated in PMID: 30649474.

Eukaryotic cell lines

Policy information about cell lines and Sex and Gender in Research

Cell line source(s)	Human white preadipocytes (PromCell, #C-12732, Lot #456Z005.1, isolated from human omentum) Human osteoblasts (Promocell, #C-12720, Lot #445Z012.2, isolated from human femoral head) Human skeletal myoblasts (PromoCell, #C-12530, Lot #451Z031.15, isolated from human musculus pectoralis major) GLP-1 secreting human cell line NCI-H716 (ATCC, CCL-251) Rat insulin-secreting INS-1E 832/13 cells (a kind gift from Dr. Brice Emanuelli, Novo Nordisk Foundation Center for Basic Metabolic Research, Faculty of Health and Medical Sciences, University of Copenhagen) Human epithelial Caco-2 cell line (ATCC, #HTB-37)
Authentication	Cell lines obtained from publicly available cell banks were not re-authenticated.
Mycoplasma contamination	All cell lines were tested negative for mycoplasma contamination.

Commonly misidentified lines (See ICLAC register)	No commonly misidentified cell lines were used.

Animals and other research organisms

Policy information about studies involving animals; ARRIVE guidelines recommended for reporting animal research, and Sex and Gender in Research

Laboratory animals	Male mice with a C57BL/6 background (specific pathogen-free grade) and with varying ages as described in detail in the manuscript were purchased from Janvier Labs (Le Genest-Saint-Isle, France). Male Sprague-Dawley (SD) rats, nine weeks old and weighing around 300 grams, were purchased from the Experimental Animal Center of Chongqing Medical University, China, or from Janvier Labs (France) with ages specified in the manuscript. Male BKS-Leprdb/db/JOrlRj mice (Mus musculus) were obtained from Janvier Laboratories (France) at eight weeks of age, with initial body weights ranging from 30 to 45 grams. In the comparative study of the effects of r-RORDEP1 and scrambled r-RORDEP1 on glucose tolerance, 45 male C57BL/6J mice at eight weeks of age were obtained from Gempharmatech (Nanjing, China).
Wild animals	No wild animals were used.
Reporting on sex	Male animals were used in this study.
Field-collected samples	This work does not utilize field-collected samples.
Ethics oversight	All protocols for mice experiments were approved by the Danish Animal Experiments Inspectorate (license numbers: 2018-15-0201-01491 for the intervention study with RT strain and 2020-15-0201-00568 for the GMO1 study), and the University of Copenhagen (project numbers: P20-392 for the intervention study with RT strain and P23-145 for the GMO1 study). The comparative study between r-RORDEP1 and scrambled r-RORDEP1 in mice was conducted with ethical approval ID: GP01-QD112-2024v1.2 at WUXI (https://www.wuxiapptec.com). The rat research protocols were reviewed and approved by the Danish Animal Experimentation Council for the intravenous infusion (approval ID: 2023-15-0201-01508) and assessment of r-RORDEP1 effects on incretin release (approval ID: 2023-15-0201-01393), and by the Animal Ethics Committee of Chongqing Medical University, China (approval ID: IACUC-CQMU-2024-0036) for the intraducdenal infusion study.

Note that full information on the approval of the study protocol must also be provided in the manuscript.

Plants

Seed stocks	NA
Novel plant genotypes	NA
Authentication	NA